University of Stavanger

Faculty of Science and Technology

MASTER THESIS

Study program/Specialization: Petroleum Geosciences	Fall Semester 2015 Open access
Writer: Jennifer E. Cunningham	…… (Writer's signature)
Faculty supervisor: Chris Townsend External supervisor(s):	
Thesis title: Modeling Synrift Sediment Infill Patterns of Synthetic Normal Faults	
Credits (ECTS): 30	
Key words: Synrift, sedimentation, sediment, rifting, extension, modeling, reservoir modeling, normal faults, faults, displacement, relay ramps, deltas, Gilbert deltas, Corinth Rift, Greece	Pages: 79 + enclosure:1 Stavanger, January 8th, 2016

MODELING 3D SYNRIFT SEDIMENT INFILL PATTERNS OF SYNTHETIC NORMAL FAULTS

Jennifer E. Cunningham

MSc University of Aberdeen, United Kingdom

BSc (Hons) Memorial University of Newfoundland, Canada

An MSc thesis presented to the Institute of Petroleum Technology at the University of Stavanger

January 2016

Abstract

Previous studies of normal faulting and their control on sedimentation have largely focussed on geometrical infill patterns from a two dimensional perspective. In order to overcome this a series of 3D models have been generated which allow 3D infill patterns to be examined in detail. This study uses a series of synthetic 3D experiments to highlight the effect of changing fault displacement parameters on synrift sedimentation patterns. Several experiments have been run using new functionalities in Roxar's RMS 2013 software (part of their uncertainty module), in particular the ability to change displacements within a structural model. A new workflow has been established which combines the different RMS functionalities to sequentially displace surface models and infill the resulting hanging wall depressions. This workflow enables the user to manipulate various fault parameters, including length, displacement field and reverse drag, plus the option to manipulate the number of faults and their evolutionary geometry.

The modifications to the structural models make it possible to generate topographic surfaces and displace them in a similar manner to faults cutting the earth's surface. The resulting hanging wall basins can then be infilled using flat surfaces. The displacement-infill sequence forms a series of evolutionary models where the relative impact of the rate of the displacement and sedimentation can be observed (these rates are user controlled). In RMS, semi-automated modeling techniques were developed to accomplish various scenarios, which allowed specific parameters to be altered and their impact assessed. The structural models have been converted to 3D grids in order to utilise RMS's visualization of layered/segmented models and optimize the presentation of the results (successive time steps, layer geometries, fault displacement view, map view and multi cross-section view).

Initial models concentrated on using a single fault model in order to test the RMS functionalities. These models have been used to develop the RMS workflow and check the resulting models produced the expected results. The initial experiments have been developed to generate more complex structural situations in order to demonstrate how these techniques can be applied to more real world scenarios. The more complex experiments include asymmetric faults (where the point of maximum displacement is not in the center of the fault), multiple faults with similar displacement rates and relay ramps. Finally, further modeling techniques were developed in order to model the formation of sedimentary lobes such as those in a Gilbert delta environment. These techniques include the use of cone-shaped infill surfaces to mimic the radial sedimentation patterns associated with Gilbert type fan deltas. These visualizations attempt to replicate field examples of synrift sedimentation from the Corinth Rift in Greece (especially the Vouraikos Delta).

Acknowledgements

The scope of this study was defined by Chris Townsend and was completed at the University of Stavanger.

I would like to thank the following people for their continued support during the completion of this MSc thesis:

Chris Townsend of the University of Stavanger for defining the project, assisting me in learning RMS software, and helping in overseeing the overall completion of this thesis.

Nestor Cardozo of the University of Stavanger for his continued support during the completion of this thesis.

Hans Kallekleiv of Roxar for the technical support required during the modeling stages of this MSc.

Without the help of Roxar, this project would not have been possible. Roxar provided the University of Stavanger with their reservoir modeling software (RMS) and provided me with invaluable assistance during the uncertainty modeling portion of this project.

Table of contents

Abstract……...……i

Acknowledgements…….……...ii

Table of contents……...……...……...…..……..……..iii-v

List of figures…….……..vi-vii

List of tables……...…….……viii

List of appendices……..……...……....……ix

Chapter 1: Thesis introduction……..…….1

1.1 Introduction

1.2 Objectives

1.3 Background and literature review

1.3.1 Normal faulting and synrift sedimentation

1.3.1.1 Structural factors

1.3.1.2 Modeling Terms

1.3.1.3 Factors effecting sedimentation

1.3.2 Fault modeling literature review

1.3.3 Introduction to RMS

Chapter 2: Data & Methods……14

2.1 Introduction

2.2 Basics of modeling

2.3 RMS and structural uncertainty modeling

2.3.1Introduction to RMS' terminology

2.3.2 Data storage in RMS

2.3.3 Workflow manager

2.3.4 Data labeling system

2.4 Basic modeling setup

2.4.1 Input fault and horizon data

2.4.2 Fault displacement data

2.4.3 Experiment model dimensions

2.4.4 Modeling steps

2.4.5 Main modeling problem

2.5 Detailed workflow

2.6 Modeling the experiments

2.7 Visualization

Chapter 3: Results……41

3.1 Experiment 1
3.2 Experiment 2
3.3 Experiment 3
3.4 Experiment 4
3.5 Experiment 5
3.6 Experiment 6
3.7 Experiment 7
3.8 Experiment 8
3.9 Experiment 9

Chapter 4: Discussion……...62

4.1 Overview of results

4.2 Successes in modeling techniques

4.3 Improvements to software

4.3.1 Horizon displacement problem

4.3.2 Fault order in RMS

4.3.3 Compaction in RMS

4.3.4 Easy Parameter Manipulation

4.4 Geological improvements

4.5 Real world Application

Chapter 5: Conclusions and recommendations……...70

5.1 Conclusions

5.2 Recommendations

References…….73-78

Appendix……...…….Appendix Pages 1-52

List of figures

Figure 1.1: A simplified cross section view showing important terminology associated with rotated fault blocks in an extensional setting.

Figure 1.2: A fault terminology figure.

Figure 1.3: Simplified normal fault evolution in a rift basin.

Figure 2.1: The basics of modeling.

Figure 2.2: Workflow interaction diagram.

Figure 2.3: An example of a standard workflow (similar to the fourth displacement in experiments 1-7) displaying the resulting output from each job in the modeling workflow.

Figure 2.4: Graphs displaying the displacement attribute data for Experiment 1.

Figure 2.5: Graphs showing the displacement attribute data for each horizon in each Structural Model for Experiment 5.

Figure 3.1: The results from Experiment 1.

Figure 3.2: The results from Experiment 2.

Figure 3.3A&B: A: An intersection view of Experiment 3 showing the problems with modeling an increasing reverse drag. B: How the application of reverse drag should be handled in RMS.

Figure 3.3C: The results from Experiment 3.

Figure 3.4: The results from Experiment 4.

Figure 3.5: The results from Experiment 5.

Figure 3.6: The results from Experiment 6.

Figure 3.7: The results from Experiment 7.

Figure 3.8A: The results from the relay structure experiment (Experiment 8).

Figure 3.8B: The oldest horizon (A) being displaced in the relay ramp experiment where the relay ramps architecture is evident.

Figure 3.9A: The results from the multiple faults experiment (Experiment 9).

Figure 3.9B: This map shows horizon contours of Horizons A-F where A is the oldest and demonstrates the 50/50 displacement distribution of the hanging wall and footwall.

Figure 3.10: The results from Experiment 10.

Figure 4.1: Gilbert delta field and RMS model comparison figure.

List of tables

Table 2.1: List of experiments.

Table 2.2: Table 2.2: List of size, fault increment and 3D grid size data from all experiments

List of appendices

Appendix 1: Horizon and fault .txt inputs

Appendix 2: All experiments modeling input data

Appendix 3: Linear displacement graphs and displacement data tables for all experiments

Appendix 4: All modeling information and workflows for Experiments 1-10

Appendix 5: Colour bars used in 3D grid experiment visualization

Appendix 6: CD with sample RMS File: Experiment 1

Chapter 1

Thesis introduction

1.1 Introduction

Faults are dislocations in the earth's crust along which displacement has occurred with one side having moved relative to the other (Twiss and Moores, 2007; Fossen, 2010). A normal fault occurs when the faults slip (relative displacement) is roughly parallel to dip of the faults surface and the hanging wall (upper fault block) moves down relative to the footwall (lower fault block) (see Figure 1.1; Twiss and Moores, 2007; Ragan, 2009). Normal faults often dip approximately 60 degrees and facilitate the extension and subsequent thinning associated with rifting of the earth's crust (Twiss and Moores, 2007; Ragan, 2009). When these faults intersect the earth's surface they allow accommodation space to develop, that can be partially or completely filled by syn-tectonic sedimentation (Leeder and Gawthorpe, 1987; Gawthorpe and Leeder, 2000; McLeod et al., 2002; Fossen, 2010). There have been numerous studies on extension, basin development, normal faults and syn-tectonic sediment fill (e.g. Gibbs, 1984; Rippon, 1985; Barnett et al., 1987; Walsh and Watterson, 1987, 1990; Peacock and Sanderson, 1991; Childs et al., 1995, 2002; Gupta et al., 1999; Gawthorpe and Leeder, 2000; Peacock, 2002; Leeder, 2012). These articles have focused specifically on computational modeling of the interaction of changing normal faults and synrift sediment deposition: Gibson et al., 1989; Syahrul, 2014.

Modern geological modeling software (RMS) allows us to create a series of experiments following the approaches of Gibson (1989) and utilizing techniques developed by Syahrul (2014), to investigate the effect changing fault parameters have on the depositional patterns in syn-tectonic sediments. Once this has been established, the next stage will to apply the findings of these experiments to real world situations such as those found in modern and ancient rift basins. In the future, these forward models can be used to help understand the tectonic processes that may have occurred during synrift deposition.

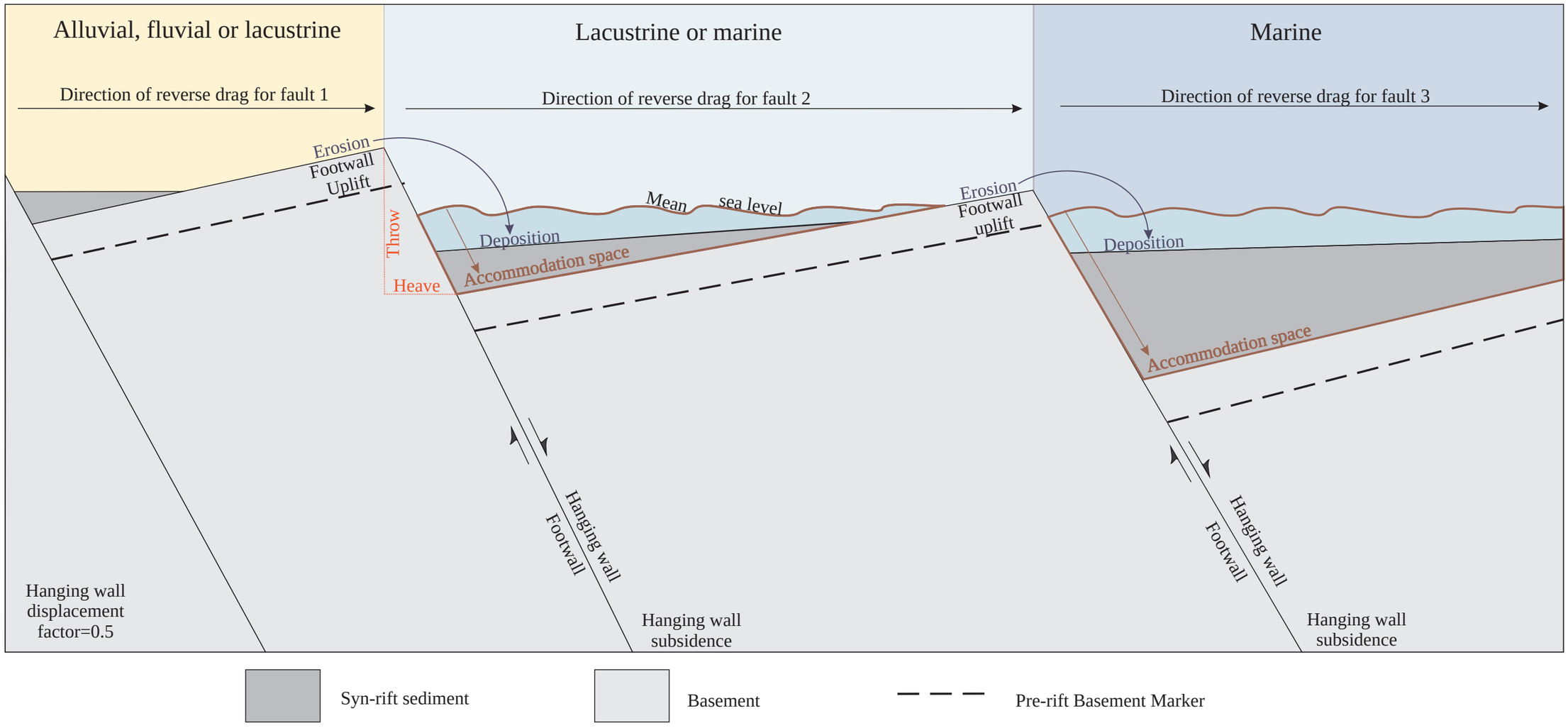

Figure 1.1: A simplified cross section view showing important terminology associated with rotated fault blocks in an extensional setting. As the faults subside accommodation is created, erosion of the footwall can occur, resulting in syn-rift sedimentation. The hanging wall displacement factor in the case of this figure is 0.5 (50% of the displacement goes to the footwall and 50% to the hanging wall side). (Modified from; Leeder & Gawthorpe, 1987, Einsele, 2000; Fossen, 2000; Peacock et al 2000; Twiss & Moore, 2007; Gawthrope & Leeder 2000, Leeder 2012 and sources cited within)

1.2 Objectives

There are four main objectives in this thesis:

1. Evaluate the current understanding of synrift deposits, extensional faulting and the link between the two through a literature evaluation including expected stratigraphic patterns.
2. To develop a series of experiments using Fault Uncertainty Modeling in RMS in order to create a library of 3D synrift sedimentation models. These experiments use a simple, idealized, planar normal fault where modifications are applied to a single fault parameter while the other parameters remain constant. This allows the effect of the single parameter on sediment growth packages to be documented. These experiments also tests the functionality of RMS and show that expected sedimentation patterns can be created.
3. Develop new 3D visualization techniques and styles to display each experiment effectively in RMS.
4. Use fault uncertainty modeling to establish the functional limitations of RMS by carrying out more geologically complex experiments. The aim here is to create models showing the following: fault asymmetry, a relay structure with syn-tectonic sedimentation and finally a model showing multiple faults displacing at different times.
5. Use the fault uncertainty functionality of RMS to model the interaction between growing Gilbert delta and faulting. Sedimentation patterns will be modeled based on literature and field observations of the ancient Vouraikos and Kerinitis Deltas, Gulf of Corinth, Greece (see Ford et al., 2009; Backert et al., 2010).

1.3 Background information and literature review

1.3.1 Normal faulting and synrift sedimentation

The topic of extensional basins is extensive and therefore it is not possible to cover everything in this introduction. A summary of key terms and processes relevant to this thesis are explained in this section.

Extensional basins are composed of faults at the margin and tilted fault block geometries basinward (Figure 1.1; Gibbs, 1984; Leeder and Gawthorpe, 1987; Gawthorpe and Leeder,

2000; Leeder, 2012). Synrift sedimentation and the patterns of sediment accumulation are controlled by a combination of structural and sedimentological factors (Gibbs, 1984; Leeder and Gawthorpe, 1987; Cohen et al., 1995; Gawthorpe and Leeder, 2000; McLeod et al., 2002; Fossen, 2010).

1.3.1.1 Structural factors

The structural factors being considered here include: tectonic subsidence, creation of accommodation space, fault surface length and growth, the faults displacement and reverse drag (Hamblin, 1965; Barnett et al., 1987; Walsh and Watterson, 1988; Gibson et al., 1989; Dawers et al., 1993; Gawthorpe et al., 1994; Gawthorpe and Leeder, 2000; Selley, 2000)**.**

1. In a marine rift system accommodation space is defined as a vertical interval between the seafloor and sea level (Figure 1.1; Einsele, 2000; Selley, 2000). Accommodation space can be affected by a change in sea level (eustasy) or by tectonic subsidence or uplift (Selley, 2000). In extensional rift systems accommodation space generation is controlled primarily by fault block rotation and basin wide (tectonic) subsidence (Leeder and Gawthorpe, 1987; Gawthorpe et al., 1994; Schlische, 1995; Ravnås and Steel, 1998; Gawthorpe and Leeder, 2000; McLeod et al., 2002; Fossen, 2010). Sediment deposition will only occur in marine basins when sufficient accommodation space is present, which allows sediment to deposit (Jervey, 1988; Gawthorpe et al., 1994; Ravnås and Steel, 1998; Selley, 2000; Fossen, 2010). When accommodation is not being generated, there is no place for sediment to deposit and the result is usually erosion (Jervey, 1988). Eustatic changes in sea level are not a consideration in this project. Accommodation is not created uniformly across a faults surface and is greatly influenced by changing fault parameters. (See below for detailed introduction into fault parameters; Gawthorpe and Leeder, 2000).

2. Faults can be described as planes or surfaces which are defined as a largely planar narrow zone in the earth's crust where the rock on one side has moved relative to the other (Twiss and Moores, 2007; Fossen, 2010 and references therein). Fault length is defined as the distance between the faults tips which is often measured on a horizontal plane (Figure 1.2; Scholz and Cowie, 1990; Peacock, 1991; Peacock et al., 2000). Fault displacement refers to the absolute movement on a faults surface relative to surface points that were originally adjacent (Leith, 1923; Peacock et al., 2000). The

A.

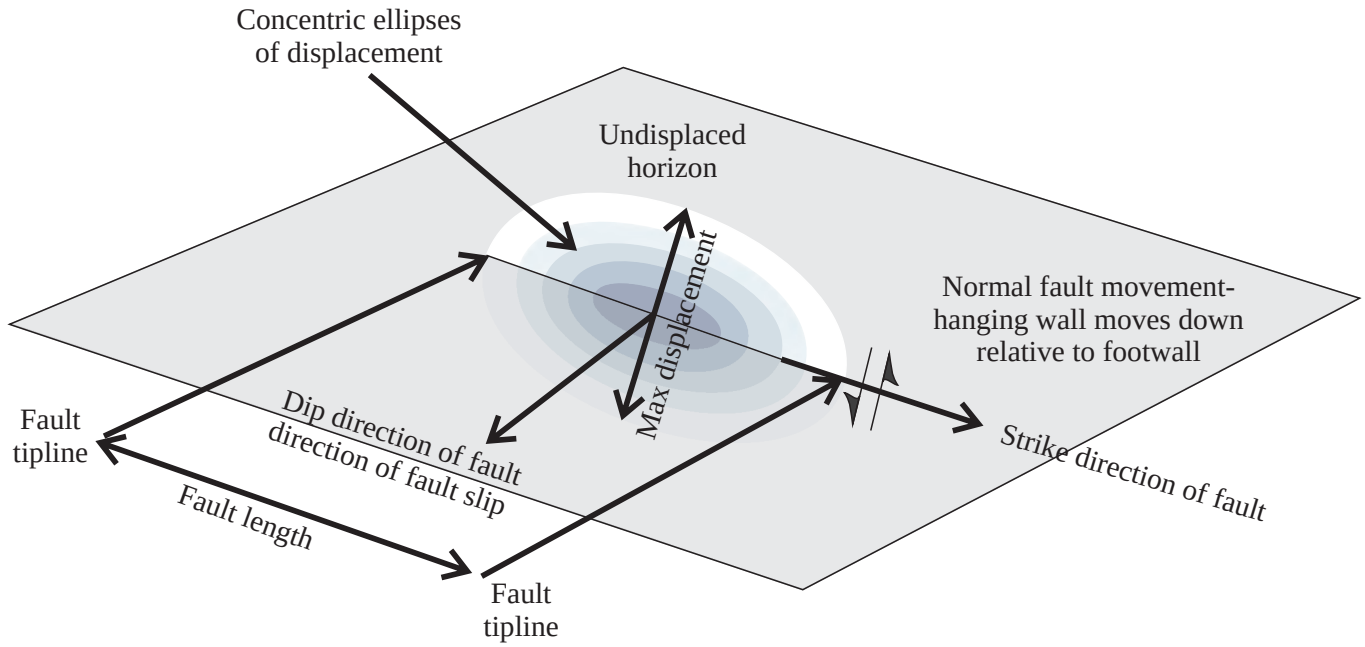

B.

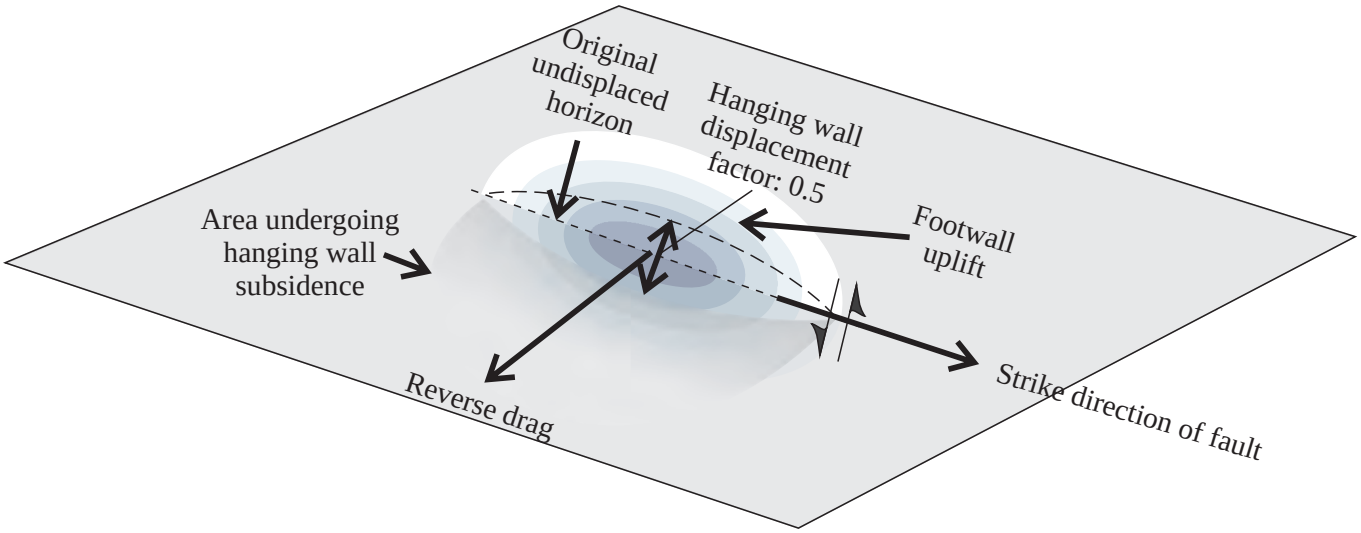

Figure 1.2: Fault terminology figure. A.) A single fault plane showing elliptical displacement field B.) Hanging wall displacement factor is set to 0.5 meaning the displacement is evenly distributed 50% to the hanging wall and 50% to the footwall. (Modified from: Leigh, 1923; Hamblin, 1965; Watterson, 1986; Barnett et al., 1987; Walsh & Watterson, 1988 & 1989; Gibson et al., 1989; Cowie & Scholz, 1992; Peacock, 1991; Gawthrope & Leeder, 2000; Peacock, 2000; Leeder, 2012 and sources cited within)

amount of displacement on a fault surface identified on the host rock often varies laterally and it is at a maximum at the center of the fault and decreases gradually to zero at the fault tipline (Figure 1.2; Barnett et al., 1987). Displacement along the faults length tends to follow a series of concentric elliptical contours (see Figure 1.2A&B; Barnett et al., 1987).

The horizontal length of normal faults is not always constant. Fault growth can be loosely defined as an increase in distance between the faults tiplines and is typical where growth faults are associated with extensional basin development (Walsh and Watterson, 1987; Gawthorpe and Leeder, 2000). Changes in fault length and normal fault interactions are often associated with the complex evolution of extensional basins (Walsh and Watterson, 1987; Gawthorpe and Leeder, 2000; Leeder, 2012). Gawthorpe & Leeder (2000) describe the evolution of a normal fault array occurring in three prominent stages:

- The initiation phase is characterized by numerous faults with small displacements, each with its own isolated depocentre (Gawthorpe and Leeder, 2000; Leeder, 2012).
- The interaction and linkage phase refers to fault growth, the linking of faults and the formation of structures linked to fault interaction which in this case are relay structures, a type of overlap structure (Childs et al., 1995; Gawthorpe and Leeder, 2000; Leeder, 2012).
- The throughgoing fault zone refers to the localization of major fault zones, the formation of these large faults can give rise to basin bounding half graben and graben faults.

3. Reverse drag was originally identified by Powell (1874) but was first defined in the modern day literature by Hamblin (1965) as the downward bending associated with normal faulting. The reverse drag dimension is defined as the point where the gradual decrease in down bending reaches zero (Figure 1.1, 1.2) and can increase or decrease with each phase of fault displacement and fault growth (Hamblin, 1965). Hamblin (1965) and Gibson (1989) also concluded that the magnitude of reverse drag for each major fault displacement is roughly proportional to the amount of displacement on the fault during the displacement event. Subsequent studies showed that reverse drag decreases systematically normal to the fault and that the changes in dips associated with the reverse drag of normal faults will increase as fault length increases (Barnett

et al., 1987). In faults less than 1km long, reverse drag affects dips by less than 5%, whereas in seismic scale faults reverse drag has a much greater effect on dips (Barnett et al., 1987). There is very little specific information available to quantify the value of reverse drag relative to the fault length or displacement amount. For this reason a reverse drag of approximately half the fault length was used. Whether or not the reverse drag remains constant in these models is more important than the actual reverse drag distance itself.

1.3.1.2 Modeling terms

Two specific terms need to be introduced in order to complete the modeling of more geologically complex environments:

1. **Relay structure**

A relay structure is a type of fault overlap that forms in an extensional regime during a normal fault growth phase (Peacock and Sanderson, 1991, 1994; Gawthorpe and Leeder, 2000; Peacock, 2002; Leeder, 2012). Relay structures were originally referred to as fault bridges (Ramsey and Huber, 1980) and transfer zones (Chadwick, 1986), before Larson (1988) introduced the modern term. In order for a relay to form, fault growth must occur between two sub parallel faults (Figure 1.3; Childs et al., 2002, 1995; Gawthorpe & Leeder, 2000; Peacock, 2002). Once the fault tips overlap, a relay ramp forms to connect faults in the intervening zone (Figure 1.3B; Chadwick, 1986; Larsen, 1988; Peacock and Sanderson, 1994; Gupta et al., 1999; Peacock, 2002; Gawthorpe et al., 2003). This evolution is consistent with what Gawthorpe & Leeder (2000) described in their "evolutionary stages" of a normal fault under the fault interaction and linkage stage. As the faults continue to grow and as displacement increases, the ramp will continue to rotate and shear strain accumulates (Figure 1.3C; Peacock and Sanderson, 1994; Long and Imber, 2011). The overlapping segments of the faults exhibit a very specific form of displacement (Figure 1.3C2) where the displacement sum of the overlapping faults is equal to the displacement of a single fault (Peacock and Sanderson, 1991; Childs et al., 1995; Walsh et al., 2003; Long and Imber, 2011). The ramp eventually reaches a point of maximum shear strain and begins to fracture/fault or breach, which alters the shape of the relay and its subsequent sediment infill patterns. (Figure 1.3D; Childs et al., 1995; Athmer and Luthi, 2011; Conneally et al., 2014).

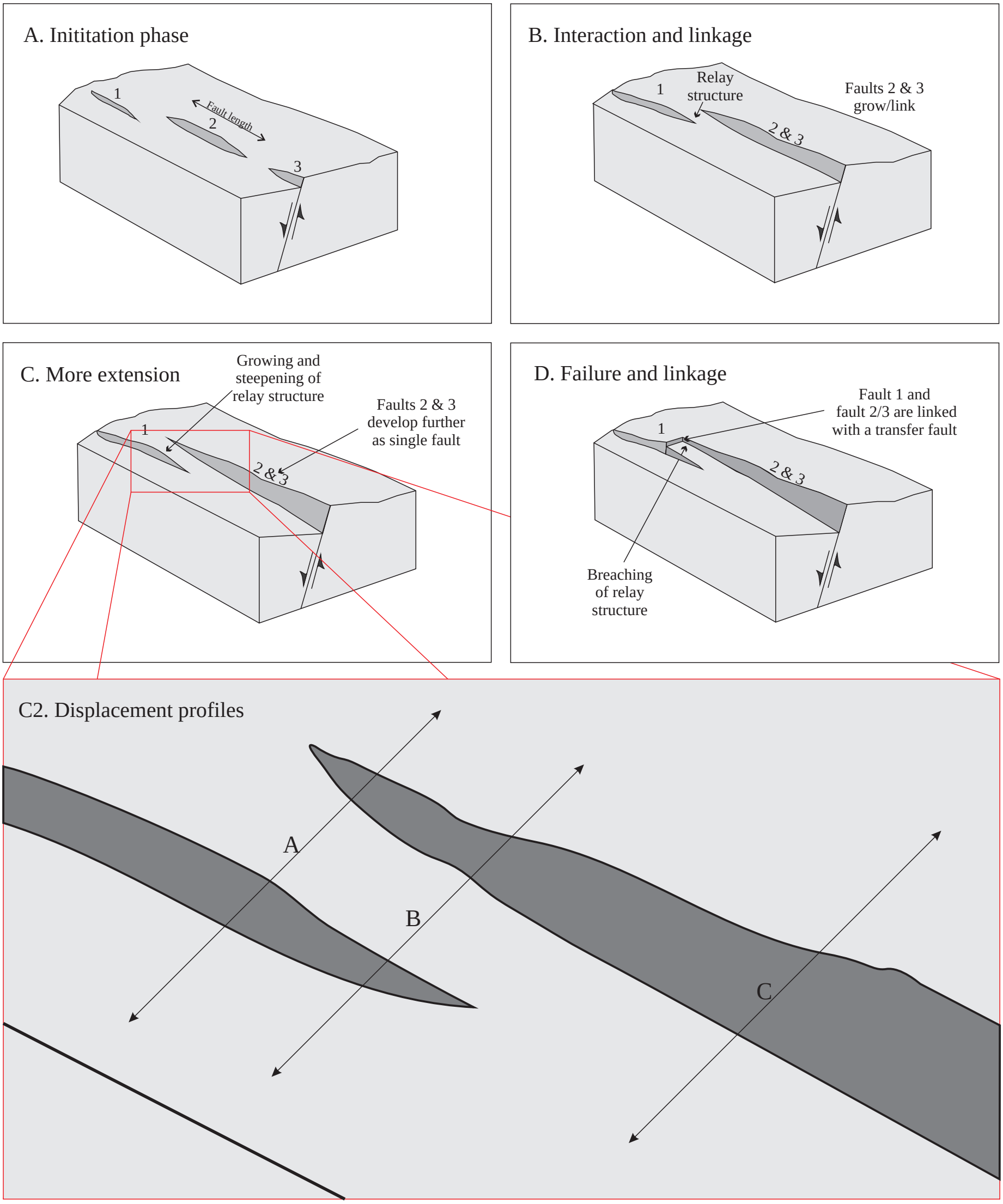

Figure 1.3: Simplified normal fault evolution in an extensional basin. A. The initiation stage of three normal faults in an extensional basin. At this point the faults are independent. B. Phase of interaction and linkage is where extension develops further which increases fault displacement amount and promotes fault growth. The result is the formation of a relay ramp (or other overlap structure) between 1&2, and the linking of faults 2&3. C. The further development of relay ramp (growth and steepening) and associated faults as well as the increase in displacement and fault length of Faults 2&3.D. The final phase of development where the relay ramp breaches causing the formation of a transfer fault between the final two faults. C2: The displacement profiles in a relay ramp suggest that the total amount of displacement A=B=C'. Refer to references for further information. This figure was modified and created from: Peacock & Sanderson, 1991, 1994; Gawthorpe & Leeder, 2000; Trudgill, 2002; Athmer & Luthi, 2011; Long & Imber, 2011; Leeder, 2012 and sources cited within.

Relay structures can be important conduits for synrift sediment transport and subsequent accumulation because they form topographic lows along basin margins (Gupta et al., 1998). An in depth analysis of relay structure sedimentation was completed by Athmer and Luthi (2011) which involved in detail the sediment transfer pathways associated with basin evolution. The modeling of a basic relay structure in this thesis will help to create a simplified understanding of associated sediment accumulation patterns in a scenario where sedimentation rate is equal to, or greater than fault displacement rates.

Relay structures are often associated with petroleum systems, thus an understanding of their formation and evolution is crucial. For example the Late Cretaceous Lysing Formation of the Norwegian North Sea is deposited east of the Vøring Basin in a structurally complex assemblage of submarine terraces (Nordland and Dønna), ridges (Træna) and relay ramps (Fugelli and Olsen, 2007; Athmer and Luthi, 2011a).

2. Gilbert fan deltas

A fan delta is defined as a type of alluvial fan deposit (a cone or fan shaped sediment accumulation deposited from a higher altitude to a lower altitude from a single point source) in a subaqueous environment (Holmes, 1965; Nemec and Steel, 1988; Leeder, 2012). A Gilbert delta (first described by Gilbert in 1885) is a type of delta that forms when a river system meets a body of water (lacustrine or marine) and where there are steep gradients and large amounts of accommodation space being generated in the body of water (Gilbert, 1885; Leeder, 2012; Gobo, 2014). Gilbert deltas are identified and comprised of three main sedimentologically significant facies types; low angle topsets, high angle foresets (up to 35°) and low angle bottom sets (Ford et al., 2009; Leeder, 2012; Gobo, 2014).

In the modeling of Gilbert type fan deltas, field observations from the Vouraikos and Kerinitis ancient deltas (Gulf of Corinth, Greece) were used (Ford et al., 2009; Backert et al., 2010). The Gulf of Corinth deltas vary in size (radius) from approximately 3-8km and can reach thicknesses up to 900m (Ford et al., 2009). The Vouraikos delta is sourced from the south, progrades northward and lies in the hanging wall of the Mamoussia-Pirgaki (MP) fault. The MP fault dips approximately ~55° and the delta's topsets, foresets and bottom sets have sub-horizontal dips, 10-35° and 5-10° dips respectively (Ford et al., 2009). The Kerinitis delta is deposited in the hanging wall of the MP Fault and the foresets dip ~25° (Backert et al., 2010). These deltas are separated on the MP fault by the

Kerinitis fault (Ford et al., 2009; Backert et al., 2010). These deltas were chosen because of the consistent source and propagation directions through the deltas evolution, making them the least sedimentologically and structurally complex of the Corinth deltas. For the purposes of this study, the delta will be modeled considering the dip values for both field locations where topset dips will vary between 0-10°, the foresets will range from 20-30° and the bottomsets 5-10°. The dip of the fault will be modeled at approximately 55° (Ford et al., 2009). A prograding succession of deltaic deposits will also be incorporated into the modeling for this experiment. These deposits will be modeled as largely cone shaped structures, where the tip of the cone is flattened at the shoreline position (similarly to Gilbert delta formation in Greece; Ford et al., 2009; Backert et al., 2010).

Gilbert deltas are a very specific delta type and although more rare than classic fluvial deltas, are responsible for the formation of petroleum reservoirs. This linkage means it is important to understand the structural and sedimentological evolution of these environments. As an example the North Sea's Oseberg Field is currently producing from Gilbert delta reservoirs of the Oseberg Formation (Ravnås and Steel, 1998).

1.3.1.3 Factors effecting sedimentation

The style of sedimentation in rift zones is dependent on the relative rates of sediment supply, accommodation space generation (i.e. faulting) and the sedimentary environment (Leeder and Gawthorpe, 1987; Ravnås and Steel, 1998).

1. **Sedimentation rate** is defined as the amount of sediment deposited per time and is a major control on the architecture of synrift sedimentation (Leeder and Gawthorpe, 1987; Ravnås and Steel, 1998; Ravnås et al., 2000). Synrift sedimentation rates are discussed in relation to fault displacement in the following contexts:
    - Sedimentation Rate > Fault Displacement: These conditions allow accommodation space to be completely filled with sediment and therefore preserve a complete record of fault growth history but not sedimentation history (Childs et al., 1993, 1995; Nicol et al., 1997). This is the case that will be applied to almost all of the synthetic models in this report (Experiments 1-9) to understand the effect fault growth has on the sediment distribution and thickness.
    - Sedimentation Rate < Fault Displacement: In this example the accommodation space does not infill with sediment and the result cannot be used to fully

understand the fault displacement over time. These conditions can be used to describe the real world experiment based on the modeling of the Gilbert delta (Experiment 10).

2. **Sedimentary environment:** The sedimentary environment controls the distribution of facies/sediment type in the synrift sediments (Selley, 2000). Gawthorpe and Leeder (2000) discuss how changes in the depositional environment influences the type of synrift deposition in an evolving normal fault array. Although this parameter is very important to reservoir characterization and facies distribution, the models produced here only consider the sedimentation rate in relation to the rate of fault displacement and not facies distribution or changes in sedimentary environment. Additionally as discussed in section 1.3.1, only the changes of accommodation space caused by tectonic events are being considered and not eustatic changes in sea level.

1.3.2 Fault modeling literature review

Gibson (1989) modeled planar faults in order to investigate the effect of changing the displacement controlling parameters and to generate synthetic horizon contours.

Syahrul (2014) was the first to use the RMS software outside its intended functionality for the purpose of forward modeling of synrift deposits. The workflow used in Syahrul's (2014) paper was analyzed and altered in order to better model the experiments highlighted in this thesis. Syahrul (2014) used a simple workflow that contained fault modeling, fault displacement estimation, horizon modeling, horizon extraction and structural modeling. Syahrul's (2014) experiments involved modeling the Kerpini fault block as it is today, and did not incorporate any structural evolution. The modeling was completed by applying changes to the fault length through the manipulation of the displacement point set where the displacement points followed an unnatural triangular shape. The correction range (reverse drag) is altered in horizon modeling. The modeling workflow explained how to create a single structural model that was the final phase of displacement but did not explain the integration of multiple displaced horizons into one horizon model or make use of a 3D grid. Although Syahrul's (2014) workflow did not integrate displaced horizons or 3D grids, it serves as an excellent starting point for designing the workflows in this study.

1.3.3 Introduction to RMS

The history of the RMS software begins with the first fault modeling software Havana, a research software developed in the late 1990's (see Hollund and Mostad, 2002). Havana was the first software designed for modeling subseismic scale faults and combined a unique functionality to allow the displacement of surfaces and 3D grids (Hollund and Mostad, 2002). In 2000, Havana developed techniques for structural uncertainty modeling which allowed the user to apply displacement functions to normal faults and change horizon positions (Hollund and Mostad, 2002). In 2013, Havana's technologies were integrated into RMS, Roxar's reservoir modeling software.

RMS is an integrated reservoir modeling software that uses workflow driven modeling techniques to provide the user with increased understanding of the petroleum system from production and economical perspectives (Roxar, 2014). The 2013 version of RMS introduced structural uncertainty modeling, which is comprised of two main functionalities: horizon modeling and fault uncertainty modeling. Horizon modeling integrates horizon input data and uses stochastic modeling techniques to simulate a range of possible modeling outcomes of depth surfaces which lie within the limits of uncertainty (Roxar, 2014). RMS' fault uncertainty modeling allows uncertainty to be applied to the faults position, dip, strike, throw and the input of uncertainty to be quantified. The cross cutting relationships of faults can be adjusted in this new version of RMS and furthermore, the integration of horizon and fault data is possible. A fault displacement estimation job applies a throw attribute point set to the structural model.

RMS is also capable of creating 3D grids, which converts the zones, surfaces and fault data from a horizon model into a 3D grid using user defined cell dimensions. Grids are used to represent the shape and volume of a reservoir and form the input for reservoir simulation. Grids can also be populated with geological rock types (facies) and sedimentary configurations. The facies can then be infilled with petrophysical properties to produce realistic models that can be used for volume calculations and more geologically realistic reservoir simulation.

Although the new displacement function was not designed for the purposes of this thesis, it is utilized to model surface displacement and infill with new surfaces to mimic the development of a faulted half graben being filled with sediment. Syahrul (2014) was the first to extend the functionality of RMS to generate synthetic structural models. The workflows that Syahrul

(2014) created were used as a baseline and were further developed to model the effects that changing fault parameters have on synrift sedimentary fill patterns.

Chapter 2

Data and methodology

2.1 Introduction

The objective of this project is to build a series of models to show realistic synrift sedimentation geometries. This will be accomplished using the new structural uncertainty functionality in RMS 2013. There will be a total of ten experiments in this report. Experiments 1-7 are run to establish a new efficient workflow and to test the functionality of RMS. The results of these experiments will be used to discover whether RMS can produce results that are representative of real world structural processes. Experiments 8-10 are more complex models including a relay structure, the interactions of multiple faults (where all faults show alternate displacement sequences) and a Gilbert delta. The delta is modeled using cone shaped deposition features as prograding sedimentary packages. Table 2.1 shows a complete list of experiments.

2.2 The basics of modeling

The basic modeling concept (Figure 2.1) behind synrift sedimentation found in experiments 1-9 is derived using the following steps:

1. A flat horizontal surface is introduced to represent the pre-faulting state of a synrift sedimentary basin (i.e. top prerift). The flat surfaces are input into RMS as points where all Z (depth) values are the same.
2. The flat horizontal surface is displaced by a fault, which elevates the footwall and subsides the hanging wall. The fault was uploaded as points with varying X, Y and Z values in order to construct dipping planar faults (in these experiments the faults dip approximately 55°).
3. A new flat horizontal surface is introduced to the hanging wall and represents the half graben fill. The same surface follows the initial displaced surface in the footwall.

	Fault parameters (All parameters change with time/A-E)		
Experiments	Fault displacement	Fault length	Reverse drag
1	Constant	Constant	Constant
2	Constant	Constant	Decreases
3	Constant	Constant	Increases
4	Constant	Increases	Constant
5	Increases	Constant	Constant
6	Decreases	Constant	Constant
7	Asymmetric	Constant	Constant
8	Fault relay structure		
9	Multiple faults		
10	Gilbert delta		

Table 2.1: List of experiments

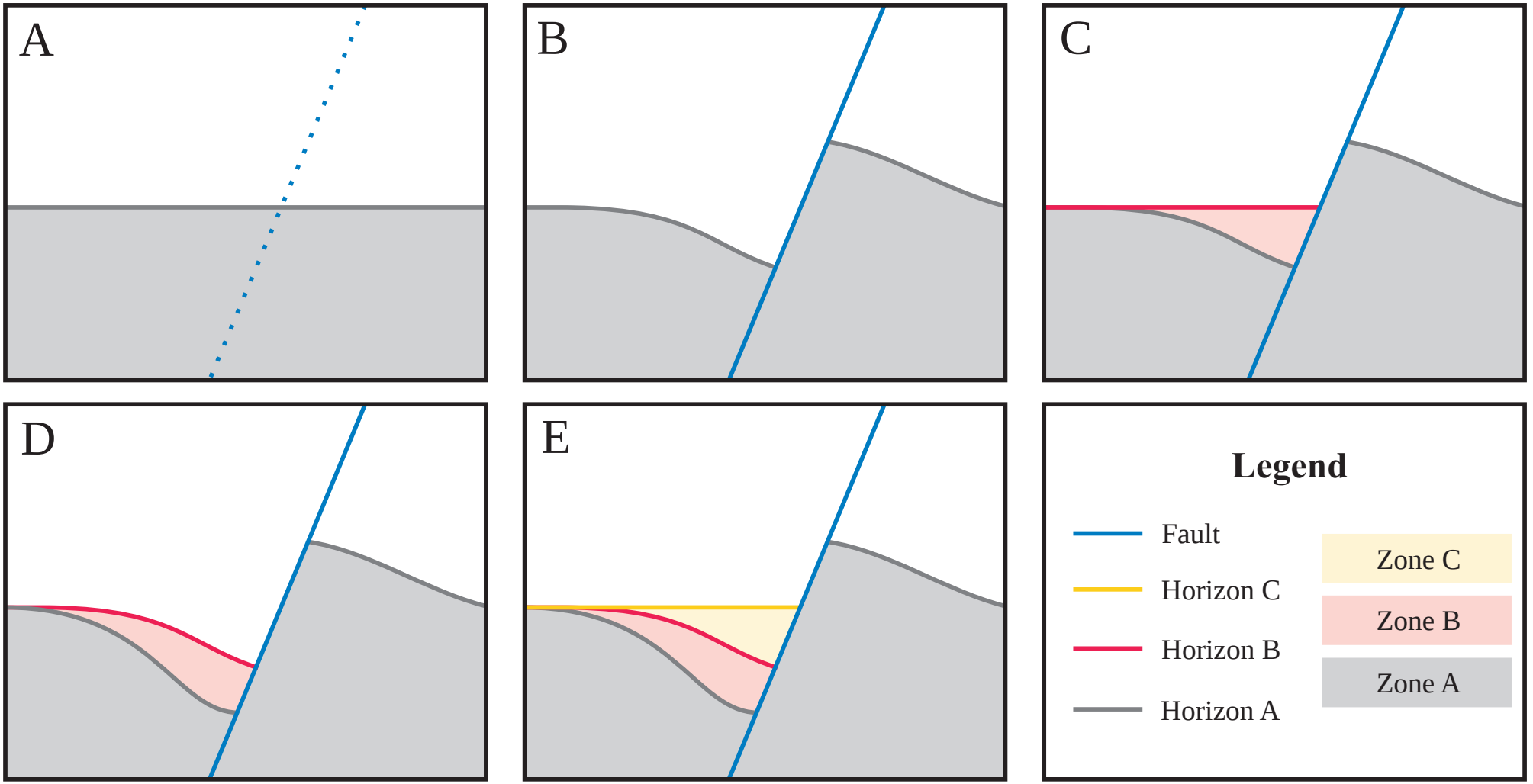

Figure 2.1: The basics of modeling. A.) Introduction of a flat horizontal surface which represents the top of the pre rift sediment. (Horizon A). B.) The flat surface is displaced by a fault where the footwall is elevated and the hanging wall subsides. C.) A new flat surface is introduced (Horizon B) which represents syn-rift fill. D.) The two surfaces are displaced again by the fault. E.) Another flat surface is introduced to fill in the new depression. Steps A-E are repeated multiple times to achieve syn-rift sedimentation in a half graben.

4. The two surfaces (displaced and flat) are then displaced creating a second depression on the hanging wall side (and an increased uplift on the footwall side).
5. Another flat horizontal surface is introduced to fill in the new depression and represents a second phase of half graben fill.
6. These steps are repeated several times to achieve a synrift fill of a developing half graben.

2.3 RMS and structural uncertainty modeling

2.3.1 Introduction to RMS terminology

RMS can be used to model synrift sediment packages through the non-standard use of its modeling processes and functionalities (Syahrul, 2014). Modeling processes are the in-built steps that are used to create 3D geomodels. Functionalities are changes that can be applied to the outputs from the modeling processes to manipulate the data (e.g. the use of a calculator, surface-surface operations etc.).

The modeling processes used to create the basic modeling discussed in Section 2.2 are as follows:

- **Stratigraphic framework setup:** Where the order of horizon deposition is specified.
- **Horizon mapping:** Used in all experiments after horizon data points are imported into RMS, this process is applied to create a contour map/surface from the points.
- **Fault modeling:** Used in all experiments to create a plane from uploaded fault points. This process is also used where the visualization of the fault grid is defined. At this point the fault is just a plane and does not have any displacement information associated with it.
- **Structural model:** This process is created by generating a fault model and is changed for every phase of displacement in the experiment. The structural model contains all data associated with the fault model and can contain any number of horizon models. If the fault model changes, it is necessary for a new structural model to be generated.

- **Fault displacement:** This modeling process is where displacement is linked to the fault surface created in the previous step. The input source for applying displacement can be set to either maximum throw or attributes (uploaded by the user).
    a. When the fault displacement is set to max 'throw' a single input value is applied at the faults center and a gradual but constant decrease in displacement is automatically applied towards the tiplines of the fault.
    b. Attributes are a user-defined point or set of points that allow the fault to be displaced to a depth of choice. In this thesis, only attributes (or displacement point sets) were used to displace faults and were uploaded as a series of points placed laterally across the faults center line at the same depth as any flat horizon to undergo displacement. The point sets (with an X, Y, Z and displacement value) have approximately 200m separation across the middle of the fault plane. There is one point set for each displaced horizon in every experiment.

  Another function of this process is the application of the hanging wall displacement fraction, a value of 0.5 for this parameter allows the displacement to be divided equally between the hanging wall and footwall for all experiments (apart from Experiment 10). When the hanging wall displacement factor is set to 1.0, all displacement is applied to the hanging wall side; when it is set to 0, all displacement is applied to the footwall side as uplift. The variogram range (smooths displacement factor), length/height ratio (estimation of fault tipline) and length/displacement ratio (estimation of fault length with respect to the faults ellipses) can also be manipulated. However these parameters were all set to the RMS default values in experiments 1-9 as preliminary experiments showed that they had no impact on the way these models were generated (Barnett et al., 1987; Peacock et al., 2000; Roxar, 2013).
- **Horizon modeling:** This process integrates horizon data (the surfaces produced in the horizon mapping process) with the fault model. Firstly the stratigraphy that will undergo horizon modeling must be selected (i.e. Horizon A, B etc.) along with the input source for this framework (mapped surfaces from horizon mapping process or extracted horizons from previous

horizon models). The application of reverse drag can be found on the modeling section of this process (correction range), where the input number is the value in meters of the envelope around the fault where the horizon is displaced. In the event of a horizon undergoing displacement, fault displacement must be selected. Other user-defined parameters were left as default values because they had no impact on preliminary tests. Horizon modeling was used for three separate occasions:

1. The displacement of single surfaces.
2. The modeling of flat horizontal surfaces.
3. Horizon modeling of all extracted surfaces (displaced and flat).

- **Create grid:** All data in a single horizon model can have a 3D grid applied which subdivides the data into cells of specified size. The cell sizes are modified in the X, Y and Z directions. There are two options when it comes to the cells associated with the fault; a pillar fault and a stair-stepped fault. In a pillar fault, the cells edge follows the same gradient as the fault surface and the gradient can be altered by moving the pillar adjustment percentage to a chosen value. Stair-stepped faults divide the slope across a series of cells of a constant width and cannot be adjusted in the same way. In experiments 1-9, the RMS default fault setting of pillar faults was used where no pillar adjustment percentage was applied. In Experiment 10 a pillar adjustment fault was used with an adjustment percentage of ~40% in order to avoid problems of the zones creeping up the fault surface.

The extract horizons, and grid parameter functionalities are used in all experiments, whereas the surface-surface operation is only used in the Gilbert delta experiment.

- **Extract horizons/isochores:** All data contained in a horizon model can be exported to be reused in another horizon model as horizons, horizon points or isochores.
- **Surface-surface operation:** These functions allow for surfaces to be mathematically altered, made equal to or eliminated relative to another chosen surface. This process is important during the modeling of the Gilbert delta, but was not used in the modeling of simplified synrift sedimentation.
- **Grid index parameter utility:** This utility or function is applied to the grid separately and allows the grids cells to be compartmentalized into various

index parameter types. For the purposes of this report only zone filters were applied to allow the grid to be coloured based on zone, and in some cases a fault block filter was applied in order to avoid unwanted thin cells on the footwall side.

- **Grid geometry parameter utility:** This utility or function is applied to the grid separately and allows the grids cells to be compartmentalized into various geometric parameters. For the purposes of this report only a Z cell thickness filter was applied to filter out unwanted thin cells from outside of the area of deformation to simplify visualization of the data.

2.3.2 Data storage in RMS

An understanding of data storage in RMS is essential for designing the most effective experiments. The easiest way to manage displacement phases is to separate each displacement event into a single structural model (structural model 1= displacement phase 1 etc.). Once data are input into RMS horizon and fault folders, they are ready to be manipulated or displaced. RMS cannot displace more than one horizon at a time in a single horizon model so each structural model contains nested workflows to allow the displacement of each horizon separately. A nested workflow allows for a smaller workflow to be run as a part of a larger workflow in RMS. The resulting data remain in the horizon model and cannot be used elsewhere until they are exported back into the original fault and horizon folders. Once the data are extracted back to the original folder it can be used as an in input for any modeling process or functionality in RMS. This extraction functionality is very important in the final horizon modeling job of each structural model because this is where all displaced horizons are combined into a single horizon model.

2.3.3 Workflow Manager

The workflow manager in RMS is where individual modeling processes and functionalities are combined into an automated list as jobs to simplify the entire structural modeling process (Figure 2.2). Workflows allow parameters in each job to be easily manipulated without having to individually run each manually and they allow for the establishment of a standardized modeling procedure. For all experiments in this report, each phase of

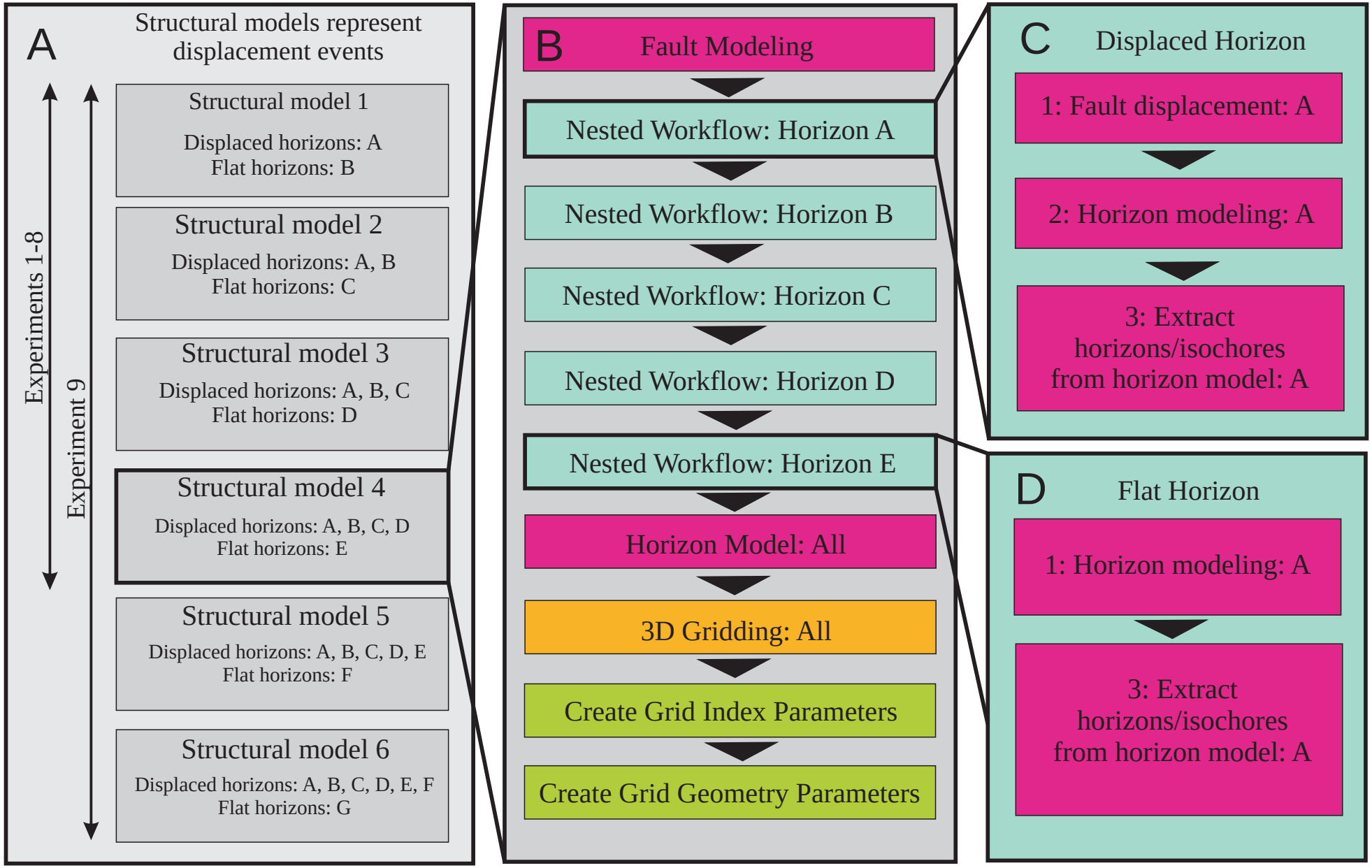

Figure 2.2: Workflow interaction diagram. A.) Structural models represent each phase of displacement in the experiment. B.) An example from experiment 1 of a workflow from structural model 4 (fourth displacement phase) where horizons A, B, C and D are displaced and E is flat. C.) Nested workflow from horizon A. D.) Nested workflow from horizon E.

displacement has its own structural model and workflow. For each phase of fault displacement/structural model, there is a separate workflow containing the following jobs (Figure 2.2, 2.3):

- **Fault model:** Models points into a plane specific to the structural model of choice (Figure 2.2B, 2.3A).
- **Nested workflows:** This functionality of RMS allows for one workflow (X) to be integrated into another larger workflow (Y) as a separate single job. The nested workflow for Displaced Horizons contains three separate jobs (Figure 2.2C):
    - Fault displacement: This job allows for the integration of the fault surface (fault modeling job) and the fault displacement point set. Figure 2.3 shows an example of four horizons undergoing displacement. Horizon D is the youngest and undergoes X meters of displacement, C undergoes 2Xm, B 3Xm and A 4X m.
    - Horizon modeling: The horizon model contained in the nested workflow is where the displacement point set data from the previous fault displacement step is combined with the fault model to displace a single horizon. Figure 2.3B shows the results of the horizon model from nested workflow A, where a displacement point set amount of 4X m was applied. Figure 2.3 C-E are the results from nested workflows B-D.
    - Extract horizons/isochores: The displaced and flat horizontal horizon modeling results from each nested workflow are extracted for later use.
- **Nested workflow for flat horizontal horizons contains two separate jobs** (Figure 2.2D):
    - Horizon Modeling: As this horizon remains flat, this horizon modeling job is responsible for integrating the horizon data with the fault location where the fault displacement is turned off (Figure 2.3F).
    - Extract Horizons/isochores: The result of the horizon model is extracted for later use.
- **Horizon model all:** This job is where all extracted horizons from the nested workflows are combined into one model. The extracted horizons are chosen as the input for this model but as they have already been displaced the fault displacement is switched off. The horizons can only be converted into a 3D grid if they are all contained in a single horizon model. The resulting objects in this horizon model are

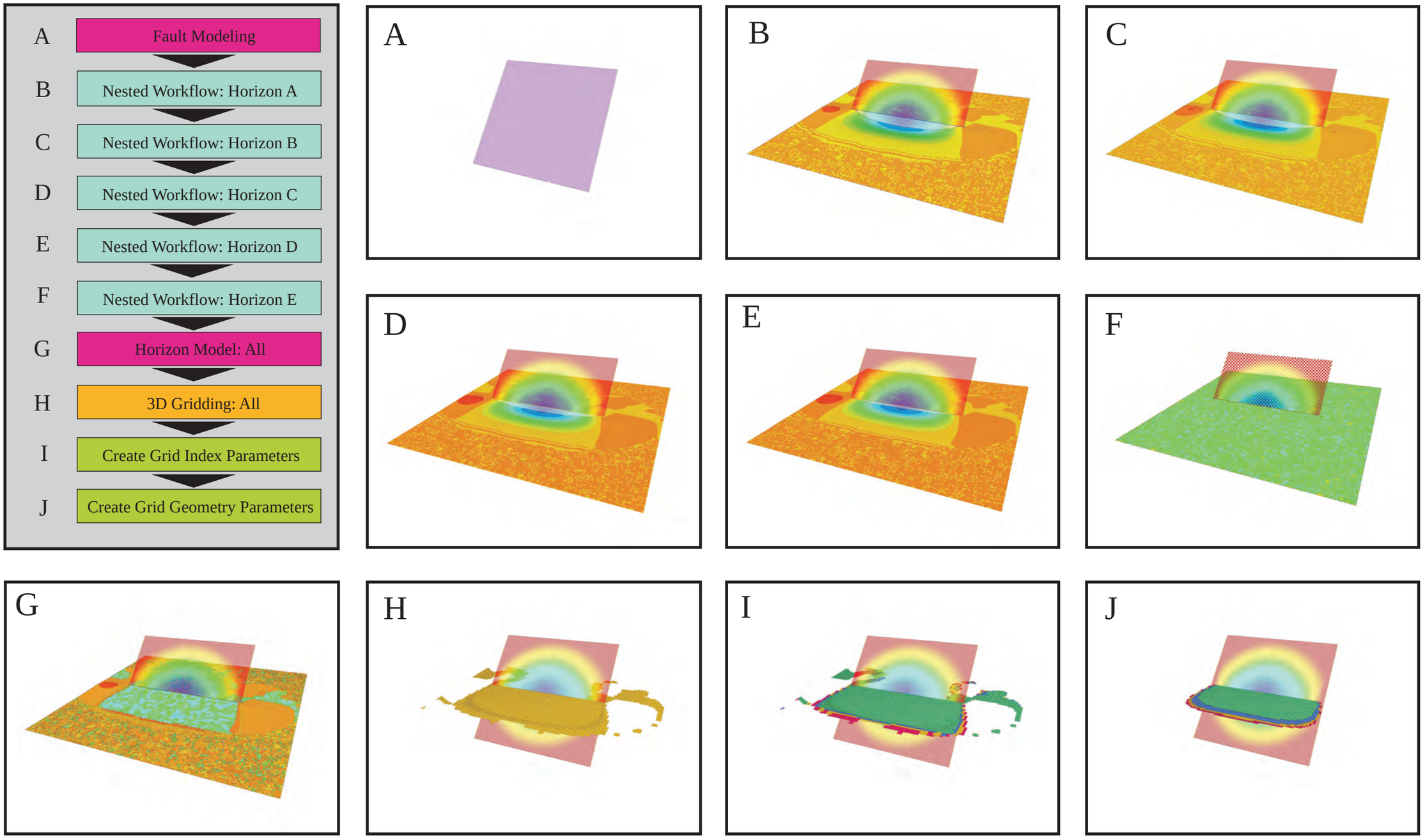

Figure 2.3: An example of a standard workflow (the fourth displacement in experiments 1-7) where four horizons are displaced and one remains flat. Pictures A-J are the resulting data from each job in the workflow. A.) The fault surface is derived from the four points imported in the setup phase. B.) The nested workflow applies displacement attribute to the fault making these deformation ellipses on the fault surface, the horizon A is displaced. C.) Fault containing displacement ellipses and horizon B is displaced. D.) Fault containing displacement ellipses and horizon C is displaced. E.) Fault containing displacement ellipses and horizon D is displaced. F.) No displacement is applied to horizon E so it remains flat. G.) The horizon model containing all exported data from the five nested workflows. H.) A grid is generated from the zones created in the previous horizon model. I.) Grid index parameters are applied so grid zones can be displayed. J.) Grid geometry parameters are applied so unwanted Z Cells can be filtered by thickness.

all displaced horizon contour maps, a flat surface contour map, the zones between the horizons, the faults and fault block division. The results of the horizon contour maps from this job are found in Figure 2.3G.

- **3D gridding:** The data from the horizon model all job is then converted to a grid where the size of the grid cells is user defined (Figure 2.3H)
- **Grid geometry parameters:** This job is applied to divide the grid into separate geometry parameters. For the purposes of this report, the Z cell thickness parameter was used to filter out unwanted cells that fall outside of the area of fault displacement.
- **Grid index parameters:** This job is applied to divide the grid into separate index parameters. For the purposes of this report the grid had a zone parameter that was used to display the grid by zone colour. The fault block parameter was applied to the grid where grid cells are divided up by their location, either on the hanging wall or footwall side of the fault. This fault block parameter was used to filter out cells that appear on the footwall side of the fault in some experiments because it was the simplest way to remove unwanted cells without losing important cell data from elsewhere in the model.

2.3.4 Data labeling system

The structural models in each experiment represent phases of displacement and are numbered sequentially starting with 1 where experiments 1-8 had a total of four structural models, experiment 9 had six and experiment 10 had two.

Horizons were labeled in a reverse sequential order starting with A as the oldest, where the younging direction continued through the stratigraphy alphabetically. This naming scheme is chosen because the total number of horizons in each experiment is not constant, leaving some room to add more horizons.

Nested workflows and horizon models are named according to the horizon(s) used as an input. If Horizon A is input the labels were: Nested workflow A and horizon model A.

In RMS, zones are defined as the volume between two horizons and are named according to the youngest horizon. For example, the zone between horizon A and B is named zone B. As there is no zone immediately beneath horizon A, experiments 1-9 all began with zone B. Experiment 10 did have a zone A as a prerift base horizon was introduced. The zones follow

the same reverse sequence as the horizons, where B is the oldest and the rest of the zones follow alphabetically.

Displacement point sets are labeled based on the structural model and the horizon undergoing displacement. For example 1A is the displacement point set for horizon A in structural model 1.

2.4 Basic model setup

2.4.1 Input fault and horizon data

To begin all experiments, the fault and horizon data is imported into RMS as a series of points (each with X, Y and Z coordinates). The point sets are first created in Microsoft Excel and are imported into RMS as a series of points that define the corners of the surface. The data can either be imported as a .txt file or copied directly from the Excel file into a created point file. These points are gridded into surfaces using Horizon Mapping after which they can be used as input into the modeling processes. All models are synthetically generated using planar fault surfaces to displace horizontal flat horizons. The input data for all experiments can be found in Appendix 1.

2.4.2 Fault displacement data

Fault displacement is applied in two modeling processes: the fault modeling process and the fault displacement estimation process. Firstly the fault(s) points are changed into a surface(s) by applying fault modeling. The fault surface resolution can also be changed here with increased resolution improving the visualization of fault displacement ellipses.

The fault displacement point set is used as the input for the fault displacement estimation modeling process, where the desired point set can be selected from a drop down list. The point set file is set up where the first line reads “Float maxthrow” then, each line after that is four numbers separated by spaces, where column one represents the x coordinate, two is the Y, three is the Z and four is the displacement value. These files are imported as new fault data by selecting the format option “internal points format text” on the RMS import window. Excel was used in a iterative process to manipulate the point sets for each experiment, then the data was copied to the original imported file. Figure 2.4 shows graphs of each horizon model’s point set data.

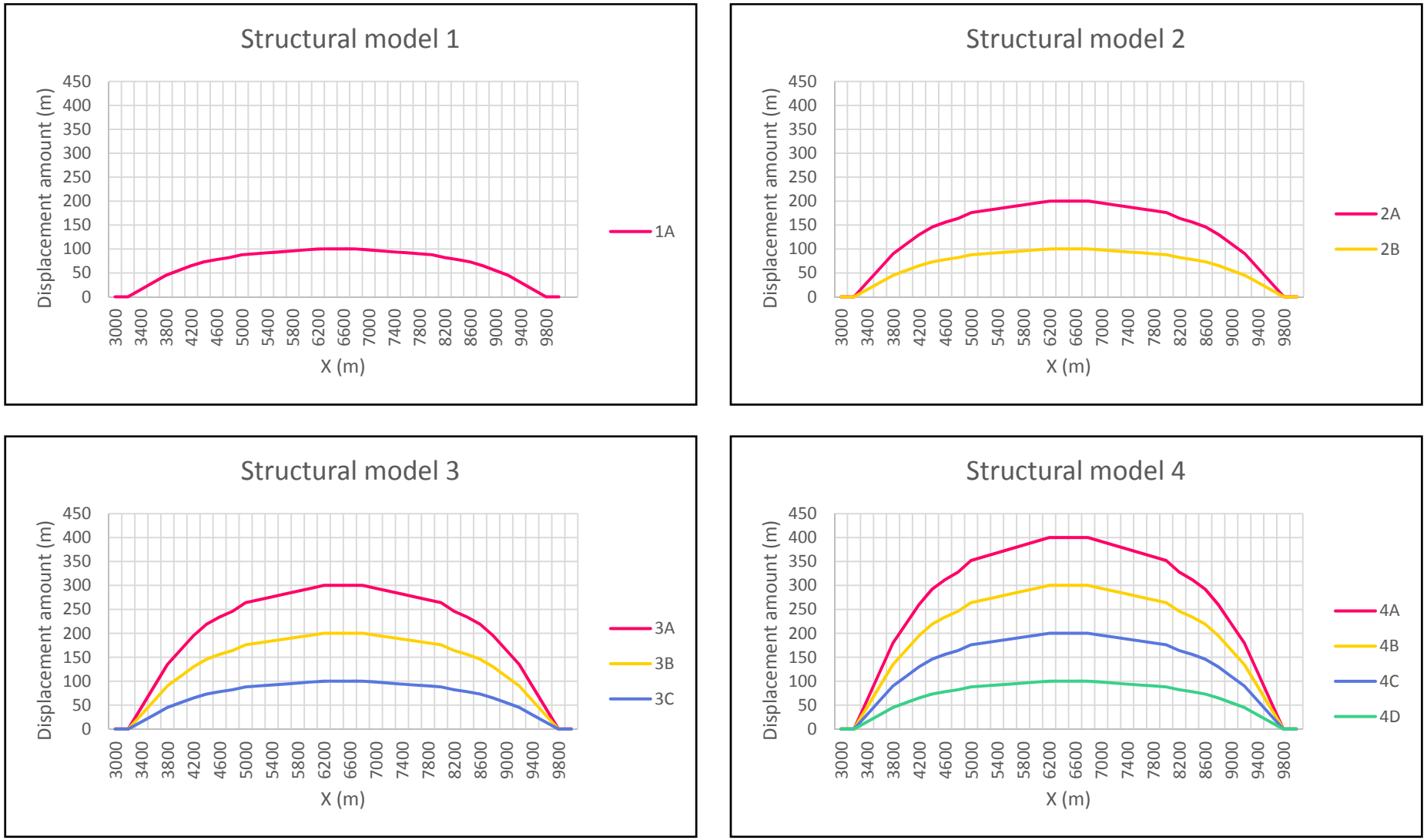

Figure 2.4: Graphs displaying the displacement attribute data for Experiment 1. Each graph shows the attribute data for each horizon in the structural model.

In general the displacement point sets were created to resemble patterns occurring in actual faults, where the point of maximum displacement lies at the center of the fault and displacement gradually decreases to zero towards the tiplines (Barnett et al., 1987). Experiments 4 and 7 were the exception to this rule: Increasing the fault length in experiment 4 was modeled by manipulating the displacement point set (rather than the length of the fault itself) and Experiment 7 models an asymmetric fault where the point of maximum displacement is offset from the fault center.

2.4.3 Experiment model dimensions

A complete list of the dimensions, fault surface increments and 3D cell size of each experiment can be found in Table 2.2.

2.4.4 Modeling steps

In Experiments 1-8 there are four structural models representing four phases of displacement and subsequent synrift fill. Experiment 9 has six structural models where one fault has six phases of displacement and two faults only three. Experiment 10 has two phases of displacement representing two large-scale fault movements after which deltaic sedimentation can take place. For each phase of displacement there is a structural model (containing horizon and fault data), a corresponding 3D grid and the grid's extracted geometric and index grid parameters.

2.4.5 Main modeling issue with RMS

While running test workflows in RMS it became apparent that it is not possible to add displacement to a horizon that has already been displaced. RMS is supposed to be able to change displacement by a factor, or add a specified displacement. For example in the first displacement event, horizon A should displace to a depth of 100m to create a depression where sediment will infill then another flat horizon is incorporated into the model. Ideally a second displacement event should add an additional 100m of displacement to horizon A, making the total displacement of 200m. However this secondary method of applying displacement results in a total displacement of slightly more than 100m, therefore the method does not correctly model a horizon already having an applied displacement at the location of the fault.

Experiment	Length	Width	Fault surface increment	3D grid cell size Xm x Ym
1	12000	12000	25	120m x 120m
2	12000	12000	25	120m x 120m
3	12000	12000	25	120m x 120m
4	12000	12000	25	120m x 120m
5	12000	12000	25	120m x 120m
6	12000	12000	25	120m x 120m
7	10000	10000	25	120m x 120m
8	20000	20000	25	200m x 200m
9	20000	20000	25	200m x 200m
10	20000	20000	100	200m x 200m

Table 2.2: List of size, fault increment and 3D grid size data from all experiments.

As a result a workaround has been devised in the modeling workflow to correct for this software malfunctioning. All displacement events are divided into their own structural models and horizons in each are displaced using attribute point sets to their final total maximum displacement in that displacement event. In an example where 100m displacement is applied, then an additional 100m, the displacement point sets would be applied as follows:

- Structural Model 1 (100m):
    - Horizon B: Flat horizontal surface
    - Horizon A: 100m maximum displacement point set
- Structural Model 2: 100+100m:
    - Horizon C: Flat horizontal surface
    - Horizon B: 100m maximum displacement point set
    - Horizon A: 200m maximum displacement point set

This pattern continues for all other structural models.

2.5 Detailed workflows

Structural model 1

- Nested workflow A: In this workflow fault displacement estimation is used to apply point set 1A to the fault and the new fault data is used to displace horizon A in horizon model A. The data is exported for use in the final horizon model. This all occurs separately from the main workflow in a nested workflow.
- Nested workflow B: The result of this workflow is horizon model B, which contains flat horizon B where no point set is applied. The data is exported for use in the final horizon model. This all occurs separately from the main workflow in a nested workflow.
- Final horizon model: All the data from the nested workflow is exported (horizons A and B) from previous steps into a single horizon model where no fault displacement is applied as horizons are already displaced or are meant to be flat undisplaced surface. The new horizon model creates zones between horizons A and B. The final horizon model generates zones that represented the synrift sediment packages.

- 3D gridding, grid index & geometry parameters: A 3D grid is created from the structural model and from which index/geometric properties are extracted. The extraction of these properties are used in the visualization of models (discussed in 2.7 Visualization).

Structural model 2

- Nested workflow A: Same as nested workflow A, structural model 1 substitute point set 1A for point set 2A.
- Nested workflow B: Displacement of horizon B with point set 2B.
- Nested workflow C: Flat surface using horizon C as described in structural model 1, nested workflow B.
- Final horizon model: As seen in structural model 1, with addition of horizon C.
- 3D gridding, grid index & geometry parameters

Structural model 3

- Nested workflow A: Same as nested workflow A, Structural model 1 substitute point set 1A for point set 3A.
- Nested workflow B: Displacement of horizon B with point set 3B.
- Nested workflow C: Displacement of horizon C with point set 3C.
- Nested workflow D: Flat surface using horizon D as described in structural model 1, Nested workflow B.
- Final horizon model: As seen in structural model 1, with addition of horizon D.
- 3D gridding, grid index & geometry parameters

Structural model 4

- Nested workflow A: Same as nested workflow A, structural model 1 substitute point set 1A for point set 4A.
- Nested workflow B: Displacement of horizon B with point set 4B.
- Nested workflow C: Displacement of horizon C with point set 4C.
- Nested workflow D: Displacement of horizon D with point set 4D.
- Nested workflow E: Flat surface using horizon E as described in structural model 1, nested workflow B.
- Final horizon model: As described in structural model 1, with addition of horizon E.

- 3D gridding, grid index & geometry parameters

Experiment 9 exceeds four structural models/phases of displacement. Here are the idealized formats of the two additional structural models:

Structural model 5

- Nested workflow A: Same as nested workflow A, structural model 1 substitute point set 1A for point set 5A.
- Nested workflow B: Displacement of horizon B with point set 5B.
- Nested workflow C: Displacement of horizon C with point set 5C.
- Nested workflow D: Displacement of horizon D with point set 5D.
- Nested workflow E: Displacement of horizon E with point set 5E.
- Nested workflow F: Flat surface using horizon F as described in structural model 1, Nested workflow B.
- Final horizon model: As described in structural model 1, with addition of horizon F.
- 3D gridding, grid index & geometry parameters

Structural model 6

- Nested workflow A: Same as nested workflow A, structural model 1 substitute point set 1A for point set 6A.
- Nested workflow B: Displacement of horizon B with point set 6B.
- Nested workflow C: Displacement of horizon C with point set 6C.
- Nested workflow D: Displacement of horizon D with point set 6D.
- Nested workflow E: Displacement of horizon E with point set 6E.
- Nested workflow F: Displacement of horizon F with point set 6F.
- Nested workflow G: Flat surface using horizon G as described in structural model 1, Nested workflow B.
- Final horizon model: As described in structural model 1, with addition of horizon G.
- 3D gridding, grid index & geometry parameters

2.6 Modeling the experiments

Ten experiments are created for this thesis. Experiments 1-7 are idealized single fault experiments with four modeling steps. Experiments 8, 9 and 10 are more geologically complex scenarios. The following presents the aims for each experiment, the parameters assigned in RMS, and required adjustments to the detailed workflow in order to successfully run the experiment.

Experiment 1

- **Purpose:** To complete an experiment where all fault parameters (length, reverse drag and displacement amount) remain constant through each phase of displacement. This experiment acts as a baseline example.
- **Modeling parameter variations:** The reverse drag (correction range) is set to 3100m, the fault length is 6000m and the displacements are 100m for each step (400 total in four displacements).
- **Basic workflow adjustments:** The basic workflow does not vary from those discussed in section 2.5.

Experiment 2

- **Purpose:** To examine the effects of a decreasing reverse drag on the synrift sedimentation patterns.
- **Modeling parameter variations:** The fault length in this experiment is 6000m, there is 100m displacement applied to each structural model (totaling 400m). The changes to reverse drag are applied in the horizon modeling process (modeling tab under the column correction range) where a value is given to each horizon in the horizon model. A flat horizon does not have any effects of reverse drag so the number for this case does not affect the outcome of the experiment. As displaced horizons are made in separate horizon models, all data exported and then combined into one single horizon model all job, the data for reverse drag that was applied for all horizon modeling jobs is as follows:
    - Structural model 1: A=3000
    - Structural model 2: A=3000, B=2500
    - Structural model 3: A=3000, B=2500, C=2000
    - Structural model 4: A=3000, B=2500, C=2000, D=1500

- **Basic workflow adjustments:** The basic workflow does not vary from those discussed in section 2.5.

Experiment 3

- **Purpose:** To examine the effects an increasing reverse drag has on the synrift sedimentation patterns.
- **Modeling parameter variations:** The fault length in this experiment is 6000m, there is 100m displacement applied to each structural model (totaling 400m). The changes for reverse drag are applied as explained in Experiment 2 but the values vary:
    - Structural model 1: A=2000
    - Structural model 2: A=2000, B=3000
    - Structural model 3: A=2000, B=3000, C=4000
    - Structural model 4: A=2000, B=3000, C=4000, D=5000
- **Basic workflow adjustments:** The basic workflow described in section 2.5 does not work for this experiment because the application of an increasing reverse drag in RMS is unsuccessful. The problem is that there is an interference in horizon data that needs to be resolved. After the nested workflows are run the horizons are exported and have a surface-surface operation applied to all horizons to resolve interference issues. The new horizon data is then imported into the final horizon model and the application of 3D gridding and grid parameters is carried out as normal.

Experiment 4

- **Purpose:** To examine the effects of increasing fault length on the synrift sedimentation patterns.
- **Modeling parameter variations:** In this experiment 100m displacement is added to each structural model (totaling 400m at the end of all displacement) and the reverse drag remains constant at 3500m. The fault length changes from 2000m in the first structural model to 4500m in the second, 6000m in the third and 7000m in the final structural model.

  This experiment required a number of preliminary attempts in order to discover the best way to model the increase in fault length. The first attempt involves a displacement profile assemblage where horizon A is smaller than B, B is smaller than C etc. However RMS is not capable of visualizing this properly and the result was a “Russian nesting doll” effect where the largest horizon D, contained smaller horizons

C, B and A respectively (horizon E remained flat). This is a problem because RMS did not recognize that A was set to occur first in the stratigraphy. In order to overcome this problem, a slightly different technique is used in the displacement attribute point set.

This modeling is accomplished by altering the fault displacement point set. In the first structural model, only about 2000m of the fault central displacement point set has a displacement applied, the rest are set to zero. In the structural models to follow for example point set 2A, the displacements are designed to mimic the shape of the previous point set first, and then follow the second phase of displacement in order to create the growth in faults and in areas where no displacement occurs the value is set to zero (Figure 2.5).

- **Basic workflow adjustments:** The basic workflow does not vary from those discussed in section 2.5.

Experiment 5

- **Purpose:** To examine the effects of increasing fault displacement on the synrift sedimentation patterns.
- **Modeling parameter variations:** In this experiment the fault length and reverse drag remain constant at 7000m and 3500m respectively. An increase in fault displacement is accomplished by manipulating the displacement point sets. In this experiment 1A has a point of maximum displacement (50m) in the center of the fault, which decreases gradually towards the fault tiplines. This allows a 50m displacement to occur in structural model 1 (the first phase of displacement). The second phase of displacement (structural model 2) is 100m and is accomplished by multiplying the entire displacement point set 1A by 2 to create point set 2B (maximum displacement 100m) and by 3 (maximum displacement 150m) to create point set 2A. Structural models 3 and 4 displace 150 and 200m respectively and this method for deriving displacement point sets is continued throughout the experiment.
- **Basic workflow adjustments:** The basic workflow does not vary from those discussed in section 2.5.

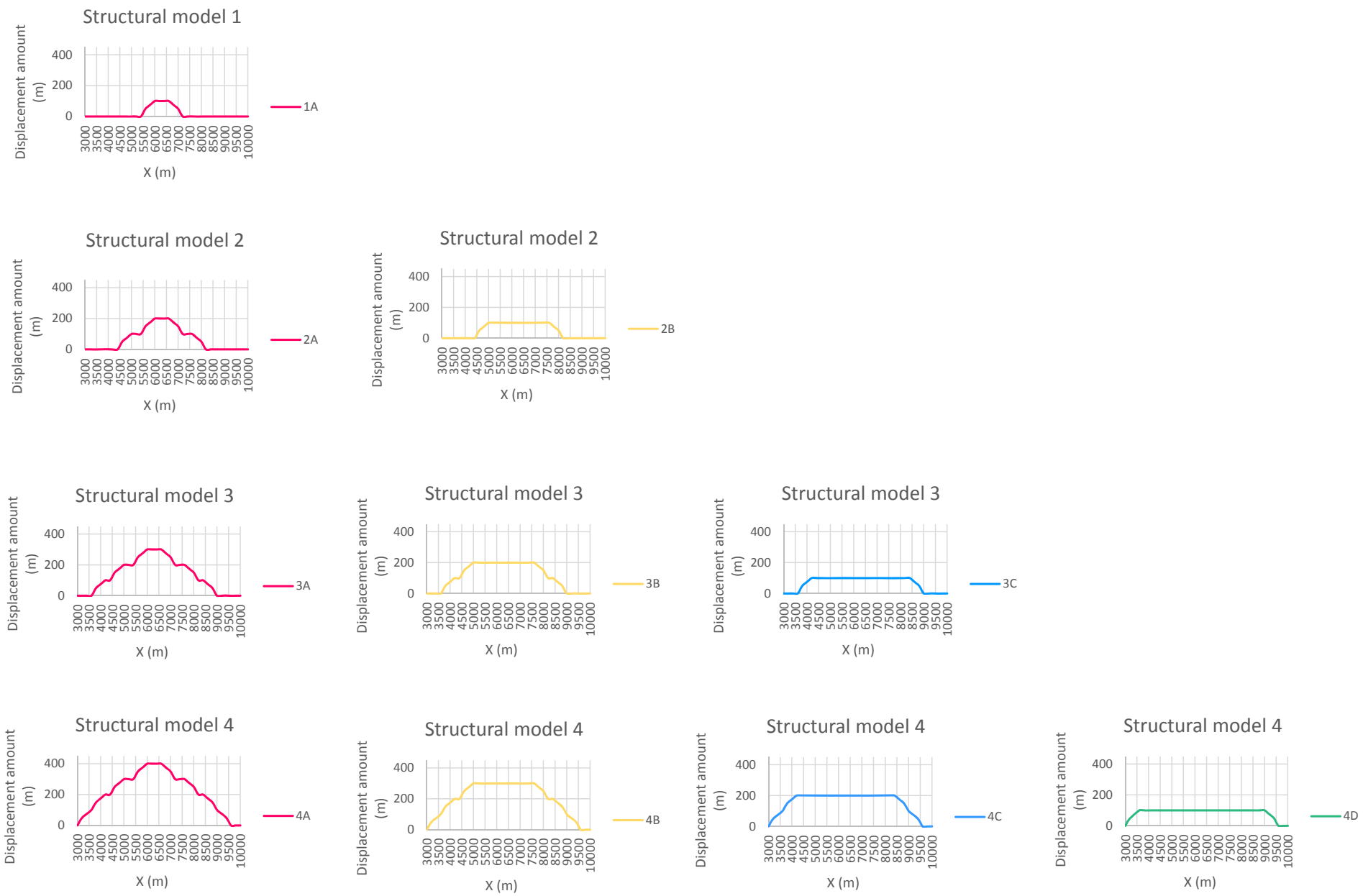

Figure 2.5: Graphs showing the displacement attribute data for each horizon in each structural model for Experiment 4.

Experiment 6

- **Purpose:** To examine the effects of decreasing fault displacement on the synrift sedimentation patterns.
- **Modeling parameter variations:** In this experiment the fault length and reverse drag remain constant at 6500m and 3500m respectively. A decrease in fault displacement with each structural model is created by applying changes to the displacement point sets. In this case a displacement point set with a maximum displacement of 50m is used for 4D (Structural Model 4, horizon D). The displacement data for each point are generated by multiplying the point set 4D by factors of X in order to create 200m displacement in the first structural model, 150m in the second, and 100m in the third and 50m in the final (used for 4D). For example structural model 1, horizon A is displaced to 200m (four times the 4D displacement point set) but in structural model 2 the faults shift 150m more so the maximum displacement of horizon A in structural model 2 (2A) is 350m (seven times the values for 4D).
- **Basic workflow adjustments:** Once the displacement point set alterations are applied and uploaded the modeling followed section 2.5.

Experiment 7

- **Purpose:** To examine the effect that fault asymmetry has on the synrift sedimentation patterns.
- **Modeling parameter variations:** The fault length and reverse drag are constant in this experiment (5500m and 2250m respectively). The displacement point sets are manipulated by shifting the point of maximum displacement from the center of the fault and applying a gradual decrease to the displacement amount towards the fault tiplines. The result is the asymmetric profile with a maximum displacement of 100m titled 1A. Since the amount of displacement per structural model remains constant, the point set values for 1A can be multiplied by 2, 3 and 4 to accomplish a displacement profile for 200, 300 and 400m. 1A, 2B, 3C and 4D use the 100m displacement profile; 2A, 3B, 4C use the 200m; 3A and 4B use the 300m and 4A use the 400m.
- **Basic workflow adjustments:** The basic workflow does not vary from those discussed in section 2.5.

Experiment 8

- **Purpose:** To examine the sedimentation patterns associated with a relay ramp structure.
- **Modeling parameter variations:** The fault lengths and reverse drags are constant at 9000m and 4500m. There are no changes to modeling parameters in this experiment. The displacement column in the point set tables are consistent with those used in Experiments 1-4, where 100m displacement is applied to each structural model (total displacement 400m). The X, Y and Z coordinates will change in the displacement point sets so that the points run along each faults center at approximately 200m separation.
- **Basic workflow adjustments:** The basic workflow remains almost identical to all previous experiments and the only change is the presence of an extra fault. In order to model two faults instead of one, both faults must be selected in the following modeling processes: fault modeling, fault displacement, horizon modeling (fault tab).

Experiment 9

- **Purpose:** To examine the sedimentation associated with fault 1 displacing six times, and faults 2 and 3 displacing at every second displacement of fault 1.
- **Modeling parameter variations:** The modeling for fault 1 remains identical to those found in previous experiments but an extra two displacements are applied in structural models 5 and 6 (additional displacement point sets: 5A-5F, 6A-6G).

  For faults 2 and 3, the displacement point sets still follow the rule where the point of maximum displacement is at the faults center but point set manipulation follows these instructions:

    - Displacement 1- No displacement, horizon A remains flat and horizontal.
    - Displacement 2- Horizons A and B are displaced to 100m and horizon C remain flat.
    - Displacement 3- No displacement occurs so horizons A and B remain at 100m, horizons C and D remain flat.
    - Displacement 4- Horizons A and B are displaced again to 200m, horizons C and D are displaced to 100m, E remains flat.

- Displacement 5- No displacement occurs so horizons A and B remain at 200m, horizons C and D remain at 100m, horizons E and F remain flat.
- Displacement 6- Horizons A and B are displaced to 300m, horizons C and D are displaced to 200m, horizons E and F are displaced to 100m and G remains flat.

- **Basic workflow adjustments:** The basic workflow does not vary from those discussed in section2.5 (with two extra structural models added).

Experiment 10

- **Purpose:** To model Gilbert delta sedimentation associated with large-scale fault movements.
- **Modeling parameter variations and basic workflow adjustments:** The Gilbert delta modeling process is unlike any other experiment. This experiment contains two structural models, which are associated with two major fault displacements. Here are the workflows for experiment 10 where the changes to modeling parameters are found in brackets next to each job.

Structural model 1

- Fault modeling (no changes from other experiments)
- Fault displacement estimation (hanging wall displacement fraction: 0.5, variogram range:1000, length/height ratio: 2, length displacement ratio:100)
- Horizon modeling: Horizon A (Correction range: 50000, in the interest of simplicity to keep horizon A as flat as possible, fault displacement: on)
- Extract horizon: Horizon A to extract horizon 1
- Surface-surface operation for all Gilbert delta sedimentation: This process eliminates the surfaces B-F where B>A, C>A etc.
- Horizon modeling: All surfaces base-A-F (inputs for horizon A: extract horizon 1, inputs for horizons base, B-F: mapped horizons, fault displacement turned off, correction range 50000)
- 3D gridding, grid index & geometry parameters (grid was set to a pillar type grid with 43% pillar adjustment)

Structural model 2

- Fault modeling: for second displacement of Horizon A
- Fault displacement estimation: for second displacement of horizon A (hanging wall displacement fraction: 0.5, variogram: 1000, length/height ratio: 1, length displacement ratio: 100)
- Horizon modeling horizon A: for second displacement of horizon A (input: horizon A: mapped horizon, correction range: 50000, fault displacement: on)
- Extract horizon: Horizon A to extract horizon phase 2
- Fault displacement estimation: displacing Gilbert delta horizons B-F (hanging wall displacement fraction: 1.00, variogram: 1000, length/height ratio: 1, length/displacement ratio: 100)
- Horizon modeling displaced Gilbert delta: Horizons base, displaced A-F (input: mapped horizons correction range: 50000, fault displacement: on)
- Extract horizon: All horizons in horizon model displaced Gilbert delta into folder extracted horizons 2
- Horizon modeling all: Horizons base, A-F and new Gilbert delta packages horizons G-K (input Base, horizons G-K: mapped horizons, input horizons A-F: extracted horizons 2, fault displacement: off)
- 3D gridding, grid index & geometry parameters (grid was set to a pillar type grid with 43% pillar adjustment)

2.7 Visualization

Displaying 3D models is not a simple process. To properly display the results found in each experiment, 3D grids are created and grid index parameters and grid geometry parameters are extracted from the grid data to show the internal geometry of the models. The following visualization steps were applied to each phase of displacement in each experiment:

- **The Z cell thickness parameter** is used to filter thin cells that fall outside the area of fault displacement. In some cases applying the cell thickness parameter was unsuccessful at filtering because it not only removed data outside of the area of fault displacement, but it also removed critical grid cells in the zone of fault displacement.

- **A fault block parameter** is only used if the cell thickness filter is unsuccessful in removing cells on the footwall side of Experiments 1-9.
- **A row column index filter** is applied in each experiment to remove for example seven of every eight columns or rows (in the X or Y direction). The display now appears as slices, which maximizes the 3D perspective view without having to take single screen shots of every horizon contour in every displacement phase.
- **Perspective or angle** of extracted images are chosen based on the angle best displaying the important features in each experiment.

Separate 3D grids were produced from each structural model (phase of displacement) in the experiment; in order to maintain constant colors for all zones in an experiment specific color tables were assigned to each grid. These tables can be found in Appendix 5.

Chapter 3

Results

Ten experiments were designed for this thesis. Experiments 1-7 demonstrate the extended functionality of RMS by manipulating single fault parameters in order to understand the effect these changes have on synrift sedimentation patterns. The results of these experiments are found in Figures 3.1-3.7. Experiment 8 is designed to show the sedimentation variation associated with a relay ramp structure (Figure 3.8A & B). Experiment 9 shows more complex modeling capabilities of RMS through the use of three faults with varying fault movements (Figure 3.9). The final experiment was created with completely different modeling workflows and techniques to explore the modeling capabilities of RMS (Figure 3.10). A CD containing an RMS project file can be found in Appendix 6 with all the structural models, input data and workflows.

3.1 Experiment 1

Experiment 1 is designed as a baseline experiment where all parameters remain constant throughout each phase of displacement. Figure 3.1 shows the lateral extent in the strike direction at a maximum in the center of the faults and a gradual thinning to zero towards the fault tiplines. In the dip direction all sediment packages remain thickest near to the fault and pinch-out away from the fault. The sediment package pinch-outs in the strike and dip directions follow the same line. Both laterally and perpendicular to the fault sequences show no progradation or retrogradation. In the Z direction (depth) the sediment grid zones exhibit consistent thickness in relation to one another. The displacement gradient for the fault plane remains constant with each displacement phase and with each added displacement the zone dip increases. These sedimentation patterns are as expected as seen in Einsele, 2000; Gibson et al., 1989.

3.2 Experiment 2

This experiment is modeled with a decrease in reverse drag with each displacement step from 3000m when horizon A is displaced, to 2500m in B, 2000m in C and 1500m in D. The results

Experiment 1-All parameters constant							
Structural model	Displaced horizons	Flat horizons	Fault length (m)	Displacement applied to model (m)	Maximum total displacement (m)	Reverse drag applied to each displaced horizon (m)	HW:FW displacement ratio
1	A	B	6000	100	100	3000	0.5
2	A, B	C	6000	100	200	3000	0.5
3	A, B, C	D	6000	100	300	3000	0.5
4	A, B, C, D	E	6000	100	400	3000	0.5

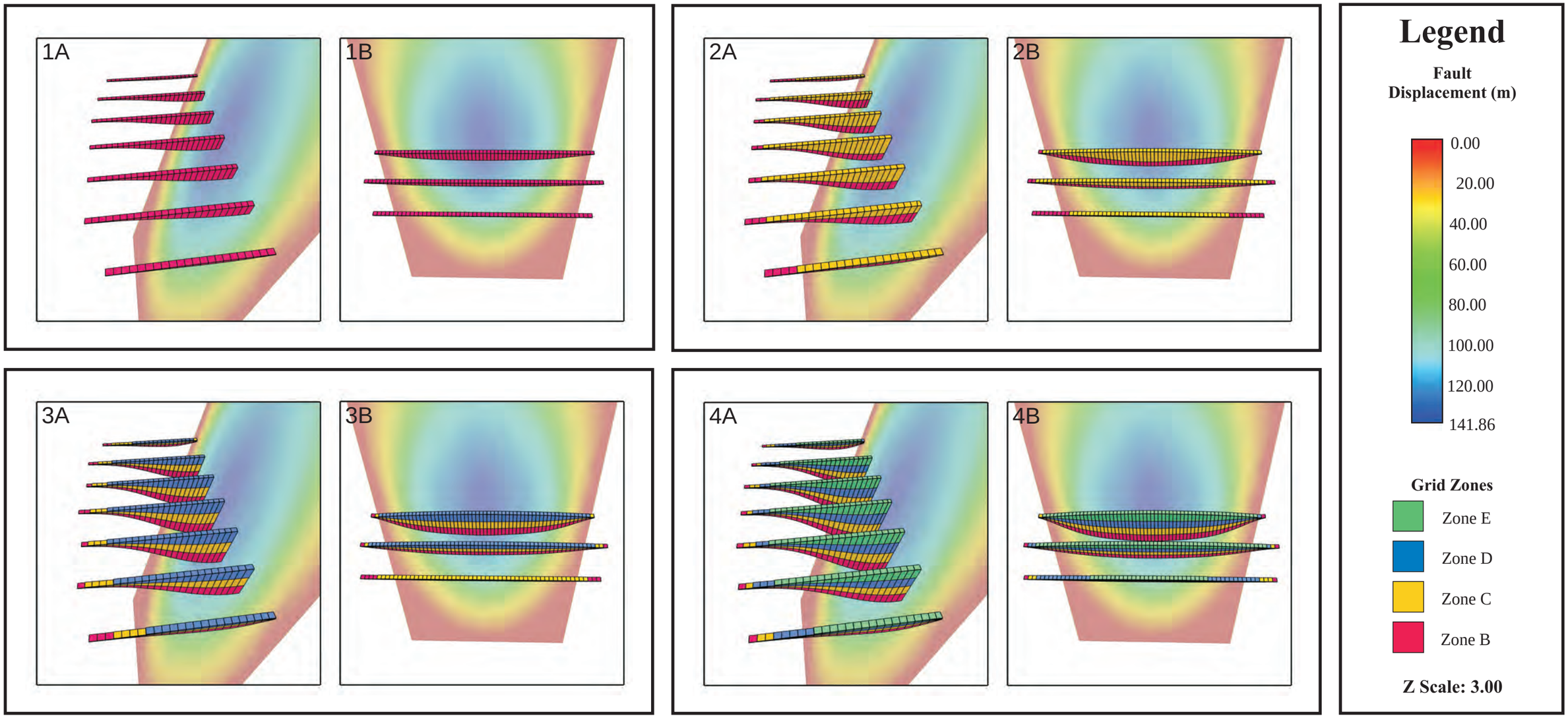

Figure 3.1: The results from experiment 1. All A figures show the resulting grid from sediment fill with a filter applied which only allows 1 of every 8 row/columns to be displayed in the X direction. The A figures are visualized from above and ~30 degrees from the strike direction. All B figures show the resulting grid from sediment fill with a filter applied which only allows 1 of every 8 row/columns to be displayed in the Y direction. The B figures are visualized from above the dip direction. 1A/B. The results after the first phase of displacement. 2A/B. The results after the second phase of displacement. 3A/B. The results after the third phase of displacement. 4A/B. The results after the final phase of displacement.

for this experiment are illustrated in Figure 3.2. Parallel to the strike of the fault there is a lateral increase in sediment thickness from one tipline to the middle of the fault and then a gradual pinch-out towards the other tipline. In the reverse drag direction, zone B shows the furthest extent, zones C, D and E progressively retrograde towards the fault plane, which is consistent with a decrease in reverse drag. The thickness of the sediment units are constant near to the fault but the thickness of zone B relative to zones C, D and E changes in the reverse drag direction. The fault displacement gradient is constant through each structural model because of the constant displacement values applied in each case.

3.3 Experiment 3

The reverse drag in experiment 3 increases with each phase of displacement from 2000m in A, 3000m in B, 4000m in C and 5000m in E. Figure 3.3A shows a cross section through the results after the final displacement phase (structural model 4) where the overlying horizons are the result of each horizon being displaced to the specific reverse drag requirements and the zones resulted from horizon model all (combining all overlying horizons into one horizon model). The results in Figure 3.3A illustrate the main modeling problem discussed in Section 2.4.5. If it were possible to displace a horizon a second time, this problem with reverse drag would not be an issue. With further investigation Figure 3.3A shows the effect that horizon A has on the shape of all zones, not the reverse drag inputs. In this experiment the user-defined stratigraphic framework in RMS results in confusion of horizon interactions and was unable to correct for horizon A cross cutting the other horizons because it is the “oldest” displaced horizon. The result is the incorrect false illusion of an increase in reverse drag and will not work for the purposes of this study.

An alternative method of modeling involves resolving the interactions between each horizon before the final horizon modeling all job by applying a surface-surface operation to each horizon. This functionality is applied to resolve each interaction by letting one horizon equal the other.

In this case the surface-surface operations are set as follows:

- For horizon A: Set A=B where A<B
- For horizon B: Set B=C where B<C
- For horizon C: Set C=D where C<D

Experiment 2- Reverse drag decreases

Structural model	Displaced horizons	Flat horizons	Fault length (m)	Displacement applied to model (m)	Maximum total displacement (m)	Reverse drag applied to each displaced horizon (m)	HW:FW displacement ratio
1	A	B	6000	100	100	A:3000	0.5
2	A, B	C	6000	100	200	A:3000, B:2500	0.5
3	A, B, C	D	6000	100	300	A:3000, B:2500, C:2000	0.5
4	A, B, C, D	E	6000	100	400	A:3000, B:2500, C:2000, D:1500	0.5

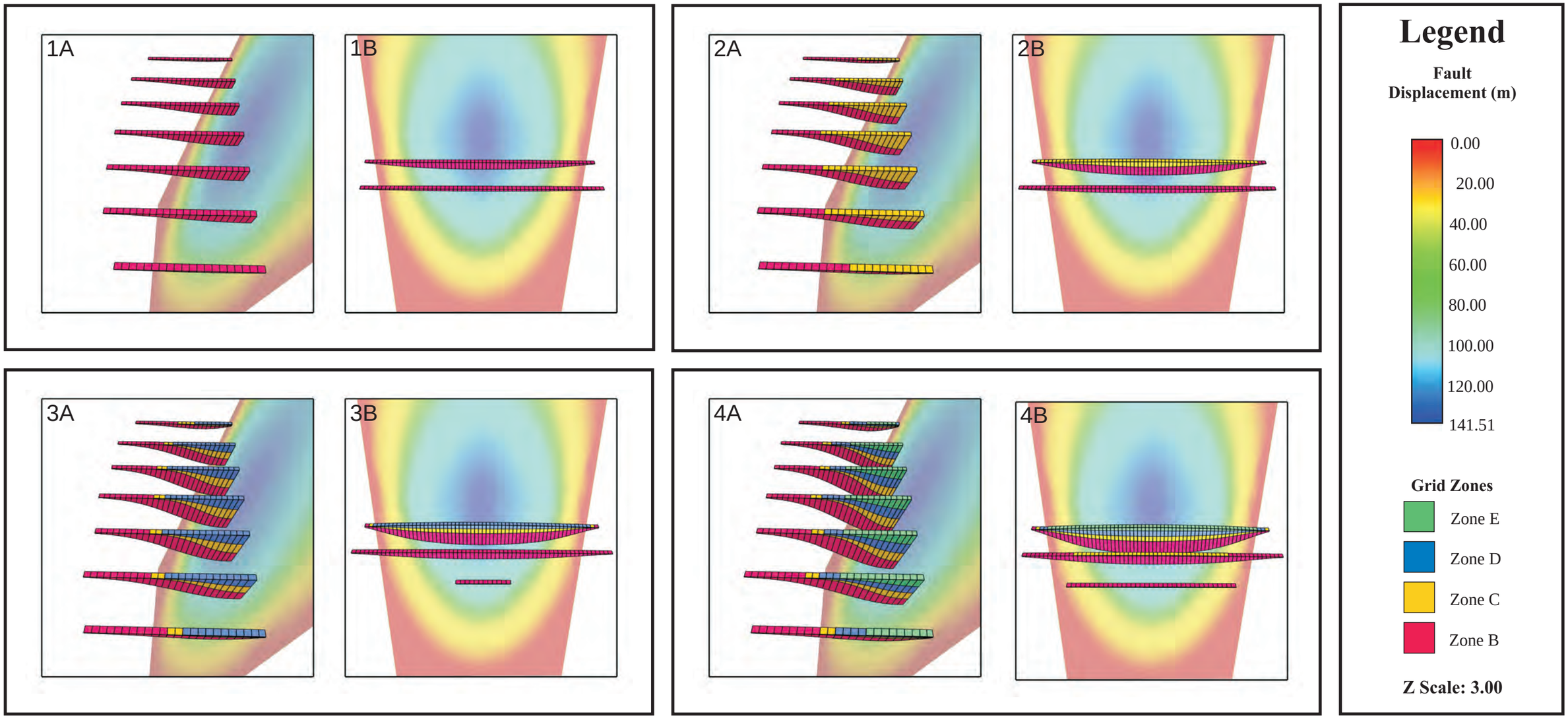

Figure 3.2:The results from experiment 2. All A figures show the resulting grid from sediment fill with a filter applied which only allows 1 of every 8 row/columns to be displayed in the X direction. The A figures are visualized from slightly above the strike direction. All B figures show the resulting grid from sediment fill with a filter applied which only allows 1 of every 8 row/columns to be displayed in the Y direction. The B figures are visualized from the dip direction. 1A/B. The results after the first phase of displacement. 2A/B. The results after the second phase of displacement. 3A/B. The results after the third phase of displacement. 4A/B. The results after the final phase of displacement.

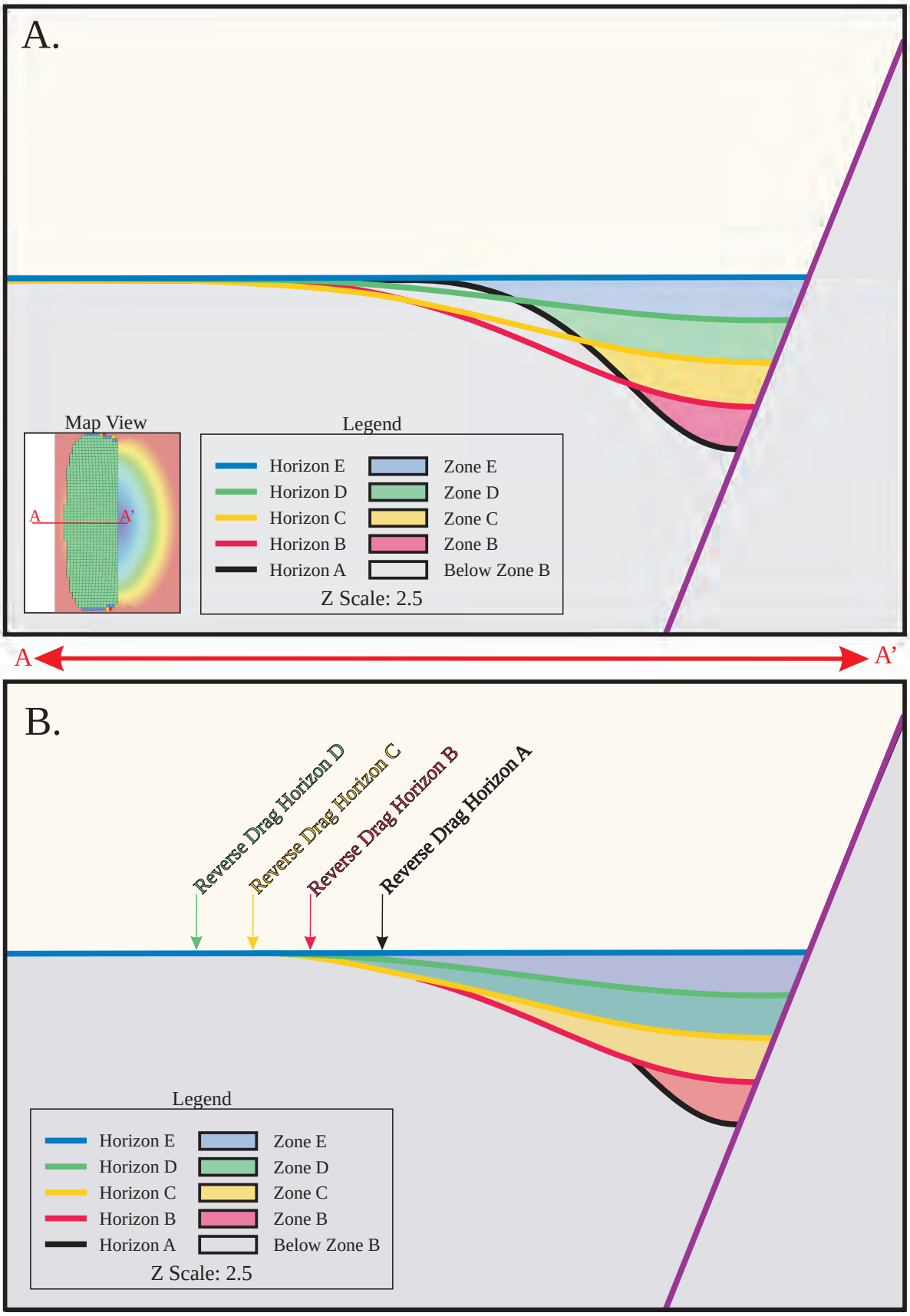

Figure 3.3: A.) An intersection view of experiment 3 showing the problems associated with modeling an increasing reverse drag. The horizons are the outputs from separate nested work flows for each horizon where displacement is applied and the zones are the result of modeling these horizon outputs into one single horizon model. The reverse drags shown on the horizons and zones are not consistent. B.) Shows a cross section of what the syn-rift sedimentation patterns should look like when horizon interactions are resolved. These results are a true 2D representation result of an increasing reverse drag, not a false positive like seen in A.

Experiment 3- Reverse drag increases

Structural model	Displaced horizons	Flat horizons	Fault length (m)	Displacement applied to model (m)	Maximum total displacement (m)	Reverse drag applied to each displaced horizon (m)	HW:FW displacement ratio
1	A	B	6000	100	100	A:2000	0.5
2	A, B	C	6000	100	200	A:2000, B:3000	0.5
3	A, B, C	D	6000	100	300	A:2000, B:3000, C:4000	0.5
4	A, B, C, D	E	6000	100	400	A:2000, B:3000, C:4000, D:5000	0.5

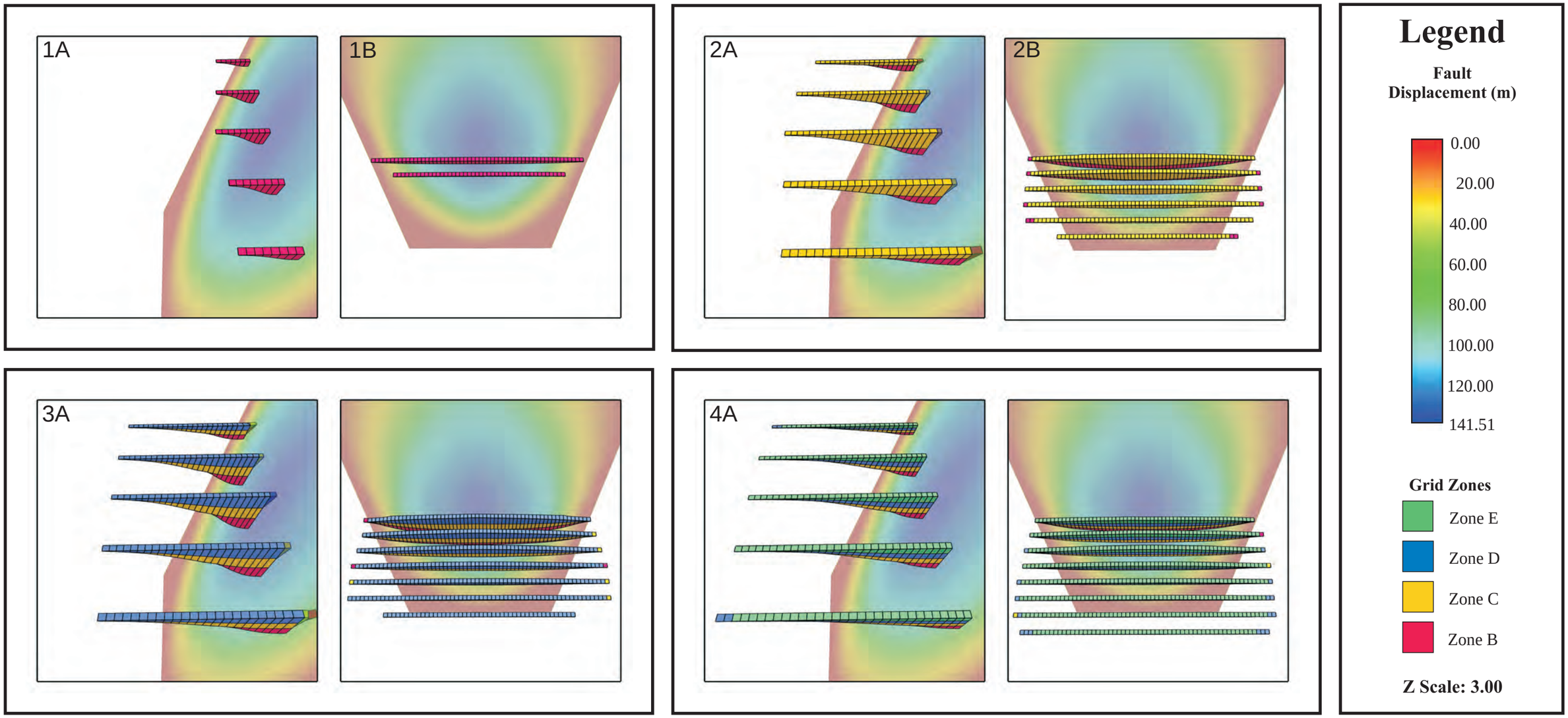

Figure 3.3C: The results from experiment 3. All A figures show the resulting grid from sediment fill with a filter applied which only allows 1 of every 10 row/columns to be displayed in the X direction. The A figures are visualized from above the strike direction. All B figures show the resulting grid from sediment fill with a filter applied which only allows 1 of every 3 row/columns to be displayed in the Y direction. The B figures are visualized from the dip direction. 1A/B. The results after the first phase of displacement. 2A/B. The results after the second phase of displacement. 3A/B. The results after the third phase of displacement. 4A/B. The results after the final phase of displacement. In 3B and 4B there are cells that fall outside of the area of subsidence which are a function of hanging wall uplift. These were filtered out using a the fault block parameter as a filter.

- For horizon D: Set D=E where D<E

The results of this modeling are almost successful, where the only problem is the fact that the surface-surface functionality was applied to both the footwall and hanging wall side, and should only be applied to the hanging wall. Since this experiment focuses on hanging wall synrift sedimentation, the modeling technique, which integrates the surface-surface operation, can be considered a partial successful.

Figure 3.3C shows the results from the newly developed modeling techniques. The distribution of synrift sediment parallel to the fault surface remains constant through all phases of displacement. The sediment thickness near to the fault surface in the Z direction is constant at the fault center and pinches-out towards the fault tiplines. The sediment thickness at the point of maximum displacement remains constant through all four phases of fault movement. Perpendicular to the fault, the lateral distribution of the synrift packages is small in the first phase of displacement (Figure 3.3C: 1A, 1B) and shows a relative increase in the lateral displacement of sediment in this direction through the remaining displacement phases. This is a function of the increasing reverse drag that was applied in the horizon modeling jobs. In the last two phases of displacement (Figure 3.3A: 3A, 3B, 4A, 4B), there were some grid cells that fall outside the area of normal fault movement, on the footwall side. The cells on the footwall side are filtered out using a fault block gridding parameter. The fault plane displacement ellipses and color bar do not change throughout this experiment as the displacement amount and fault length remain constant.

3.4 Experiment 4

Fault length increases in this experiment by manipulating the displacement point sets, not the fault surface (Appendix 3) In Figure 3.4, there is an overall increase in the lateral extent of zones B-E towards the faults tiplines (parallel with the fault) where zone B is the least laterally extensive followed by C, D and E; this change in lateral extent shows an onlapping of zone relative to the other. Each individual zone has the point of maximum displacement at the center of the fault, with a gradual pinch-out towards the tiplines, but the point where the displacement reaches zero is different for each zone. In the dip direction the reverse drag remains constant where all zones pinch-out to zero thickness at approximately the same place, this outcome is important as the reverse drag inputs remain constant throughout the

Experiment 4- Fault length increases

Structural model	Displaced horizons	Flat horizons	Fault length (m)	Displacement applied to model (m)	Maximum total displacement (m)	Reverse drag applied to each displaced horizon (m)	HW:FW displacement ratio
1	A	B	2000	100	100	3500	0.5
2	A, B	C	4500	100	200	3500	0.5
3	A, B, C	D	6000	100	300	3500	0.5
4	A, B, C, D	E	7000	100	400	3500	0.5

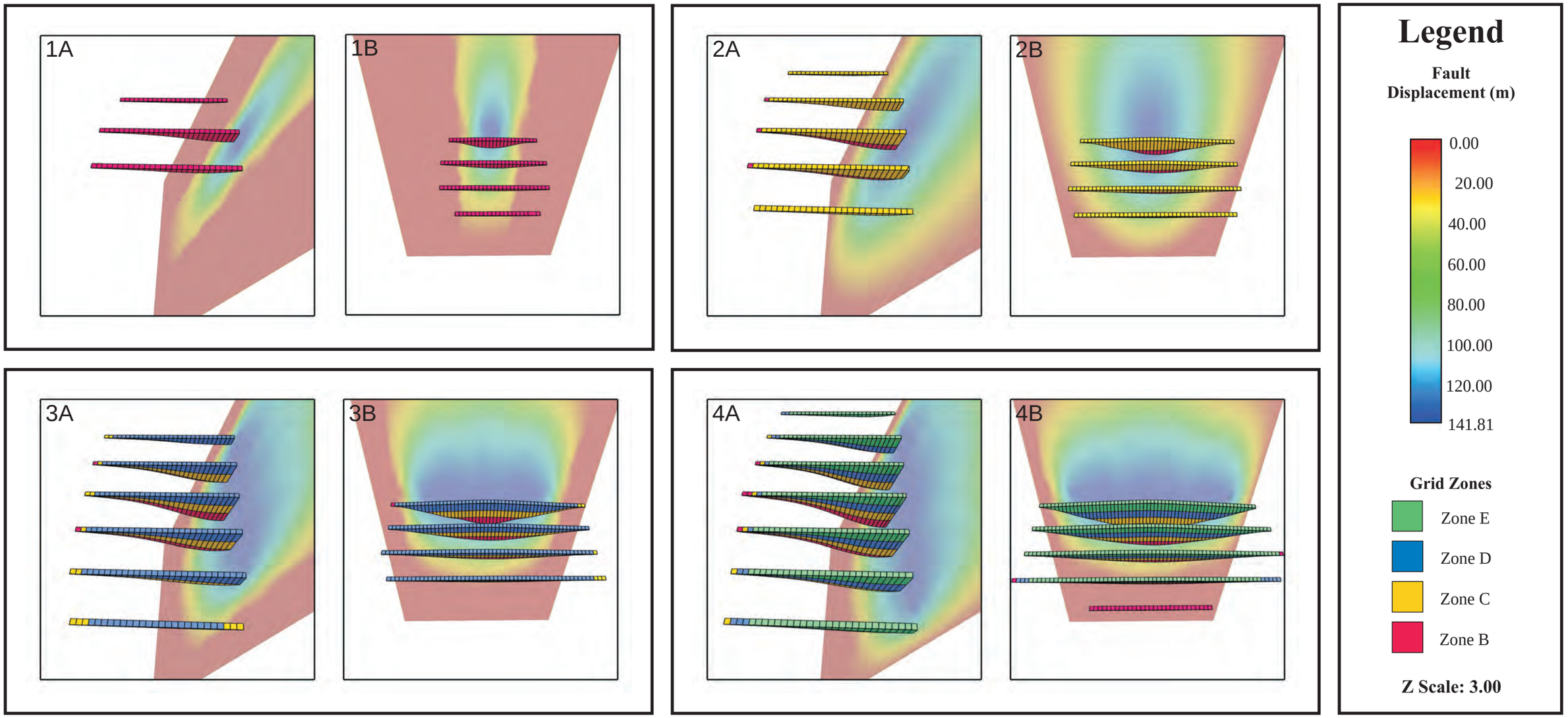

Figure 3.4: The results from experiment 4. All A figures show the resulting grid from sediment fill with a filter applied which only allows 1 of every 8 row/columns to be displayed in the X direction. The A figures are visualized from above the strike direction. All B figures show the resulting grid from sediment fill with a filter applied which only allows 1 of every 8 row/columns to be displayed in the Y direction. The B figures are visualized from the dip direction. 1A/B. The results after the first phase of displacement. 2A/B. The results after the second phase of displacement. 3A/B. The results after the third phase of displacement. 4A/B. The results after the final phase of displacement.

experiment. The thickness of the zones in the Z (depth) direction is constant close to the fault center, because the movement applied in each phase of displacement is 100m at each step. Although the fault surface does not change, the area of the fault being displaced is manipulated (Figure 3.4; the variation in the ellipsoid patterns seen on the fault plane) as a function of fault length.

3.5 Experiment 5

The results of this experiment are illustrated in Figure 3.5. The modeling in this experiment is designed to show an increase in fault displacement from zone B through, D and E. In the strike direction the sequence pinch-out is the same for all zones, which is expected when the fault length is constant. In the reverse drag direction the point where thickness of each zone pinches out is also constant due to the constancy of the reverse drag. The thickness in the Z direction varies from its thinnest for zone B and progressively increases to zone E. The fault length, and the shape of the fault displacement pattern does not change but the color bar values do change from one structural model to the next, which is a function of a constant fault length and an incremental fault displacement.

3.6 Experiment 6

See Figure 3.6 for the results of this experiment. This experiment allows the fault displacement to progressively decrease with each step where the displacement is set to 200m for the first model followed by 150m, 100m and 50m in the second, third and final stages. As the length of the fault is constant the lateral extent of the synrift packages in the strike direction is thickest at the middle of the fault and pinches-out towards tiplines at the same distance for each zone. Synrift packages are at their thickest close to the fault and thin gradually in the reverse drag direction. The reverse drag appears to decrease to zero thickness at different distances from the fault when the inputs should have forced its uniformity. Much like the fault in Experiment 5, the shape of displacement contours is constant for each phase of displacement in this experiment, but the values associated with the color bars in each displacement phase decrease. This change in the color bar is a function of a constant fault length but with a decreasing displacement per each subsequent phase of displacement.

Experiment 5: Fault displacement increases

Structural model	Displaced horizons	Flat horizons	Fault length (m)	Displacement applied to model (m)	Maximum total displacement (m)	Reverse drag applied to each displaced horizon (m)	HW:FW displacement ratio
1	A	B	6000	50	50	3000	0.5
2	A, B	C	6000	100	150	3000	0.5
3	A, B, C	D	6000	150	300	3000	0.5
4	A, B, C, D	E	6000	200	500	3000	0.5

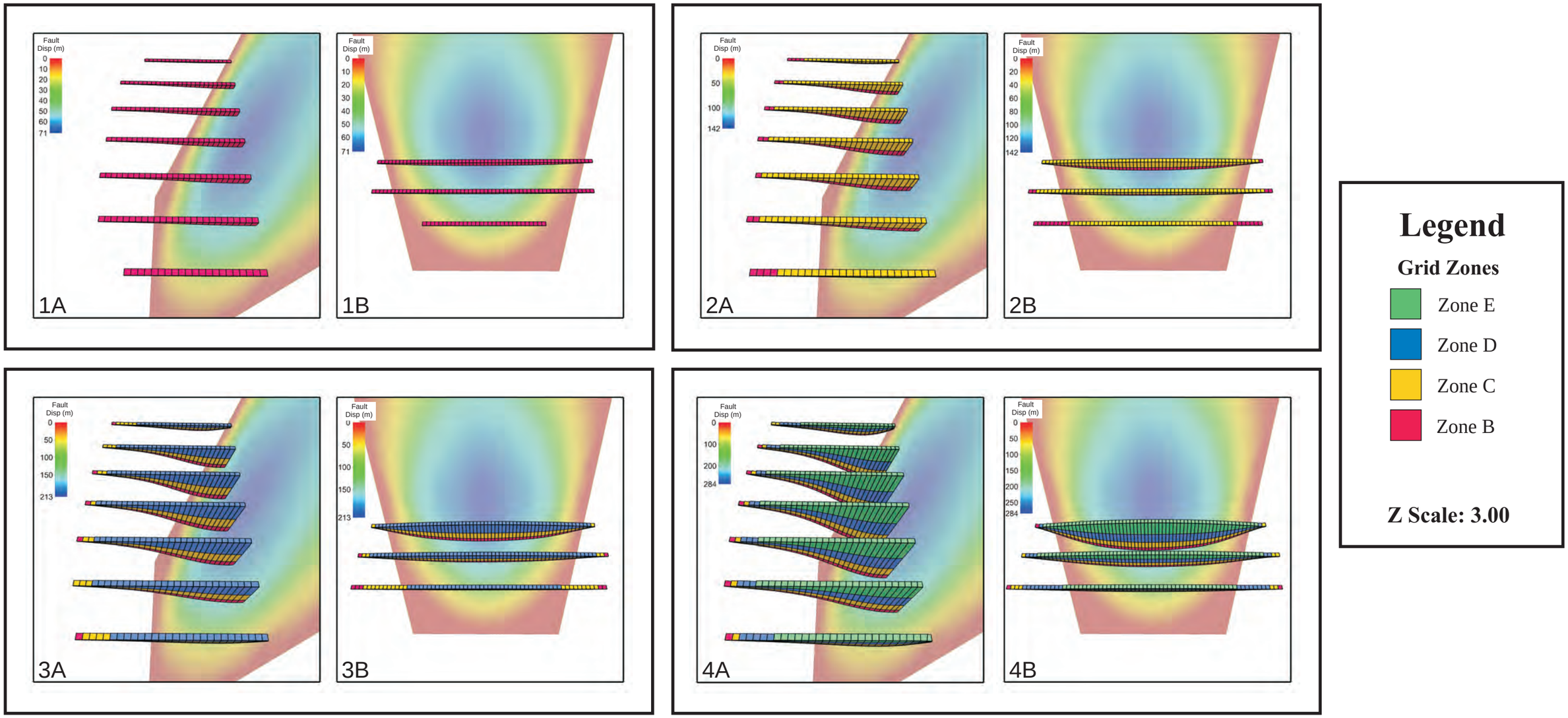

Figure 3.5: The results from experiment 5. All A figures show the resulting grid from sediment fill with a filter applied which only allows 1 of every 8 row/columns to be displayed in the X direction. The A figures are visualized from above the strike direction. All B figures show the resulting grid from sediment fill with a filter applied which only allows 1 of every 8 row/columns to be displayed in the Y direction. The B figures are visualized from the dip direction. 1A/B. The results after the first phase of displacement. 2A/B. The results after the second phase of displacement. 3A/B. The results after the third phase of displacement. 4A/B. The results after the final phase of displacement.

Experiment 6: Fault displacement decreases

Structural model	Displaced horizons	Flat horizons	Fault length (m)	Displacement applied to model (m)	Maximum total displacement (m)	Reverse drag applied to each displaced horizon (m)	HW:FW displacement ratio
1	A	B	6000	200	200	3000	0.5
2	A, B	C	6000	150	350	3000	0.5
3	A, B, C	D	6000	100	450	3000	0.5
4	A, B, C, D	E	6000	50	500	3000	0.5

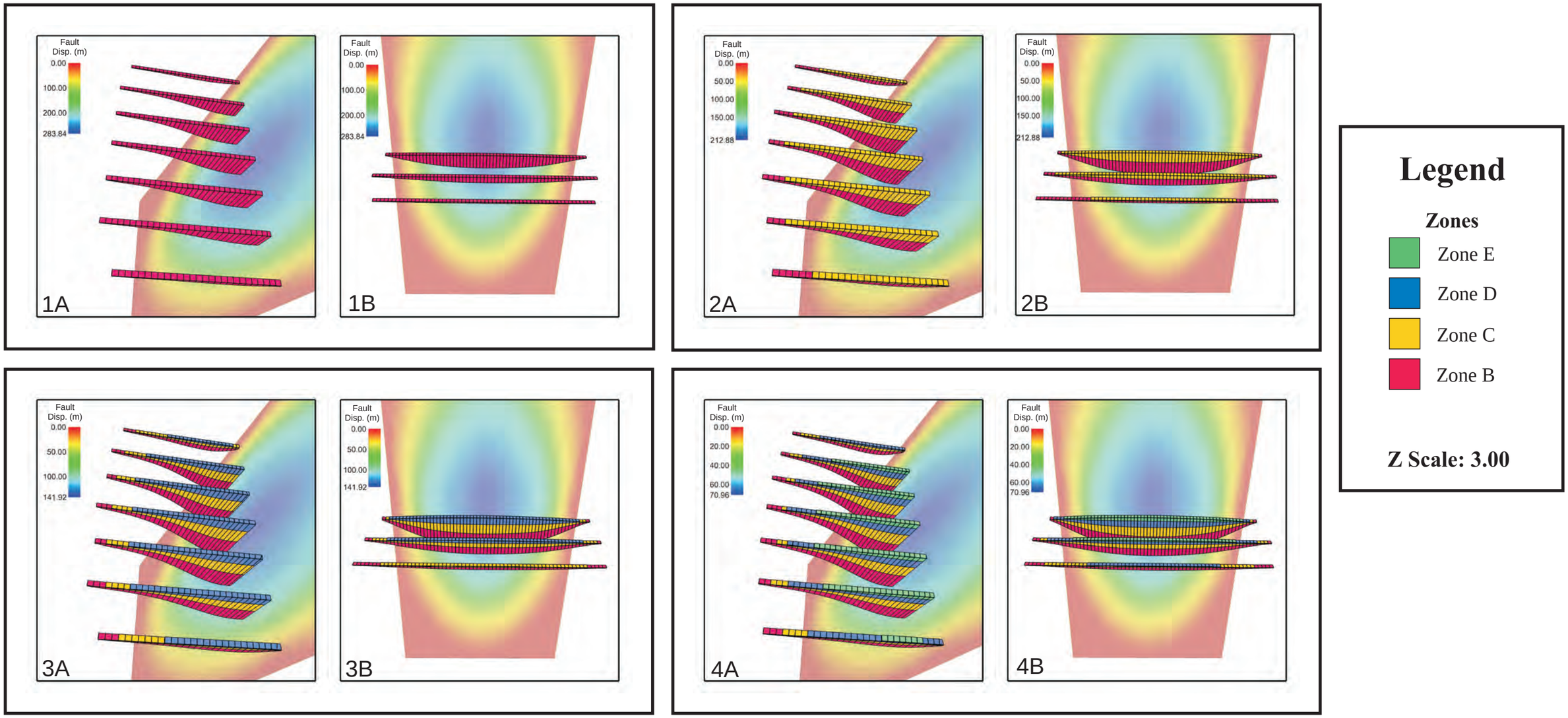

Figure 3.6: The results from experiment 6. All A figures show the resulting grid from sediment fill with a filter applied which only allows 1 of every 8 row/columns to be displayed in the X direction. The A figures are visualized from above and ~30 degrees from the strike direction. All B figures show the resulting grid from sediment fill with a filter applied which only allows 1 of every 8 row/columns to be displayed in the Y direction. The B figures are visualized from the dip direction. 1A/B. The results after the first phase of displacement. 2A/B. The results after the second phase of displacement. 3A/B. The results after the third phase of displacement. 4A/B. The results after the final phase of displacement.

3.7 Experiment 7

This experiment was created to visualize the effect that fault displacement asymmetry has on synrift sediment accumulation. The results for this experiment are illustrated in Figure 3.7. In the strike direction the lateral thickness of the sedimentary beds is unlike anything displayed thus far. The point of maximum displacement is not at the fault center. The sediments maintain a gradual asymmetrical pinch-out from the maximum displacement towards the tiplines, reflecting the displacement pattern. Similar to the results found in experiment 6, the reverse drag appears to have a slight decrease with each phase of displacement. Despite constant reverse drag (correction range) inputs through each displacement phase, the sediment packages maintain a gradual thinning in the reverse drag direction of the fault, but the pinch-out point for each zone is not constant. The fault asymmetry affects the shape of each synrift package but does not influence the consistency of the sediment thickness through each phase of displacement. The displacement gradient values of the fault do not change throughout the experiment, but the fault displacements are asymmetric. The point of maximum displacement is not located at the center of the fault and it decreases gradually and asymmetrically towards the faults tiplines.

3.8 Experiment 8

There are two figures associated with this relay structure experiment; Figure 3.8A displays an experiment summary and Figure 3.8B shows a horizon contour map showing the relay ramp morphology. Figure 3.8A contains two faults, which form a relay structure in the zone of fault overlap. The displacement attribute data for each fault is almost identical (meaning the amount of displacement per phase is the same for both faults). The point of maximum displacement is in the middle of each fault and decreases towards the fault tiplines. The zone of overlap shows a different style of sedimentation compared to the standard synrift accumulations of each fault. On the relay structure there is an overall thickening of the sediment packages that is not evident in any other lateral direction outside of the zone of overlap. The synrift sediment packages associated with fault 1 all pinch out at the same reverse drag distance of ~3500m. Those associated with fault 2 follow a similar pattern but pinch-out at a reverse drag distance of ~2300m. The value input into the model was a reverse

Experiment 7: Asymmetric fault

Structural model	Displaced horizons	Flat horizons	Fault length (m)	Displacement applied to model (m)	Maximum total displacement (m)	Reverse drag applied to each displaced horizon (m)	HW:FW displacement ratio
1	A	B	6000	100	100	3000	0.5
2	A, B	C	6000	100	200	3000	0.5
3	A, B, C	D	6000	100	300	3000	0.5
4	A, B, C, D	E	6000	100	400	3000	0.5

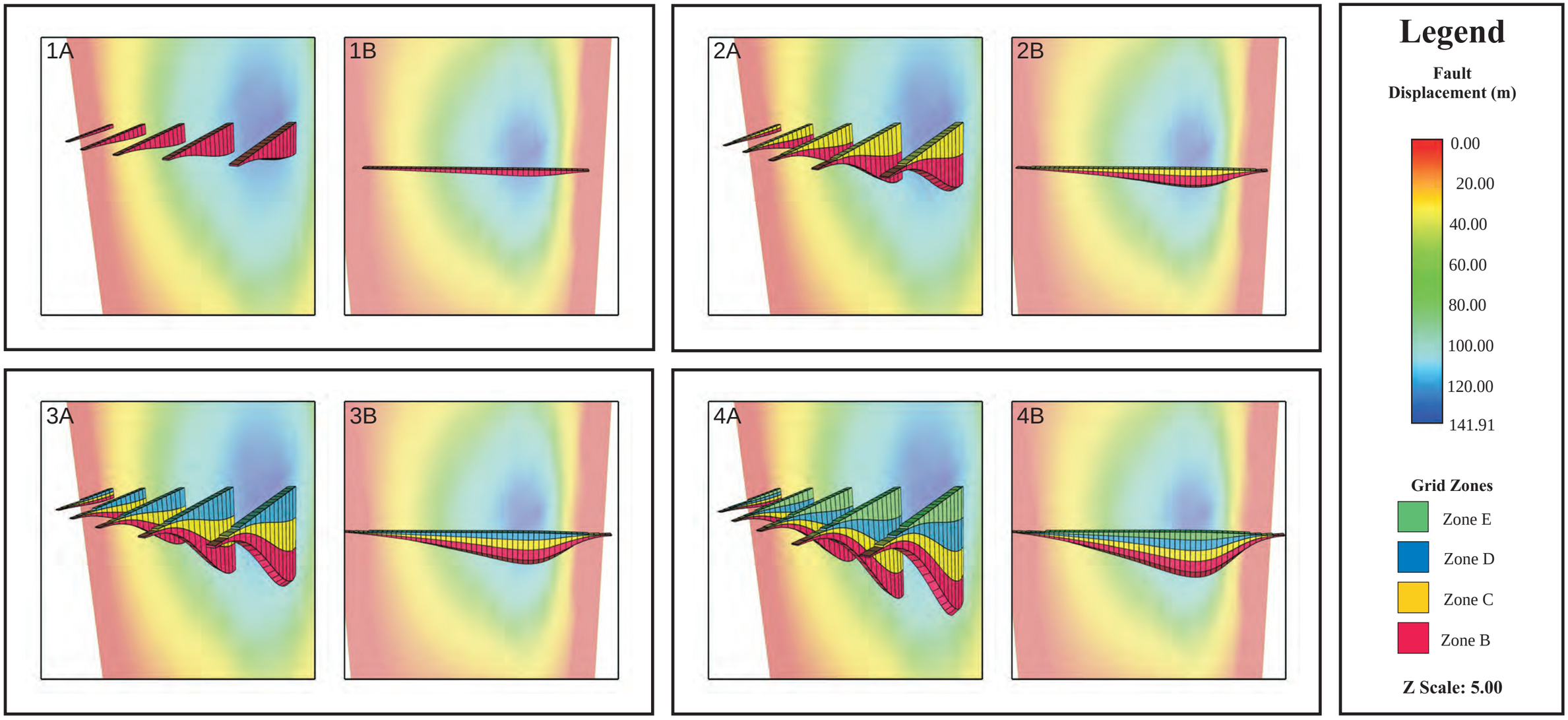

Figure 3.7: The results from experiment 7. All A figures show the resulting grid from sediment fill with a filter applied which only allows 1 of every 8 row/columns to be displayed in the X direction. The A figures are visualized ~45 degrees from the strike direction. All of the B figures show the resulting grid from sediment fill with a filter applied which allows only 1 row/column to be displayed in the Y direction. The B figures are visualized from the dip direction. 1A/B. The results after the first phase of displacement. 2A/B. The results after the second phase of displacement. 3A/B. The results after the third phase of displacement. 4A/B. The results after the final phase of displacement.

Experiment 8: Relay ramp

Structural model	Displaced horizons	Flat horizons	Length of faults (m)	Displacement applied to model (m)	Maximum total displacement (m)	Reverse drag applied to each displaced horizon (m)	HW:FW displacement ratio
1	A	B	9000	100	100	4500	0.5
2	A, B	C	9000	100	200	4500	0.5
3	A, B, C	D	9000	100	300	4500	0.5
4	A, B, C, D	E	9000	100	400	4500	0.5

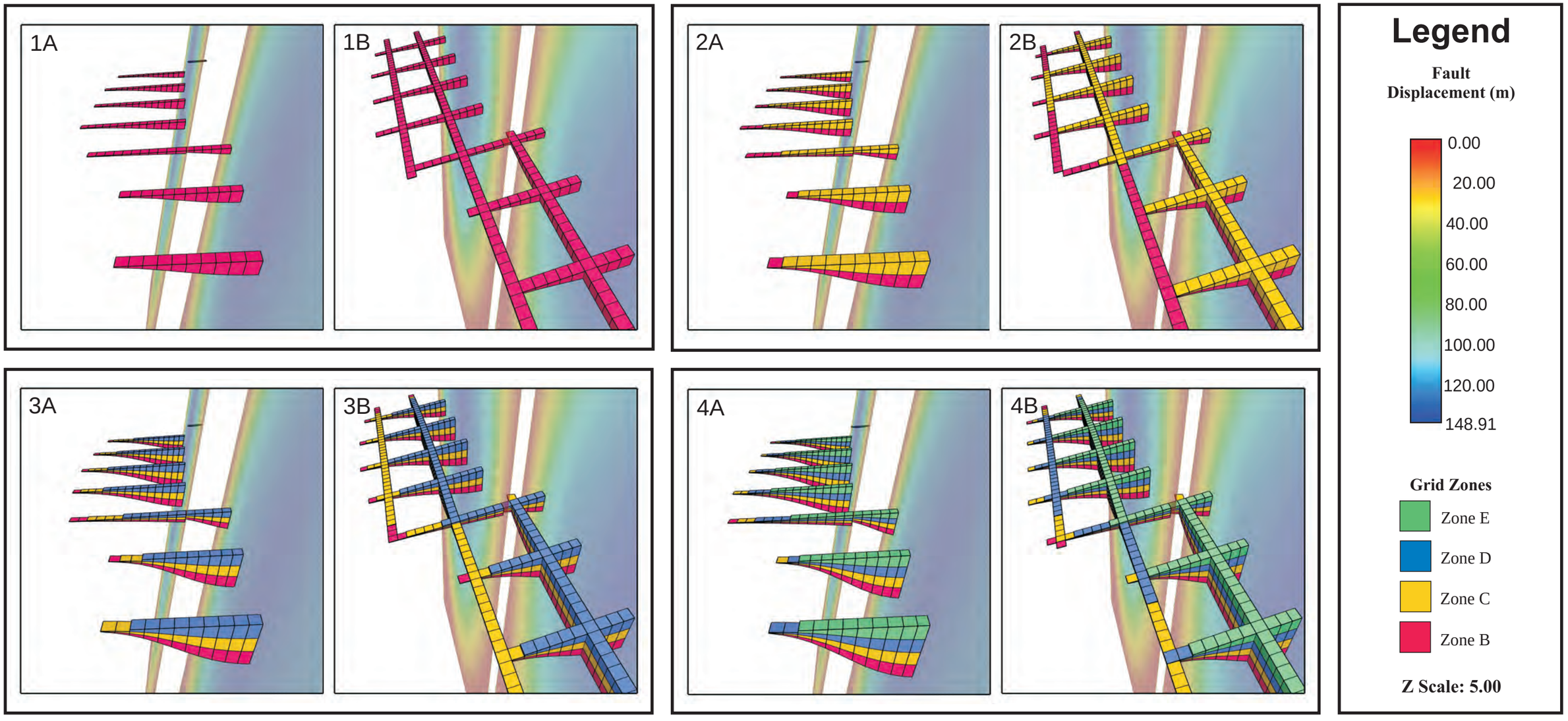

Figure 3.8A: The results from experiment 8. All A figures show the resulting grid from sediment fill with a filter applied which only allows 1 of every 8 row/columns to be displayed in the X direction. The A figures are visualized from the strike direction with emphasis on the relay ramp sediment fill. All B figures show the resulting grid from sediment fill with a filter applied which only allows 1 of every 8 row/columns to be displayed in the X and Y direction and are zoomed in to show the relay ramp sediment fill (~45 degrees to the strike and dip directions). 1A/B. The results after the first phase of displacement. 2A/B. The results after the second phase of displacement. 3A/B. The results after the third phase of displacement. 4A/B. The results after the final phase of displacement.

Experiment 8: Relay structure horizon A after final displacement

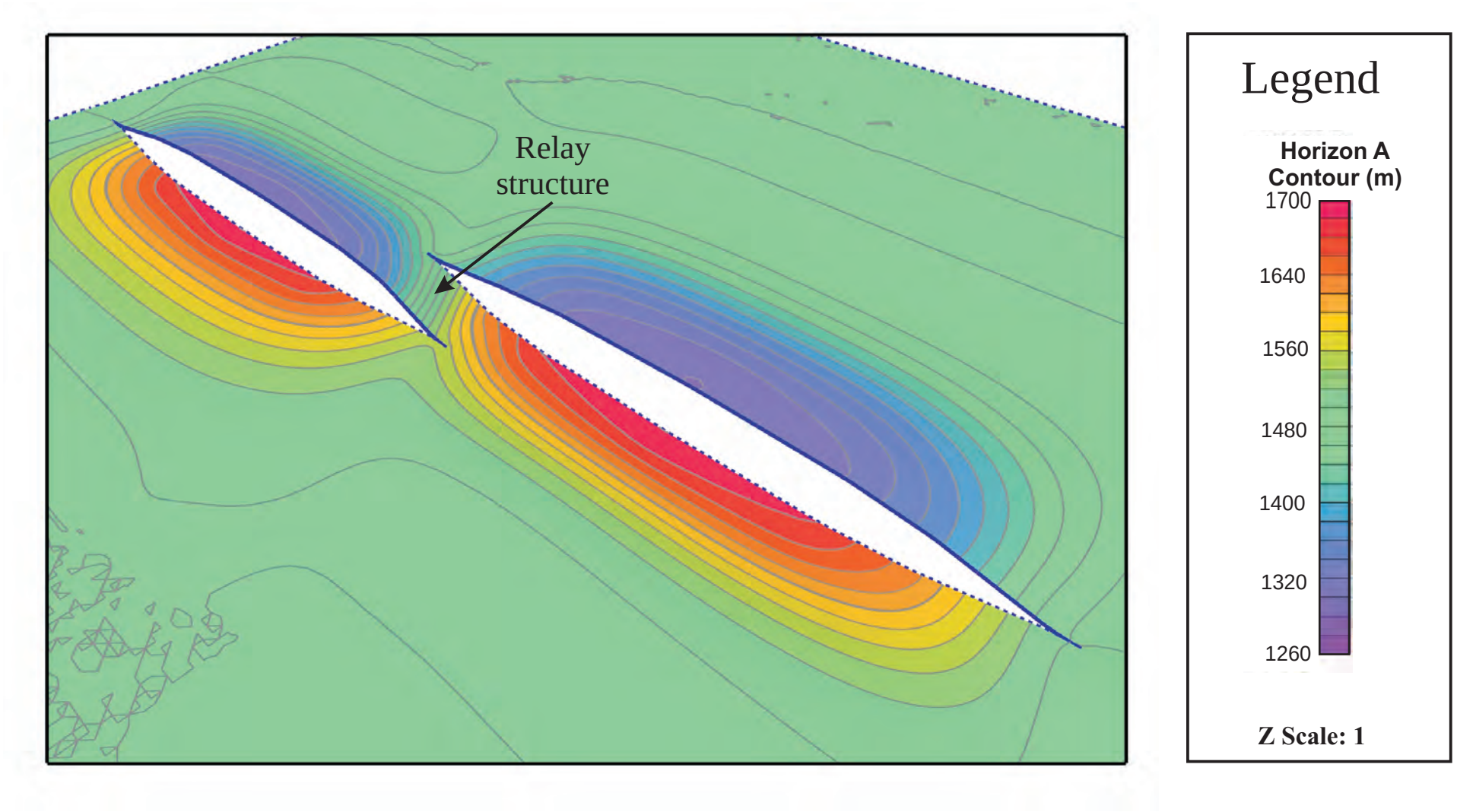

Figure 3.8B: The oldest horizon (A) being displaced in the relay ramp experiment where the architecture of the relay ramps is evident.

drag distance of 4500m. This inconsistency is interpreted as a problem with RMS and the way it deals with fault interactions. As the fault length and displacement amounts are constant, the fault displacement ellipsoids are unchanged throughout the experiment. As discussed in Chapter 1, the morphology of a relay structure is dependent on specific fault interactions where if the displacement of the overlapping units were summed, the result would be the displacement of a single fault in the system (Figure 1.3C2). These structural morphologies mimic the displacement point sets for this experiment to create a geologically accurate relay structure.

3.9 Experiment 9

This experiment shows fault 1 displacing six times, and faults 2 and 3 displacing every second time relative to Fault 1. The synrift fill for all faults follows a familiar pattern parallel with the strike direction of the fault where the point of maximum displacement is at the fault centers and displacement decreases towards the tiplines. In this experiment the reverse drag (correction range in RMS) input for all faults is constant. In the reverse drag direction the synrift sedimentation for faults 2 and 3 behave as expected, showing the thickest sediment packages close to the fault and thickness pinch-outs in the reverse drag direction. Fault 1 shows synrift packages at their thickest near to the fault and thinning gradually in the reverse drag direction until the sedimentation is cross-cut by the presence of faults 2 and 3. The thickness of all synrift sediment packages is constant with each displacement event, which was a function of the same applied displacement. In this experiment the hanging wall displacement ratio is set to 0.5 (displacement is equally divided to the hanging wall subsidence and footwall uplift). As seen in Figure 3.9B the equivalent hanging wall: footwall displacement distribution inputs and the results do not relate. The largest fault shows hanging wall subsidence and footwall uplift as expected. However the smaller two faults show displacement with hanging wall subsidence but do not show expected patterns of footwall uplift. There are some minor areas of uplift occurring on the crests of Faults 2 and 3 that measure approximately 150m height (half of the displacement of these faults) as expected. The problem with these uplifted areas is that they are only about 300m wide on the footwall side and the distance the uplifted area covers cannot be manipulated in RMS.

Experiment 9:Three faults with separate displacements

Structural model	Fault 1 length (m)	Displaced horizon	Applied displacement (m)	Maximum displacement (m)	Fault 2 & 3 length (m)	Displaced horizons	Applied displacement (m)	Maximum displacement (m)	Reverse drag (m)	HW:FW displacement ratio
1	15500	A	100	100	8000	None	0	0	7000	0.5
2	15500	A, B	100	200	8000	B	100	100	7000	0.5
3	15500	A, B, C	100	300	8000	None	0	100	7000	0.5
4	15500	A, B, C, D	100	400	8000	B, D	100	200	7000	0.5
5	15500	A, B, C, D, E	100	500	8000	None	0	200	7000	0.5
6	15500	A, B, C, D, E, F	100	600	8000	B, D, F	100	300	7000	0.5

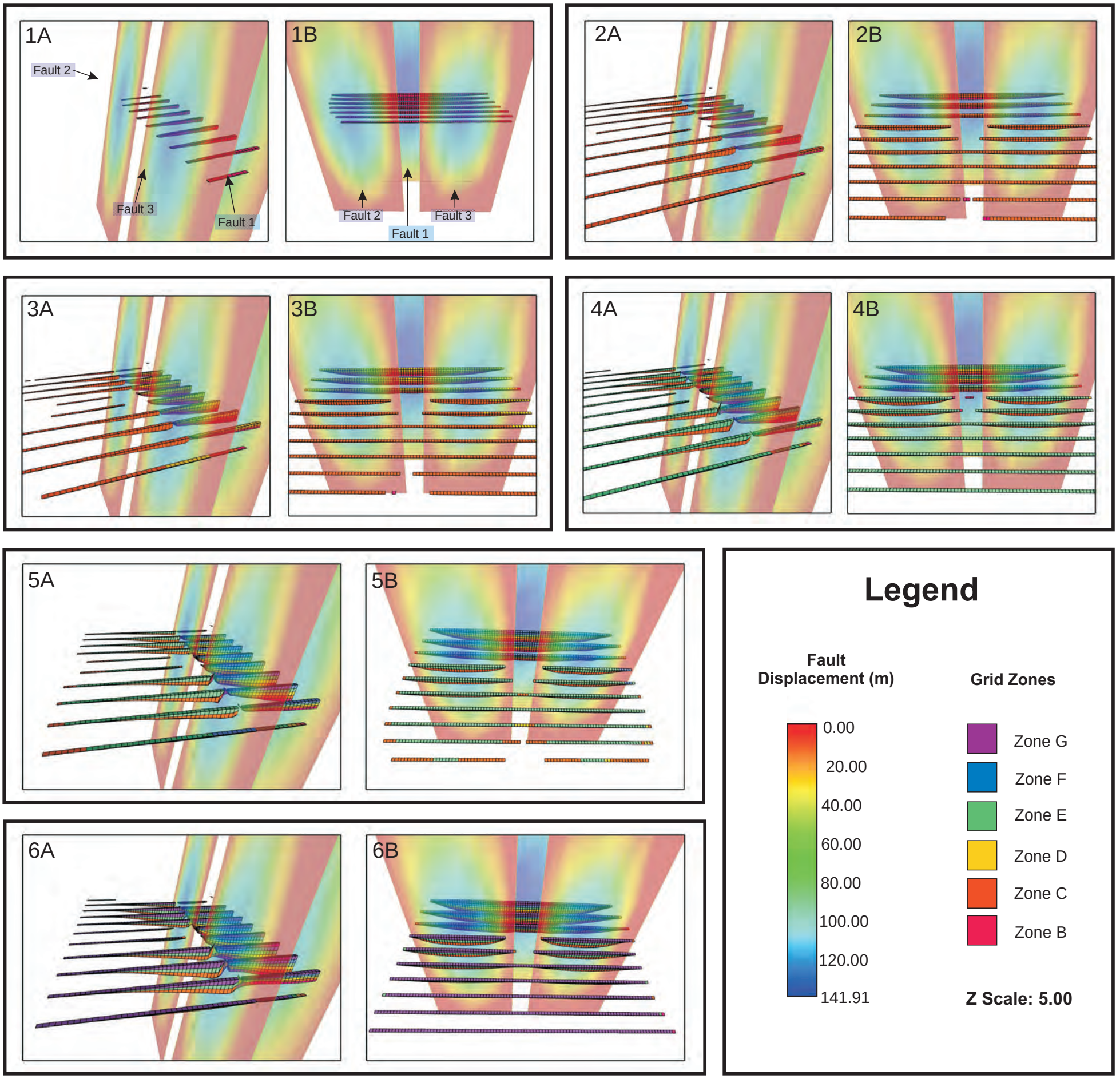

Figure 3.9A: The results from experiment 9. All A figures show the resulting grid from sediment fill with a filter applied which only allows 1 of every 8 row/columns to be displayed in the X direction. The A figures are visualized from the strike direction. All B figures show the resulting grid from sediment fill with a filter applied which only allows 1 of every 5 row/columns to be displayed in the Y direction. The B figures are visualized from above the dip direction. 1A/B. The results after the first phase of displacement. 2A/B. The results after the second phase of displacement. 3A/B. The results after the third phase of displacement. 4A/B. The results after the fourth phase of displacement. 5A/B. The results after the fifth phase of displacement. 6A/B. The results after the final phase of displacement. In this experiment both the cell thickness parameter and the fault block grid parameter were used to filter out cells that fell outside the area of fault displacement.

Experiment 9: Multiple faults

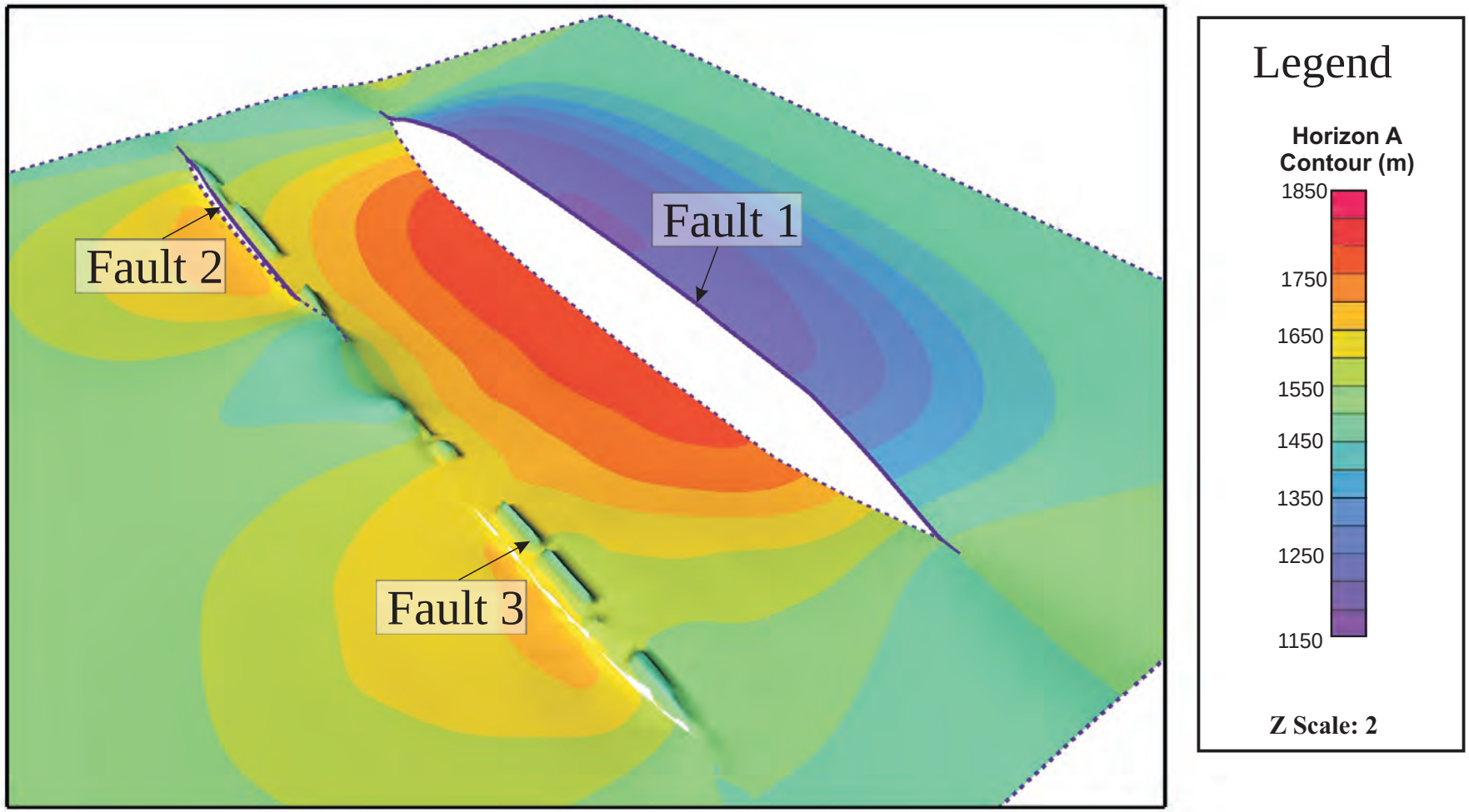

Figure 3.9B: This map shows horizon contours of horizons A-F where A is the oldest and demonstrates the 50/50 displacement distribution of the hanging wall and footwall. Fault 1 shows a normal displacement distribution. Faults 2 and 3 show hanging wall subsidence as normal, but the footwall uplift is localized only on the crest of the footwall which is not a normal uplift distribution.

3.10 Experiment 10

The Gilbert delta model is based on the ancient Vouraikos and Kerinitis Gilbert deltas, Gulf of Corinth, Greece (Ford et al., 2009; Backert et al., 2010). In this experiment (in the interest of simplification) two large displacement events of 400m were applied instead of multiple smaller 100m displacements. In the first major displacement event, Horizon A (the pre-rift horizon) is faulted approximately 400m total (200m footwall uplift and hanging wall subsidence), then the first phase of Gilbert delta sedimentation is introduced to the system. The sediment packages are modeled using conate surfaces for synrift sediment infill, where cones are moved sequentially upwards and basinwards to mimic real Gilbert delta deposition. When the conate surfaces meet sea level they are truncated by manipulating the horizon point set (see Backert et al., 2010; Ford et al., 2009). When the surfaces meet the fault surface they are also truncated as Gilbert delta sedimentation only occurs on the hanging wall (Ford et al., 2009; Backert et al., 2010). Lastly, on the footwall side, the Gilbert delta sediments are truncated by the presence of the fault pre-rift horizon (Horizon A). Another 400m displacement is applied to both the pre-and synrift Gilbert delta sediment and a second phase of delta sediments are deposited on top of the first deltaic sediments. This method of modeling was chosen to show proof of concept and can be further developed to incorporate a more complex system with respect to sedimentology and structural framework.

The results from the first displacement stage of the Gilbert delta experiment show a grid zone that acts as the framework for deltaic deposition (zone A) and five progradational Gilbert delta synrift sedimentation packages. In this example the sedimentation rate is less than the rate of accommodation space generation, which is evident in the shape of zones B-F and the mean sea level. The deltaic sediments follow a conate shape that increases in thickness through time where zone B is the smallest, and least laterally extensive, and zone F is the youngest and most laterally extensive. Zone B shows the most conate shape with a preserved apex as deposition occurred below sea level so no erosion occurred due to the presence of sufficient accommodation space. In zones C-F, the preservation of the apex of the cones decreases towards sea level and the delta top of zone F's is almost completely flattened at mean sea level due to erosion or a lack of accommodation space. These spatial observations are generally consistent with those discussed in the Introduction (section 1.3; Ford et al., 2009; Backert et al., 2010; Leeder, 2012).

Experiment 10- Gilbert delta						
Structural model	Displaced horizons	Gilbert delta gedimentation	Fault length (m)	Displacement applied to model (m)	Reverse drag applied to each displaced horizon (m)	HW:FW displacement ratio
1	A	B-F	2000	400	3000	0.5
2	A-F	G-K	2000	400	3000	0.5

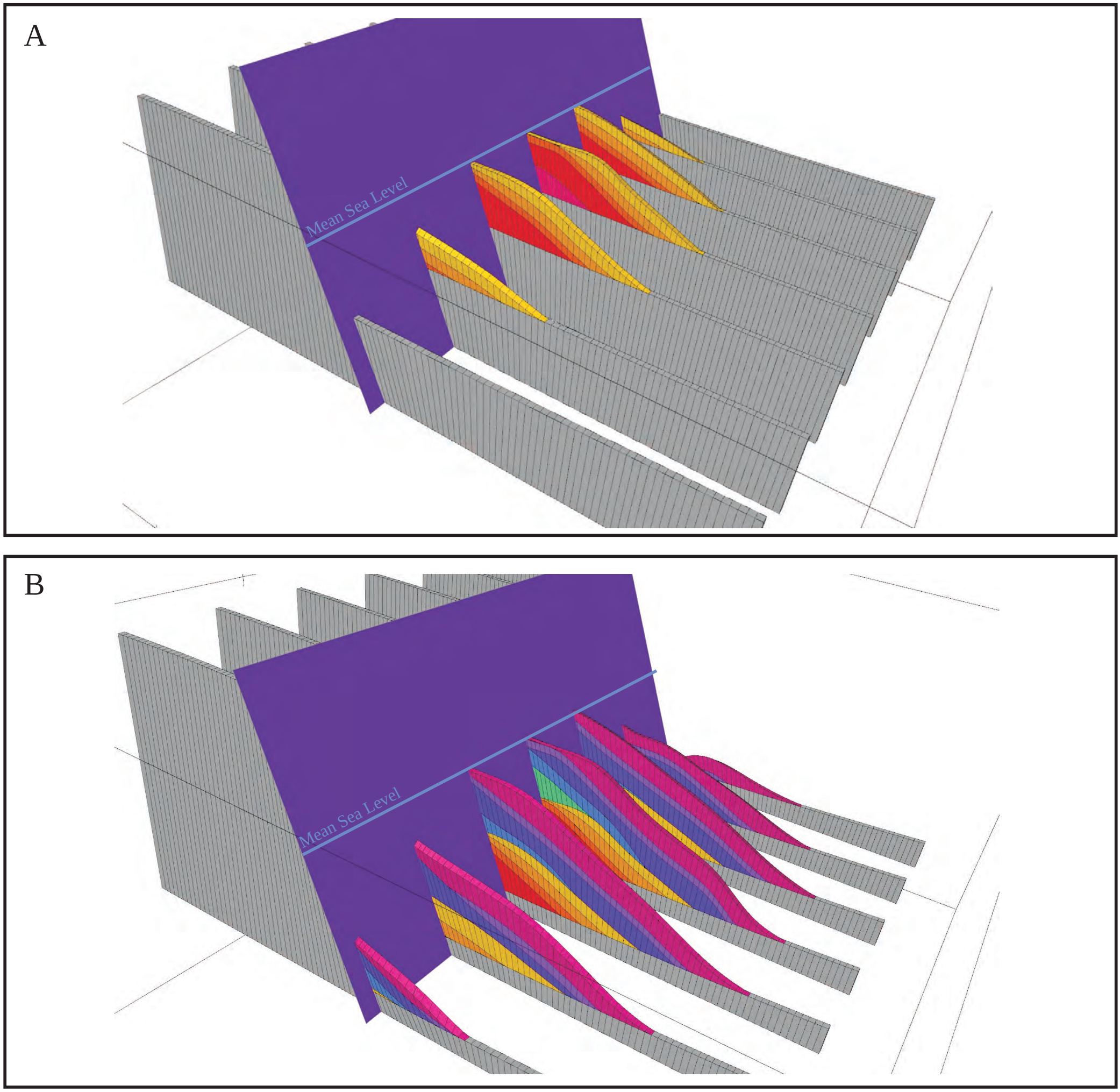

Figure 3.10: The results from experiment 10. A.) The resulting grid from displacing horizon A and introducing prograding deltaic sedimentation (horizons B-F). B.) The resulting grid after a second displacement is applied to both horizon A and all of the Gilbert delta sediments that were introduced in A. A second set of prograding deltaic sediment is also introduced after the second displacement. The results from both A and B are filtered to show 1 of every 10 grid columns in the dip direction. The fault ellipses are not imaged here because the fault was altered to displace equally across the entire surface.

Structural model 2 shows a second further displacement event for zone A and the first stage delta deposits (zones B-F). A second phase of delta progradation is deposited on top of zones B-F, where zone G has a preserved cone structure, with a clear apex, and zones H-J become progressively flatter relative to mean sea level. The lateral extent of these zones is smallest in zone G and increases through zones H-J. These new deltaic deposits drape over the original five zones (B-F) as the shape of accommodation space is irregular with the presence of the first stage of deltaic deposits. The flattened part of the zones nearest to the fault represent the deltas topsets, the dipping portions of the zones represent the deltas foresets and the distal portion of each zone (where there is a gradual flattening) represents the bottomset. The pro delta deposits will have sub-horizontal dips after the last deltaic zone (J) thins to zero, and are on top of zone A.

Chapter 4

Discussion

4.1 Overview of results

Three fault parameters (fault displacement, fault length, reverse drag) were manipulated to generate seven simplified experiments, to show the impact fault geometries have on synrift sedimentation. Three more complex scenarios were also created in order to demonstrate the functionality that this type of modeling has in real world geological situations. The main findings of these experiments were:

- The creation of accommodation space is affected by the amount of displacement, the fault length and the reverse drag.
- When all parameters in Experiment 1 remain constant, the amount of accommodation space and subsequent synrift sedimentation patterns also remains constant.
- An increase or decrease in reverse drag causes an increase or decrease in accommodation space perpendicular to the fault. Regardless if the reverse drag was changing, the shape of the accommodation space and synrift fill was always thickest near to the fault and gradually thinned to zero perpendicular to the fault.
- An increase in fault length allowed for the creation of accommodation space to increase parallel to the fault plane. The result of an increasing fault length was an increase in the lateral extent of each synrift sediment package.
- When the fault displacement increases or decreases, so does the accommodation space in the Z direction (depth). An increase in displacement results in thicker synrift sedimentation and vice versa. The shape of these synrift deposits would only vary in a lateral sense (parallel or perpendicular to the fault plane) if the fault length or reverse drag was increasing or decreasing.
- When the point of maximum displacement was not at the center of the fault, this was reflected by the generation of asymmetric accommodation space resulting in asymmetric synrift deposits.
- Relay structures have been extensively analyzed with respect to sedimentation and structural development (Larsen, 1988; Peacock and Sanderson, 1991, 1994; Childs et al., 1995; Peacock, 2002; Athmer and Luthi, 2011a; Long and Imber, 2011; Conneally

et al., 2014) however this thesis is the first known study to use RMS to forward model relay structures. Through these new modeling techniques, the parameters affecting a relay structure can now be adjusted to best fit real-world examples.

- The techniques used in modeling the interactions of multiple faults (Experiments 8 and 9) can be used to forward model a multitude of structurally complex scenarios. The methods can be used in future works to forward model other structurally complex scenarios, or even to make simplified models of entire basins.
- The techniques used in this thesis to model the interactions of multiple faults are very valuable to future works on the topic of reservoir modeling and can be used to compare changing fault interactions in RMS to field and seismic observations.
- The modeling of the Gilbert delta introduced the idea of modeling sedimentary environments where sedimentation amount is less than the rate of fault displacement. The modeling of these deltas is an invaluable way to visualize more complicated sedimentological situations in three dimensions. These techniques may allow for the modeling of other more sedimentologically complex systems. Figure 4.1 is a comparison between a field example from Greece and the RMS model from the Gilbert delta experiment.

4.2 Successes in modeling techniques

For the most part every experiment in this thesis was a success in that they generally gave the expected results as compared to observations from seismic, outcrop and 2D modeling (Barnett et al., 1987; Gibson et al., 1989; Gawthorpe and Leeder, 2000; Ravnås et al., 2000). The modeling techniques that were used were based on a framework workflow used in Syahrul (2014). The most successful adjustments to his modeling techniques included:

- Displacement point set manipulation: With the latest RMS software update (2013), came the ability to upload displacement point set attributes. This development is invaluable for the completion of these experiments. Files for each horizon undergoing displacement were uploaded containing four columns (X, Y, Z and displacement). These files could be easily manipulated using Microsoft Excel.
- Multi surface displacement workflow: In this development each horizon was displaced separately in a nested workflow that contained a fault displacement

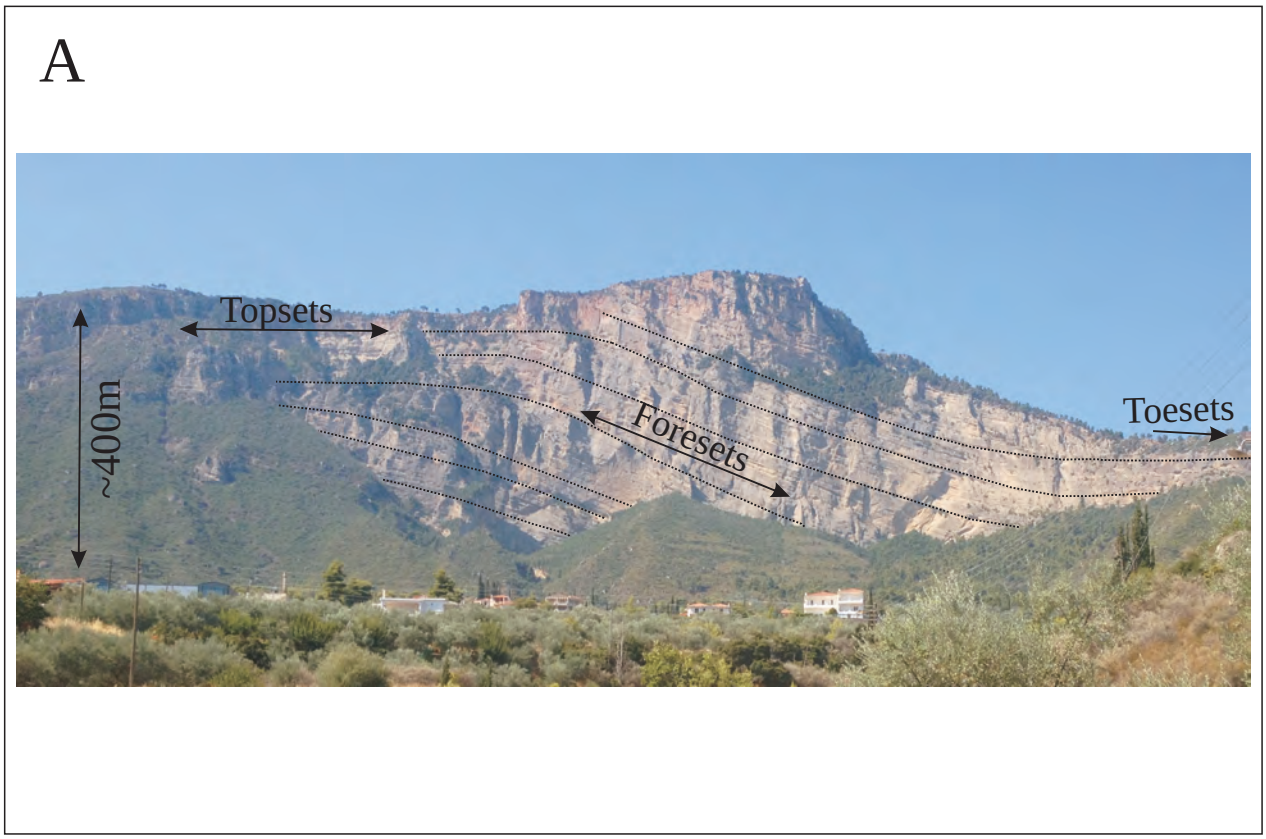

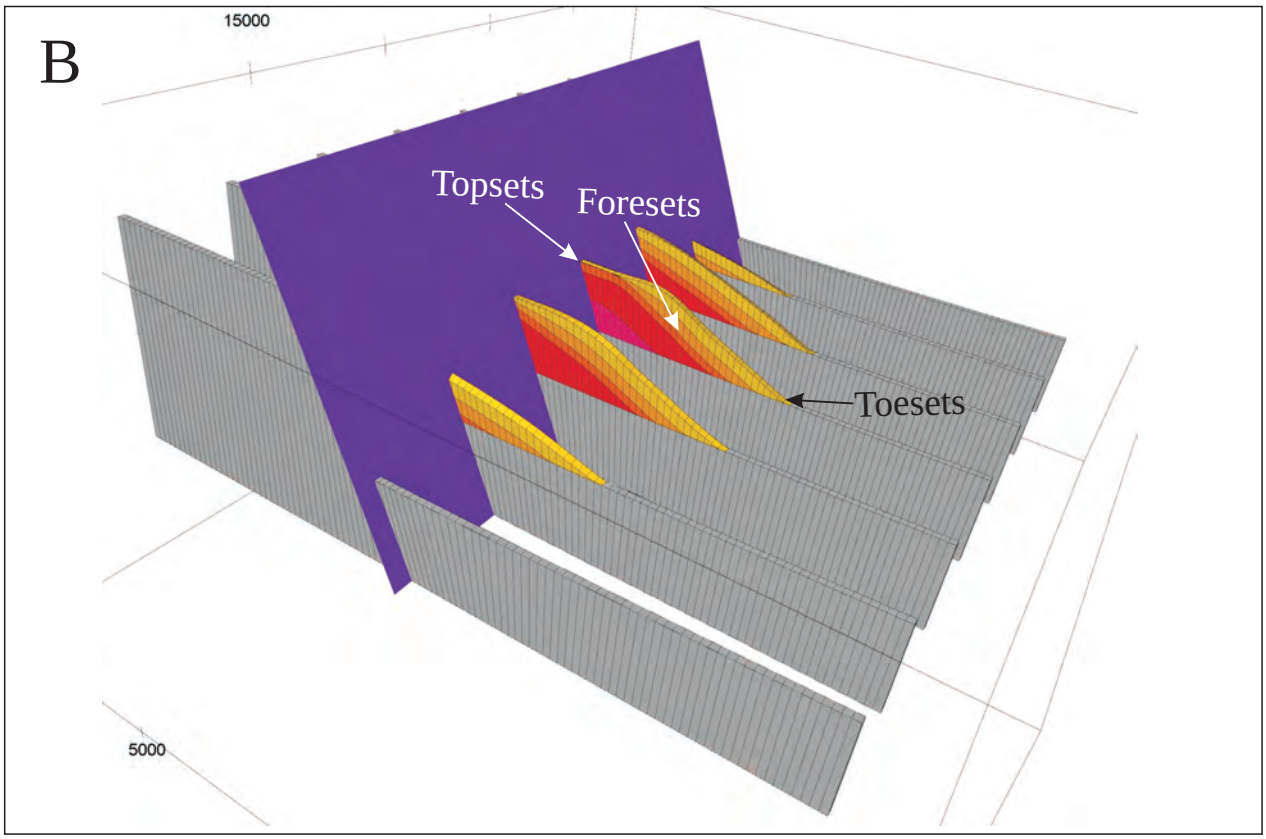

Figure 4.1: Gilbert delta comparison figure A.) A field example (Kerinitis Delta, Corinth Rift) B.) RMS model from experiment 10 (Gilbert delta exeriment)

estimation job, a horizon modeling job and an export job. Surfaces remaining flat did not undergo fault displacement estimation. All horizons that were extracted from these nested workflows were combined into a single horizon model which could then be used as input to build a 3D grid.

- 3D grid integration: When visualizing these experiments in 3D, the gridding process in RMS is fundamental. Filtering the cells in the grid to appear as slices allows for the most efficient and simple display of 3D data without the need to show horizon contour maps for each displaced horizon in every experiment.
- Complicated geological situations: The modeling of the relay ramp, the multi-fault displacement experiment, asymmetric faults and the most intricate Gilbert delta were for the most part successful. These structural environments were modeled and visualized in three dimensions and the techniques used have established an extensive list of potential structural and sedimentological situations to be modeled in the future.

4.3 Improvements to the software

4.3.1 Horizon displacement problem

Experiments were conducted so that all the changes in displacement were controlled by the manipulation of the displacement point sets. This modeling method was chosen to fix the problem with applying multiple displacements to one horizon that was originally discussed in Section 2.4.5 and may have been the source of multiple modeling inaccuracies in Experiment 3, 6 and 7. By fixing this bug in RMS the workflows used for the modeling in this thesis and other reservoir models would be simplified and the results may have been more geologically accurate.

- Experiment 3: As discussed in Section 3.3 and displayed in Figure 3.3A and B, when the basic modeling techniques were not altered, the reverse drag in this experiment was an illusion created from the shape of the first displaced horizon which controlled the modeling of all zones which were later deposited. This is a problem with the functionality of RMS which is caused by the inability to displace a horizon multiple times (Section 2.4.5). This issue with modeling was resolved by applying a surface-surface operation to each horizon interaction to eliminate surface X relative to Y,

where X>Y. These operations were applied to the horizon data that was exported from the nested workflows before it was input into the horizon model all job.

- Experiment 6: In this experiment, despite the inputs for reverse drag being consistent, the resulting synrift packages show a decrease in reverse drag. The only possible explanation for this occurrence is that decreasing fault displacement amounts are influencing the reverse drag independently from the horizon models input by the user. As this program is being used outside the limits of its typically intended functionality for this study, this is not likely to be a problem that most users will experience, but it might be fixed if the problem discussed in Section 2.4.5 is resolved.
- Experiment 7: This decrease in reverse drag appears to be a function of the fault asymmetry and is most inconsistent nearest to the point of maximum displacement. This is likely to be the same program error causing the problems with Experiment 6.

4.3.2 Fault order in RMS

During the modeling of these experiments the following questions arose: Do faults displace in a specific order? If there is an order what is it? Within the software the order of fault movement cannot be defined. When referring to the order in which faults displace either the faults all occur simultaneously when modeled, or in the order in which they are imported into RMS.

For Experiments 8 and 9 there is more than one fault undergoing displacement. Experiment 9 shows a problem with the footwall uplift of both Faults 2 and 3, where it seems the uplift is localized near to the fault; Fault 1 does not have this issue. These observations could suggest that fault 1 occurred first and did influence the way Faults 2 and 3 were modeled.

The fault order problem in RMS was not solved and it is unclear whether or not this might have influenced the shape of synrift infill patterns of the models. More investigation into this modeling problem is necessary to discover how the order of faults is determined in RMS. This problem is not exclusive to the functionality of RMS but it is also geologically significant to understand what effect the faulting order might have on the subsequent synrift sedimentation patterns.

4.3.3 Compaction

Another improvement to consider is the application of sediment compaction when one zone is buried by one or more other zones in the experiment. In a general sense, sediment undergoes subsidence and subsequent burial where compaction occurs (Allen and Allen, 1990). Compaction considers an exponential decrease of porosity with depth (Allen and Allen, 1990). Compaction can be quantified by calculating the porosity of a sediment unit at depth z using porosity before burial, the lithology (density) of both the compacted sediment and overburden sediment and the depth of compacted sediment (Allen and Allen, 1990).

Although this equation is fairly simple to solve, the results are not easily quantifiable in a three dimensional sense and it is very difficult to apply to each horizon that undergoes some form of compaction. To resolve the compaction problem a knowledge of porosity and lithology is required, and in the case of these synthetic models both parameters were not considered. If porosity and lithology were estimated the only way of applying this to our models without a computer program would be to take a maximum and minimum value for compaction and apply the average to the entire horizon by adding a value of X meters to the displacement point set of the compacted Horizon. A computer program could calculate this for each zone, and it is also possible that this equation could be incorporated into the calculator function in RMS with the help of Roxar.

4.3.4 Easy Parameter Manipulation

In RMS the manipulation of parameters is not simple. For example, to change the reverse drag (correction range in RMS) in a Structural Model it is necessary to open every horizon model contained in the structural model. Then the value for each horizon in each horizon model can be altered. There is a similar situation for manipulating fault parameters. This could easily be simplified by introducing an interface or plug-in that allows these parameters to be altered by entering a single value and applying it to the entire horizon, horizon model, structural model or everything contained in the RMS file.

4.4 Geological Improvements

There are several ways that the Gilbert delta model could be improved for geological accuracy:

- Incorporate an incised valley into the footwall side of the system
- Improve the modeling of toesets so they terminate in a more distal position, and more horizontally. This can be accomplished by horizon point manipulation.
- Instead of two large displacement events, it could be worth utilizing multiple smaller scale displacement phases to see the impact on subsequent Gilbert delta synrift sedimentation.
- Incorporate a variation in sea level over time.

The relay structure experiment shows how constant fault movement allows the accumulation of synrift sedimentation on the relay and near its corresponding faults. The accuracy of this model could improve through modeling the evolution of the structure from start to finish as follows:

- Two faults are present but do not interact.
- Fault growth occurs, no interaction
- Fault growth with interaction and formation of shallow relay structure
- Fault growth furthers the development and subsequent steepening of the relay
- Introduction of a third fault which breaches the relay ramp

Concepts of relay structure formation, evolution and breaching can be found in Larsen, 1988; Peacock and Sanderson, 1991, 1994; Childs et al., 1995; Peacock, 2002; Athmer and Luthi, 2011; Long and Imber, 2011; Conneally et al., 2014 and references within.

4.5 Real World Application

The experiments in this thesis generate 3D synrift assemblages that could improve the interpretation of synrift sedimentation on seismic data. Comparing seismic to these experiments might help the user to understand the evolution and geometries of synrift patterns in extensional tectonic settings.

When considering the application of thesis to the petroleum industry it is important to consider the more structurally complex experiments.

- Relay structures (experiment 8): As relay structures create accommodation space they are generally a point of interest for sediment accumulation associated with oil

and gas plays (Athmer and Luthi, 2011). For example in the Norwegian North Sea the deposition of the Shadd turbidite complex is controlled by relay ramp architectures between the Dønna Terrace and Nordland Ridge (Athmer and Luthi, 2011). The Magnus area of the UK North Sea and the Murchison-Statfjord North Fault Zone of the Norwegian North Sea are more examples of a relay ramp controlling the deposition of sediment in petroleum systems (Young et al., 2001; Athmer and Luthi, 2011).

By modeling a displacing relay structure, as is completed in this thesis, a greater understanding of these structures has been accomplished. In the further works section of this report is has been discussed that the relay ramp could be modeled with more geologic accuracy by taking into account the entire evolution of the structure from start to finish. To begin this evolution two faults would displace where there is no area of overlap. The faults will grow and in the zone of overlap a relay will begin to form as seen in the Murchison-Statfjord North Fault Zone (Young et al., 2001; Athmer and Luthi, 2011). The relay structure will steepen and elongate with further fault growth until a point where it reaches its maximum strain. At this point the relay would breach or fail with the formation of a third fault that links together the original two relay forming faults (Murchison-Statfjord North Fault Zone; Young et al., 2001; Athmer and Luthi, 2011). The completion of this simplified model help to gain a further knowledge of relay ramp formation and sediment infill. Once a baseline model is developed, the geometries observed in actual fields can be incorporated into the model for increased field accuracy. These models could also be used to forward model sediment deposition of submarine fans using numerical modeling techniques (Meiburg et al., 2015).

- Multiple faults (experiment 9): The problems associated with fault order application in RMS were problematic. If these bugs could be resolved and a specific user defined fault order is incorporated into RMS this experiment could be very useful. As an example, the North Sea's structural history does not occur in one time period but evolves in phases (Gibbs, 1984). The Gulf of Corinth (Greece) also has a continuously evolving structural history that cannot be modeled in one single application of faults (Skourtsos and Kranis, 2009; Ford et al., 2013). If the fault

order problem could be resolved RMS would be capable of modeling synrift sedimentation as extensional basins evolve.

- Gilbert delta (experiment 10): Coarse-grained, sand-rich, high net-to-gross deposits of Gilbert deltas can be important and volumetrically significant hydrocarbon reservoirs in settings where sediment deposition occurs with fault activity (i.e. synrift intervals). Well known examples of Gilbert deltas in the Norwegian North Sea include the Huldra, Oseberg and Vesselfrikk fields, where the Toarcian-Bajocian age Oseberg Formation can form significant parts of the Brent Group reservoir (Færseth and Ravnås, 1998; Ravnås and Steel, 1998; Leren, 2007). Understanding the formation, evolution and interaction of Gilbert deltas with existing topography, and the effects of continued faulting on Gilbert delta development has clear implications for hydrocarbon exploration and production. The techniques used in this thesis prove that RMS is capable of simulating the evolution of a Gilbert delta (Figure 4.1). Enhancing the geological accuracy of these modeling techniques (as mentioned in section 4.4) can improve the understanding of deltaic systems in a three dimensional sense. In future experiments it may be possible to apply field-specific fault and fault block geometries to experiments in RMS. The Vouraikos and Kerinitis deltas were chosen as the base model for this thesis because they run fairly straight; the models can also be manipulated so that the sourcing fluvial channel of the delta does not run perpendicular to the fault plane. Such experiments/ reservoir models could be used to forward model and predict potential facies distributions in order to better understand how faulting effects the reservoir architecture, net-to-gross and reservoir connectivity. Fluid production simulation can also be applied to these models to increase the understanding of the Gilbert delta field development through time.

Chapter 5

Conclusions and Recommendations

5.1 Conclusions

1. RMS can be used successfully in the synthetic modeling of synrift sedimentation and for the modeling of more complicated geological environments.
2. Workflows were effectively developed using Syahrul's (2014) thesis as a framework to show an evolution of synrift deposition through time.
3. The modeling of synrift sedimentation associated with normal faulting was completed in order to discover the functionality within RMS and to understand if synthetic modeling can be carried out honouring geological concepts. The results in all experiments concluded that:
    a. Displacement point sets can be used to accurately apply fault displacement where the point of maximum displacement is centered on the fault, and displacement gradually decreases towards the tiplines. This concept is geologically accurate according to Barnett et al. (1987).
    b. Concentric ellipses representing how displacement occurs across a fault surface can be displayed and manipulated in RMS and are true to geological studies (Barnett et al., 1987).
    c. Synrift sedimentation can be accurately modeled to represent a rift basin where sedimentation is greater than or equal to fault displacement through the use of displaced and flat surfaces (Einsele, 2000). This is accomplished through the manipulation of horizon points in RMS. The software is also capable of accurately modeling specific geomorphologies such as a Gilbert delta (Ford et al., 2009; Backert et al., 2010; Gobo, 2014).
4. The synrift sedimentation patterns that resulted from ten synthetic faulting experiments showed:
    a. A change in fault length and a changing reverse drag influence the lateral distribution of synrift deposits parallel with the fault surface.
    b. In the direction perpendicular to the fault surface the reverse drag distance affects the lateral distribution and thickness of the synrift sediment package.
    c. The displacement magnitude on the fault influences the thickness of synrift sedimentation in the Z direction (depth).

5. The application of reverse drag was not consistent with RMS inputs for three experiments (3, 6 and 7). The inconsistencies between the input value and the displayed reverse drag found in experiment 3 were solved by applying a surface-surface operation functionality of RMS in order to resolve horizon interactions. The same inconsistencies (as those in experiment 3) were also found in Experiments 6 and 7 and were not satisfactorily resolved.
6. It is not clear in RMS how multiple faults in an experiment are displaced relative to one another. There was evidence in experiment 9 that something was modeled incorrectly with the footwall uplift of both Faults 2 and 3. It is unclear if this fault ordering issue is the cause of the footwall uplift inconsistencies or if it could cause other problems with modeling other scenarios.
7. The accuracy of the experiments can be improved by integrating associated compaction with the synrift deposits. There is no simple way of carrying this through in the current version of RMS.
8. The results found in these ten experiments, along with the standardized modeling workflow can provide essential information on the distribution of synrift sediments. The 3D models can be used to understand sediment packages associated with fault displacement and can aid in the interpretation of seismic and field data. This work can also be further developed to assist the petroleum industry in understanding basin evolution, synrift sediment prediction, predicting lateral distribution of reservoirs and simulating fluid production.

5.2 Recommendations

- For improved geological modeling:
    - Gilbert Delta
        - Toesets: These can be modeled with more geological accuracy by importing more points into each Gilbert delta horizon point set. The result of this manipulation is toesets that continue distally as observed in the Kerinitis and Vouraikos deltas of the Corinth Rift (Ford et al., 2009; Backert et al., 2010).
        - Incised Valley: On the footwall side of the fault an incised valley could be modeled by applying more points into Horizon A to create a v-

shaped valley at approximately sea level (Ford et al., 2009; Backert et al., 2010; Gobo, 2014). The points could be assembled based on shapes from specific incised valleys found in the Gulf of Corinth (Ford et al., 2009; Backert et al., 2010; Gobo, 2014).

        - Decrease displacement amount and increase number of displacements: For increased geological accuracy more frequent smaller phases of displacement can be created. Each displacement could be associated with a single sedimentation package for further accuracy (Ford et al., 2009; Backert et al., 2010; Gobo, 2014).
        - Sea level change: As sea level through time is often not constant, the Gilbert delta model could be improved by incorporating sedimentation with a rise in sea level and erosion with a fall in sea level (Jervey, 1988; Ravnås and Steel, 1998; Gobo, 2014).
    - Relay ramp structure
        - Model all phases of development from pre-fault interaction to relay ramp breach.
    - Model structural scenarios incorporating transfer faults
    - Consider compaction
    - Investigate the order of fault displacement in RMS.
- Simplify modeling workflow
    - This is only possible if RMS fixes the horizon modeling fault from Section 2.4.5.

References

Allen, P., & Allen, J. (1990) *Basin Analysis: Principles & Applications:* Oxford, London, Edinburgh, Boston, Melbourne: Blackwell Scientific.

Athmer, W., & Luthi, S. M. (2011). The effect of relay ramps on sediment routes and deposition: A review. *Sedimentary Geology, 242*(1-4), 1–17. http://doi.org/10.1016/j.sedgeo.2011.10.002

Backert, N., Ford, M., & Malartre, F. (2010). Architecture and sedimentology of the Kerinitis Gilbert-type fan delta, Corinth Rift, Greece. *Sedimentology, 57*(2), 543–586. http://doi.org/10.1111/j.1365-3091.2009.01105.x

Barnett, J. A. M., Mortimer, J., Rippon, J. H., Walsh, J. J., & Watterson, J. (1987). Displacement geometry in the volume containing a single normal fault. *American Association of Petroleum Geologists Bulletin, 71*(8), 925–937. http://doi.org/10.1306/948878ED-1704-11D7-8645000102C1865D

Chadwick, R. A. (1986). Extension tectonics in the Wessex Basin, southern England. *Journal of the Geological Society, 143*(3), 465–488. http://doi.org/10.1144/gsjgs.143.3.0465

Childs, C., Easton, S. J., Vendeville, B. C., Jackson, M. P. A., Lin, S. T., Walsh, J. J., & Watterson, J. (1993). Kinematic analysis of faults in a physical model of growth faulting above a viscous salt analogue. *Tectonophysics, 228*(3-4), 313–329. http://doi.org/10.1016/0040-1951(93)90346-L

Childs, C., Nicol, A., Walsh, J. J., & Watterson, J. (2002). The growth and propagation of synsedimentary faults. *Journal of Structural Geology, 25*(4), 633–648. http://doi.org/10.1016/S0191-8141(02)00054-8

Childs, C., Watterson, J., & Walsh, J. J. (1995). Fault overlap zones within developing normal fault systems. *Journal of the Geological Society, 152*, 535–549. http://doi.org/10.1144/gsjgs.152.3.0535

Cohen, H. A., Dart, C. J., Akyuz, H. S., & Barka, A. (1995). Syn-rift sedimentation and structural development of the Gediz and Buyuk Menderes graben, western Turkey. *Journal of the Geological Society, 152*(4), 629–638.

Conneally, J., Childs, C., & Walsh, J. J. (2014). Contrasting origins of breached relay zone geometries. *Journal of Structural Geology, 58*, 59–68. http://doi.org/10.1016/j.jsg.2013.10.010

Cowie, P. A., & Scholz, C. H. (1992). Physical explanation for the displacement-length relationship of faults using a post-yield fracture mechanics model. *Journal of Structural Geology, 14*(10), 1133–1148. http://doi.org/10.1016/0191-8141(92)90065-5

Dawers, N. H., Anders, M. H., & Scholz, C. H. (1993). Growth of normal faults: displacement-length scaling. *Geology, 21*(12), 1107–1110.

Einsele, G. (2000). *Sedimentary Basins- Evolution, Facies, and Sediment Budget* (2nd ed.). Heidelberg, Germany: Springer.

Færseth, R., and R. Ravnås, (1998) Evolution of the Oseberg Fault-Block in context of the northern North Sea structural framework: *Marine and Petroleum Geology*, *15*(5), 467–490, doi:10.1016/S0264-8172(97)00046-9.

Ford, M., Williams, E. A., Malartre, F., & Popescu, S.-M. (2009). Stratigraphic architecture, sedimentology and structure of the Vouraikos Gilbert-type fan delta, Gulf of Corinth, Greece. *Sedimentary Processes, Environments and Basins*, (1), 49–90. http://doi.org/10.1002/9781444304411.ch4

Ford, M., Rohais, S., Williams, E., Bourlange, S., Jousselin, D., Backert, N., & Malartre, F. (2013). Tectono-sedimentary evolution of the western Corinth rift (Central Greece). *Basin Research, 25*(1), 3–25. http://doi.org/10.1111/j.1365-2117.2012.00550.x

Fossen, H. (2010). *Structural Geology* (1st ed.). Edinburgh: Cambridge University Press.

Fugelli, E., & Olsen, T. (2007) Delineating confined slope turbidite systems offshore mid-Norway: The Cretaceous deep-marine Lysing Formation. *AAPG Bulletin, 91*(11), 1577-1601. http://doi.org/ 10.1306/07090706137

Gawthorpe, R. L., Fraser, A. J., & Collier, R. E. (1994). Sequence stratigraphy in active extensional basins: implications for the interpretation of ancient basin-fills. *Marine and Petroleum Geology, 11*(6), 642–658.

Gawthorpe, R. L., Jackson, C. a L., Young, M. J., Sharp, I. R., Moustafa, A. R., & Leppard, C. W. (2003). Normal fault growth, displacement localization and the evolution of normal fault populations: The Hammam Faraun fault block, Suez rift, Egypt. *Journal of Structural Geology, 25*(6), 883–895. http://doi.org/10.1016/S0191-8141(02)00088-3

Gawthorpe, R. L., & Leeder, M. R. (2000). Tectono-sedimentary evolution of active extensional basins. *Basin Research, 12*, 195–218. http://doi.org/10.1046/j.1365-2117.2000.00121.x

Gibbs, A. D. (1984). Structural evolution of extensional basin margins. *Journal of the Geological Society, 141*(4), 609–620. http://doi.org/10.1144/gsjgs.141.4.0609

Gibson, J. R., Walsh, J. J., & Watterson, J. (1989). Modelling of bed contours and cross-sections adjacent to planar normal faults. *Journal of Structural Geology, 11*(3), 317–328. http://doi.org/10.1016/0191-8141(89)90071-0

Gilbert, G.H. (1885). The topographic features of lake shores. *United States Geological Survey, Annual Report, 5*, 69-123.

Gobo, K. (2014). *Development of Gilbert-type deltas: sedimentological case studies from the Plio-Pleistocene of Corinth Rift, Greece.* University of Bergen.

Gupta, S., Cowie, P. A., Dawers, N. H., & Underhill, J. R. (1998). A mechanism to explain rift-basin subsidence and stratigraphic patterns through fault-array evolution. *Geology, 26*(7), 595–598. http://doi.org/10.1130/0091-7613(1998)026<0595:AMTERB>2.3.CO

Gupta, S., Underhill, J. R., Sharp, I. R., & Gawthorpe, R. L. (1999). Role of fault interactions in controlling synrift sediment dispersal patterns: Miocene, Abu Alaqa Group, Suez Rift, Sinai, Egypt. *Basin Research, 11*(2), 167–189.

Hamblin, W. . (1965). Origin of "Reverse Drag" on the downthrown side of normal faults. *Geological Society of America Bulletin, 76*(10), 1145–1164.

Hollund, K., & Mostad, P. (2002). Havana - a fault modeling tool. *Norwegian Petroleum Society Special Publications, 11*(October), 157–171. http://doi.org/10.1016/S0928-8937(02)80013-3

Holmes, A. (1965). *Principles of Physical Geology* (2nd ed.). London, UK: Thomas Nelson.

Jervey, M. T. (1988). Quantitative geological modeling of siliciclastic rock sequences and their seismic expression. *SEPM Special Publications, 42*(42), 47–69. http://doi.org/10.2110/pec.88.01.0047

Larsen, P.-H. (1988). Relay structures in a Lower Permian basement-involved extension system, East Greenland. *Journal of Structural Geology, 10*(1), 3–8. http://doi.org/10.1016/0191-8141(88)90122-8

Leeder, M. R. (2012). *Sedimentology and Sedimentary Basins: From Turbulence to Tectonics* (2nd ed.). West Sussex, UK: Wiley-Blackwell.

Leeder, M. R., & Gawthorpe, R. L. (1987). Sedimentary models for extensional tilt-block/half-graben basins. *Geological Society, London, Special Publications, 28*(1), 139–152.

Leith, C. K. (1923). *Structural Geology*. New York: Holt.

Long, J. J., & Imber, J. (2011). Geological controls on fault relay zone scaling. *Journal of Structural Geology, 33*(12), 1790–1800. http://doi.org/10.1016/j.jsg.2011.09.011

McLeod, A., Underhill, J. R., Davies, S. J., & Dawers, N. H. (2002). The influence of fault array evolution on synrift sedimentation patterns: Controls on deposition in the Strathspey-Brent-Statfjord half graben, northern North Sea. *American Association of Petroleum Geologists Bulletin, 86*(6), 1061–1093.

Meiburg, E., Barbara, S., Radhakrishnan, S., & Barbara, S. (2015). *Modeling Gravity and Turbidity Currents: Computational Approaches and Challenges, 67*(July), 1–23. http://doi.org/10.1115/1.4031040

Nemec, W., & Steel, R. J. (1988). What is a fan delta and how do we recognize it? *Fan Deltas; Sedimentology and Tectonic Settings.* 3–13.

Nicol, A., Walsh, J. J., Watterson, J., & Underhill, J. R. (1997). Displacement rates of normal faults. *Nature, 390*(6656), 157–159. http://doi.org/10.1038/36548

Peacock, D. C. P. (1991). Displacements and segment linkage in strike-slip fault zones. *Journal of Structural Geology, 13*(9), 1025–1035. http://doi.org/10.1016/0191-8141(91)90054-M

Peacock, D. C. P. (2002). Propagation, interaction and linkage in normal fault systems. *Earth-Science Reviews, 58*(121-142). http://doi.org/10.1016/S0012-8252(01)00085-X

Peacock, D. C. P., Knipe, R. J., & Sanderson, D. J. (2000). Glossary of normal faults. *Journal of Structural Geology, 22,* 291–305. http://doi.org/10.1016/S0191-8141(00)80102-9

Peacock, D. C. P., & Sanderson, D. J. (1991). Displacements, segment linkage and relay ramps in normal fault zones. *Journal of Structural Geology, 13*(6), 721–733. http://doi.org/10.1016/0191-8141(91)90033-F

Peacock, D. C. P., & Sanderson, D. J. (1994). Geometry and development of relay ramps in normal fault systems. *American Association of Petroleum Geologists Bulletin, 78*(2), 147–165. http://doi.org/10.1306/BDFF9046-1718-11D7-8645000102C1865D

Ragan, D. M. (2009). Structural Geology: An Introduction to Geotechnical Techniques (4th ed.). New York: Cambridge University Press.

Ramsey, J. G., & Huber, M. (1980). *The Techniques of Modern Structural Geology Volume 2: Folds and Fractures* (6th ed., Vol. 2). London, UK: Academic Press.

Råvnas, R., Nøttvedt, A., Steel, R. J., & Windelstad, J. (2000). Synrift sedimentary architectures in the Northern North Sea. *Geological Society, London, Special Publications, 167*(1), 133–177. http://doi.org/10.1144/GSL.SP.2000.167.01.07

Råvnas, R., & Steel, R. J. (1998). Architecture of marine rift-basin successions. *American Association of Petroleum Geologists Bulletin, 82*(1), 110–146. http://doi.org/10.1306/1D9BC3A9-172D-11D7-8645000102C1865D

Rippon, J. H. (1985). Contoured patterns of the throw and hade of normal faults in the Coal Measures (Westphalian) of north-east Derbyshire. *Proceedings of the Yorkshire Geological Society, 45*(3), 147–161. http://doi.org/10.1144/pygs.45.3.147

Roxar. (2013). RMS Help. Retrieved from http://127.0.0.1:49342/rms/en_gb/helpsys/docs/user/other/entry.html

Roxar. (2014). *Structural Uncertainty and Uncertainty Management in RMS*.

Schlische, R. W. (1995). Geometry and origin of fault-related folds in extensional settings. *American Association of Petroleum Geologists Bulletin, 79*(11), 1661–1678. http://doi.org/10.1306/7834DE4A-1721-11D7-8645000102C1865D

Scholz, C. H., & Cowie, P. A. (1990). Determination of total strain from faulting using slip measurements. *Nature, 346*(6287), 837–839. http://doi.org/10.1038/346837a0

Selley, R. C. (2000). *Applied Sedimentology* (2nd ed.). San Diego, CA: Academic Press.

Skourtsos, E., & Kranis H. (2009) Structure and evolution of the western Corinth Rift, through new field data from the Northern Peloponnesus: *Geological Society, London, Special Publications*, *321*(1), 119–138, doi:10.1144/SP321.6.

Syahrul, R. (2014). *Fault Controlled Sedimentation: A Case Study of the Kerpini Fault, Greece*. University of Stavanger.

Trudgill, B. D. (2002). Structural controls on drainage development in the Canyonlands grabens of southeast Utah. *American Association of Petroleum Geologists Bulletin*, *86*(6), 1095–1112. http://doi.org/10.1306/61EEDC2E-173E-11D7-8645000102C1865D

Twiss, R. J., & Moores, E. M. (2007). *Structural Geology* (2nd ed.). New York: W.H. Freeman and Company. http://doi.org/10.1017/s0016756808004627

Walsh, J. J., Bailey, W. R., Childs, C., Nicol, A., & Bonson, C. G. (2003). Formation of segmented normal faults: A 3-D perspective. *Journal of Structural Geology, 25*, 1251–1262. http://doi.org/10.1016/S0191-8141(02)00161-X

Walsh, J. J., & Watterson, J. (1987). Distributions of cumulative displacement and seismic slip on a single normal fault surface. *Journal of Structural Geology, 9*(8), 1039–1046. http://doi.org/10.1016/0191-8141(87)90012-5

Walsh, J. J., & Watterson, J. (1988). Analysis of the relationship between displacements and dimensions of faults. *Journal of Structural Geology*, *10*(3), 239–247. http://doi.org/10.1016/0191-8141(88)90057-0

Walsh, J. J., & Watterson, J. (1989). Displacement gradients on fault surfaces. *Journal of Structural Geology, 11(*3), 307–316. http://doi.org/10.1016/0191-8141(89)90070-9

Walsh, J. J., & Watterson, J. (1990). New methods of fault projection for coalmine planning. *Proceedings of the Yorkshire Geological Society*, *42*(2), 209–219.

Watterson, J. (1986). Fault dimensions, displacements and growth. *Pure and Applied Geophysics, 124*(1-2), 365–373. http://doi.org/10.1007/BF00875732

Young, M., Gawthorpe, R., & Hardy, S. (2001). Growth and linkage of a segmented normal fault zone; the Late Jurassic Murchison-Statfjord North Fault, Northern North Sea. *Journal of Structural Geology 23*(12), 1933-1952. http://doi.org/10.1016/S0191-8141(01)00038-4

Appendix

Appendix 1: Horizon and fault .txt inputs

Experiment 1					
Horizons A-E			Fault		
X	Y	Z	X	Y	Z
0	0	1500	10000	8000	4000
0	10000	1500	10000	3000	-1000
10000	10000	1500	3000	3000	-1000
10000	0	1500	3000	8000	4000
0	0	1500	10000	8000	4000

Experiment 2					
Horizon A-E			Fault		
X	Y	Z	X	Y	Z
0	0	1500	10000	8000	4000
0	10000	1500	10000	3000	-1000
10000	10000	1500	3000	3000	-1000
10000	0	1500	3000	8000	4000
0	0	1500	10000	8000	4000

Experiment 3					
Horizons A-E			Fault		
X	Y	Z	X	Y	Z
0	0	1500	10000	8000	4000
0	10000	1500	10000	3000	-1000
10000	10000	1500	3000	3000	-1000
10000	0	1500	3000	8000	4000
0	0	1500	10000	8000	4000

Experiment 4					
Horizons A-E			Fault		
X	Y	Z	X	Y	Z
0	0	1500	10000	8000	4000
0	10000	1500	10000	3000	-1000
10000	10000	1500	3000	3000	-1000
10000	0	1500	3000	8000	4000
0	0	1500	10000	8000	4000

Experiment 5					
Horizons A-E			Fault		
X	Y	Z	X	Y	Z
0	0	1500	10000	8000	4000
0	10000	1500	10000	3000	-1000
10000	10000	1500	3000	3000	-1000
10000	0	1500	3000	8000	4000
0	0	1500	10000	8000	4000

Experiment 6					
Horizons A-E			Fault		
X	Y	Z	X	Y	Z
0	0	1500	10000	8000	4000
0	10000	1500	10000	3000	-1000
10000	10000	1500	3000	3000	-1000
10000	0	1500	3000	8000	4000
0	0	1500	10000	8000	4000

Experiment 7					
Horizons A-E			Fault		
X	Y	Z	X	Y	Z
0	0	1500	10000	8000	4000
0	10000	1500	10000	3000	-1000
10000	10000	1500	3000	3000	-1000
10000	0	1500	3000	8000	4000
0	0	1500	10000	8000	4000

Experiment 8								
Horizons A-E			Fault 1			Fault 2		
X	Y	Z	X	Y	Z	X	Y	Z
0	0	1500	1000	11000	-1000	8550	12000	-1000
0	10000	1500	10000	11000	-1000	17550	12000	-1000
10000	10000	1500	10000	5500	4000	17550	6500	4000
10000	0	1500	1000	5500	4000	8550	6500	4000
0	0	1500	1000	11000	-1000	8550	12000	-1000

Experiment 9											
Horizons A-E			Fault 1			Fault 2			Fault 3		
X	Y	Z	X	Y	Z	X	Y	Z	X	Y	Z
0	0	1500	2000	15000	-1000	1000	10500	-1000	11000	10500	-1000
0	10000	1500	17550	15000	-1000	9000	10500	-1000	19000	10500	-1000
10000	10000	1500	17550	9500	4000	9000	5500	4000	19000	5500	4000
10000	0	1500	2000	9500	4000	1000	5500	4000	11000	5500	4000
0	0	1500	2000	15000	-1000	1000	10500	-1000	11000	10500	-1000

Appendix 2: All experiment modeling input data

Modelling Data Table Part 1							
Experiment 1: All Parameters Constant							
	Displaced Horizons	Flat Horizons	Fault Length (m)	Structural Model Displacement (m)	Total Displacement (m)	Reverse Drag (m)	HW:FW Displacment Ratio
Structural Model 1	A	B	6000	100	100	3000	0.5
Structural Model 2	A, B	C	6000	100	200	3000	0.5
Structural Model 3	A, B, C	D	6000	100	300	3000	0.5
Structural Model 4	A, B, C, D	E	6000	100	400	3000	0.5
Experiment 2: Reverse Drag Decreases							
	Displaced Horizons	Flat Horizons	Fault Length (m)	Structural Model Displacement (m)	Total Displacement (m)	Reverse Drag (m)	HW:FW Displacment Factor
Structural Model 1	A	B	6000	100	100	A:3000	0.5
Structural Model 2	A, B	C	6000	100	200	A:3000, B: 2500	0.5
Structural Model 3	A, B, C	D	6000	100	300	A:3000, B: 2500, C:2000	0.5
Structural Model 4	A, B, C, D	E	6000	100	400	A:3000, B: 2500, C:2000, D:1500	0.5
Experiment 3: Reverse Drag Increases							
Experiment 3	Displaced Horizons	Flat Horizons	Fault Length (m)	Structural Model Displacement (m)	Total Displacement (m)	Reverse Drag (m)	HW:FW Displacment Factor
Structural Model 1	A	B	6000	100	100	A: 1500	0.5
Structural Model 2	A, B	C	6000	100	200	A: 1500, B: 2000	0.5
Structural Model 3	A, B, C	D	6000	100	300	A: 1500, B: 2000, C:2500	0.5
Structural Model 4	A, B, C, D	E	6000	100	400	A: 1500, B: 2000, C:2500, D:3000	0.5
Experiment 4							
	Displaced Horizons	Flat Horizons	Fault Length (m)	Structural Model Displacement (m)	Total Displacement (m)	Reverse Drag (m)	HW:FW Displacment Factor
Structural Model 1	A	B	2000	100	100	3500	0.5
Structural Model 2	A, B	C	4500	100	200	3500	0.5
Structural Model 3	A, B, C	D	6000	100	300	3500	0.5
Structural Model 4	A, B, C, D	E	7000	100	400	3500	0.5
Experiment 5							
	Displaced Horizons	Flat Horizons	Fault Length (m)	Structural Model Displacement (m)	Total Displacement (m)	Reverse Drag (m)	HW:FW Displacment Factor
Structural Model 1	A	B	6000	50	50	3000	0.5
Structural Model 2	A, B	C	6000	100	150	3000	0.5
Structural Model 3	A, B, C	D	6000	150	300	3000	0.5
Structural Model 4	A, B, C, D	E	6000	200	500	3000	0.5
Experiment 6							
	Displaced Horizons	Flat Horizons	Fault Length (m)	Structural Model Displacement (m)	Total Displacement (m)	Reverse Drag (m)	HW:FW Displacment Factor
Structural Model 1	A	B	6000	200	200	3000	0.5
Structural Model 2	A, B	C	6000	150	350	3000	0.5
Structural Model 3	A, B, C	D	6000	100	450	3000	0.5
Structural Model 4	A, B, C, D	E	6000	50	500	3000	0.5
Experiment 7							
	Displaced Horizons	Flat Horizons	Fault Length (m)	Structural Model Displacement (m)	Total Displacement (m)	Reverse Drag (m)	HW:FW Displacment Factor
Structural Model 1	A	B	6000	100	100	3000	0.5
Structural Model 2	A, B	C	6000	100	200	3000	0.5
Structural Model 3	A, B, C	D	6000	100	300	3000	0.5
Structural Model 4	A, B, C, D	E	6000	100	400	3000	0.5

Modelling Data Table Part 2							
Experiment 8 Fault 1							
	Displaced Horizons	Flat Horizons	Fault Length (m)	Structural Model Displacement (m)	Total Displacement (m)	Reverse Drag (m)	HW:FW Displacment Factor
Structural Model 1	A	B	9000	100	100	4500	0.5
Structural Model 2	A, B	C	9000	100	200	4500	0.5
Structural Model 3	A, B, C	D	9000	100	300	4500	0.5
Structural Model 4	A, B, C, D	E	9000	100	400	4500	0.5
Experiment 8 Fault 2							
	Displaced Horizons	Flat Horizons	Fault Length (m)	Structural Model Displacement (m)	Total Displacement (m)	Reverse Drag (m)	HW:FW Displacment Factor
Structural Model 1	A	B	9000	100	100	4500	0.5
Structural Model 2	A, B	C	9000	100	200	4500	0.5
Structural Model 3	A, B, C	D	9000	100	300	4500	0.5
Structural Model 4	A, B, C, D	E	9000	100	400	4500	0.5
Experiment 9 Fault 1							
	Displaced Horizons	Flat Horizons	Fault Length (m)	Structural Model Displacement (m)	Total Displacement (m)	Reverse Drag (m)	HW:FW Displacment Factor
Structural Model 1	A	B	15000	100	100	7000	0.5
Structural Model 2	A, B	C	15000	100	200	7000	0.5
Structural Model 3	A, B, C	D	15000	100	300	7000	0.5
Structural Model 4	A, B, C, D	E	15000	100	400	7000	0.5
Structural Model 5	A, B, C, D, E	F	15000	100	500	7000	0.5
Structural Model 6	A, B, C, D, E, F	G	15000	100	600	7000	0.5
Experiment 9 Fault 2							
	Displaced Horizons	Flat Horizons	Fault Length (m)	Structural Model Displacement (m)	Total Displacement (m)	Reverse Drag (m)	HW:FW Displacment Factor
Structural Model 1	None	A/B	8000	0	0	7000	0.5
Structural Model 2	A/B	C	8000	100	100	7000	0.5
Structural Model 3	A/B	C/D	8000	0	100	7000	0.5
Structural Model 4	A/B, C/D	E	8000	200	200	7000	0.5
Structural Model 5	A/B, C/D	E/F	8000	0	200	7000	0.5
Structural Model 6	A/B, C/D, E/F	G	8000	300	300	7000	0.5
Experiment 9 Fault 3							
	Displaced Horizons	Flat Horizons	Fault Length (m)	Structural Model Displacement (m)	Total Displacement (m)	Reverse Drag (m)	HW:FW Displacment Factor
Structural Model 1	None	A/B	8000	0	0	7000	0.5
Structural Model 2	A/B	C	8000	100	100	7000	0.5
Structural Model 3	A/B	C/D	8000	0	100	7000	0.5
Structural Model 4	A/B, C/D	E	8000	200	200	7000	0.5
Structural Model 5	A/B, C/D	E/F	8000	0	200	7000	0.5
Structural Model 6	A/B, C/D, E/F	G	8000	300	300	7000	0.5

Appendix 3: Displacement graphs and displacement Tables for all experiments

Experiment 1												
Displacement Point Location			Structural Model 1	Structural Model 2		Structural Model 3			Structural Model 4			
X	Y	Z	1A	2A	2B	3A	3B	3C	4A	4B	4C	4D
3000	5500	1500	0	0	0	0	0	0	0	0	0	0
3200	5500	1500	0	0	0	0	0	0	0	0	0	0
3400	5500	1500	15	30	15	45	30	15	60	45	30	15
3600	5500	1500	30	60	30	90	60	30	120	90	60	30
3800	5500	1500	45	90	45	135	90	45	180	135	90	45
4000	5500	1500	55	110	55	165	110	55	220	165	110	55
4200	5500	1500	65	130	65	195	130	65	260	195	130	65
4400	5500	1500	73	146	73	219	146	73	292	219	146	73
4600	5500	1500	78	156	78	234	156	78	312	234	156	78
4800	5500	1500	82	164	82	246	164	82	328	246	164	82
5000	5500	1500	88	176	88	264	176	88	352	264	176	88
5200	5500	1500	90	180	90	270	180	90	360	270	180	90
5400	5500	1500	92	184	92	276	184	92	368	276	184	92
5600	5500	1500	94	188	94	282	188	94	376	282	188	94
5800	5500	1500	96	192	96	288	192	96	384	288	192	96
6000	5500	1500	98	196	98	294	196	98	392	294	196	98
6200	5500	1500	100	200	100	300	200	100	400	300	200	100
6400	5500	1500	100	200	100	300	200	100	400	300	200	100
6600	5500	1500	100	200	100	300	200	100	400	300	200	100
6800	5500	1500	100	200	100	300	200	100	400	300	200	100
7000	5500	1500	98	196	98	294	196	98	392	294	196	98
7200	5500	1500	96	192	96	288	192	96	384	288	192	96
7400	5500	1500	94	188	94	282	188	94	376	282	188	94
7600	5500	1500	92	184	92	276	184	92	368	276	184	92
7800	5500	1500	90	180	90	270	180	90	360	270	180	90
8000	5500	1500	88	176	88	264	176	88	352	264	176	88
8200	5500	1500	82	164	82	246	164	82	328	246	164	82
8400	5500	1500	78	156	78	234	156	78	312	234	156	78
8600	5500	1500	73	146	73	219	146	73	292	219	146	73
8800	5500	1500	65	130	65	195	130	65	260	195	130	65
9000	5500	1500	55	110	55	165	110	55	220	165	110	55
9200	5500	1500	45	90	45	135	90	45	180	135	90	45
9400	5500	1500	30	60	30	90	60	30	120	90	60	30
9600	5500	1500	15	30	15	45	30	15	60	45	30	15
9800	5500	1500	0	0	0	0	0	0	0	0	0	0
10000	5500	1500	0	0	0	0	0	0	0	0	0	0

Experiment 1: Fault Displacement Attribute Data

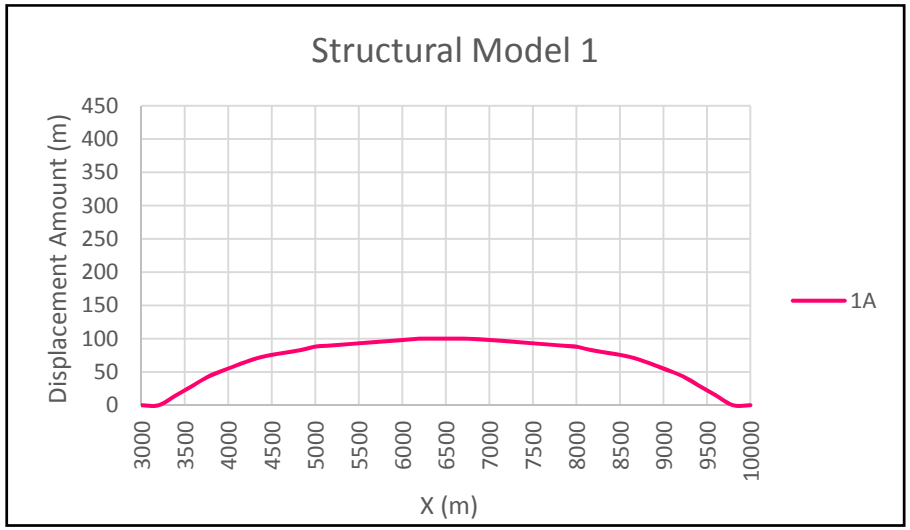

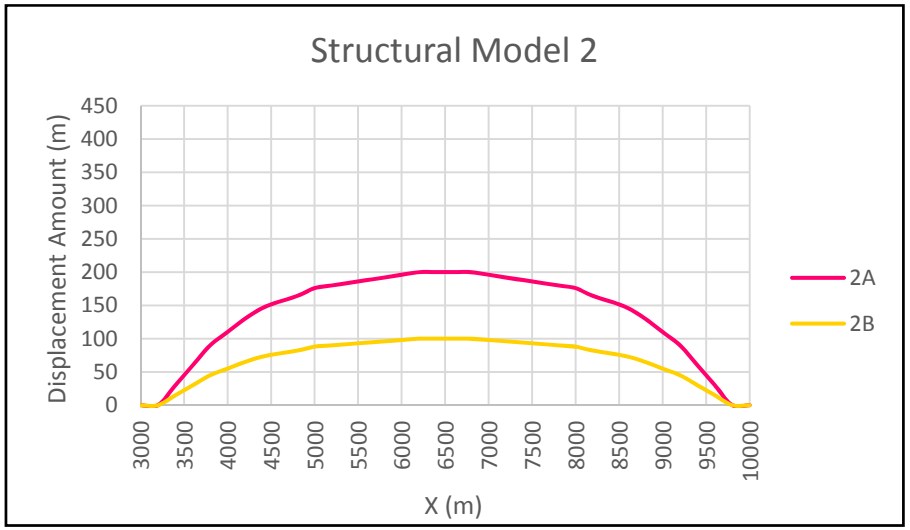

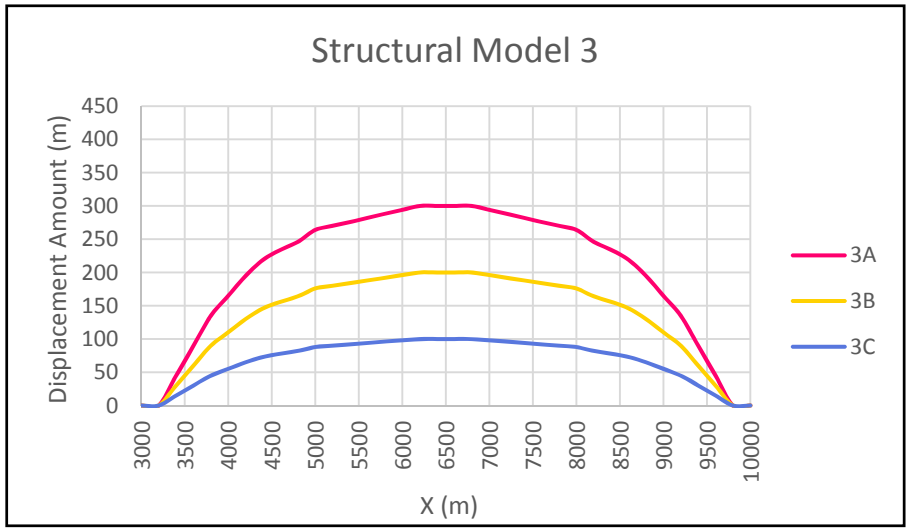

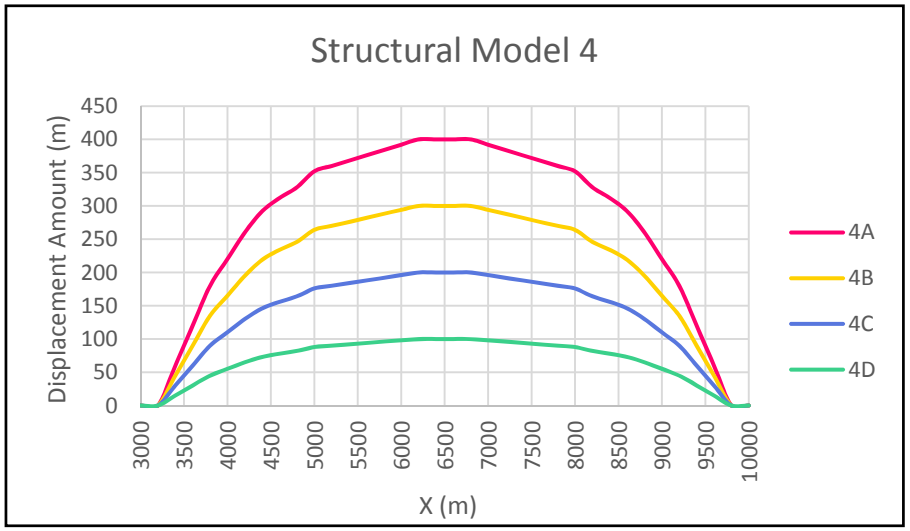

Experiment 2: Fault displacement attribute data linear charts

Experiment 2												
Displacement Point Location			Structural Model 1	Structural Model 2		Structural Model 3			Structural Model 4			
X	Y	Z	1A	2A	2B	3A	3B	3C	4A	4B	4C	4D
3000	5500	1500	0	0	0	0	0	0	0	0	0	0
3200	5500	1500	0	0	0	0	0	0	0	0	0	0
3400	5500	1500	15	30	15	45	30	15	60	45	30	15
3600	5500	1500	30	60	30	90	60	30	120	90	60	30
3800	5500	1500	45	90	45	135	90	45	180	135	90	45
4000	5500	1500	55	110	55	165	110	55	220	165	110	55
4200	5500	1500	65	130	65	195	130	65	260	195	130	65
4400	5500	1500	73	146	73	219	146	73	292	219	146	73
4600	5500	1500	78	156	78	234	156	78	312	234	156	78
4800	5500	1500	82	164	82	246	164	82	328	246	164	82
5000	5500	1500	88	176	88	264	176	88	352	264	176	88
5200	5500	1500	90	180	90	270	180	90	360	270	180	90
5400	5500	1500	92	184	92	276	184	92	368	276	184	92
5600	5500	1500	94	188	94	282	188	94	376	282	188	94
5800	5500	1500	96	192	96	288	192	96	384	288	192	96
6000	5500	1500	98	196	98	294	196	98	392	294	196	98
6200	5500	1500	100	200	100	300	200	100	400	300	200	100
6400	5500	1500	100	200	100	300	200	100	400	300	200	100
6600	5500	1500	100	200	100	300	200	100	400	300	200	100
6800	5500	1500	100	200	100	300	200	100	400	300	200	100
7000	5500	1500	98	196	98	294	196	98	392	294	196	98
7200	5500	1500	96	192	96	288	192	96	384	288	192	96
7400	5500	1500	94	188	94	282	188	94	376	282	188	94
7600	5500	1500	92	184	92	276	184	92	368	276	184	92
7800	5500	1500	90	180	90	270	180	90	360	270	180	90
8000	5500	1500	88	176	88	264	176	88	352	264	176	88
8200	5500	1500	82	164	82	246	164	82	328	246	164	82
8400	5500	1500	78	156	78	234	156	78	312	234	156	78
8600	5500	1500	73	146	73	219	146	73	292	219	146	73
8800	5500	1500	65	130	65	195	130	65	260	195	130	65
9000	5500	1500	55	110	55	165	110	55	220	165	110	55
9200	5500	1500	45	90	45	135	90	45	180	135	90	45
9400	5500	1500	30	60	30	90	60	30	120	90	60	30
9600	5500	1500	15	30	15	45	30	15	60	45	30	15
9800	5500	1500	0	0	0	0	0	0	0	0	0	0
10000	5500	1500	0	0	0	0	0	0	0	0	0	0

Experiment 2: Fault displacement attribute data

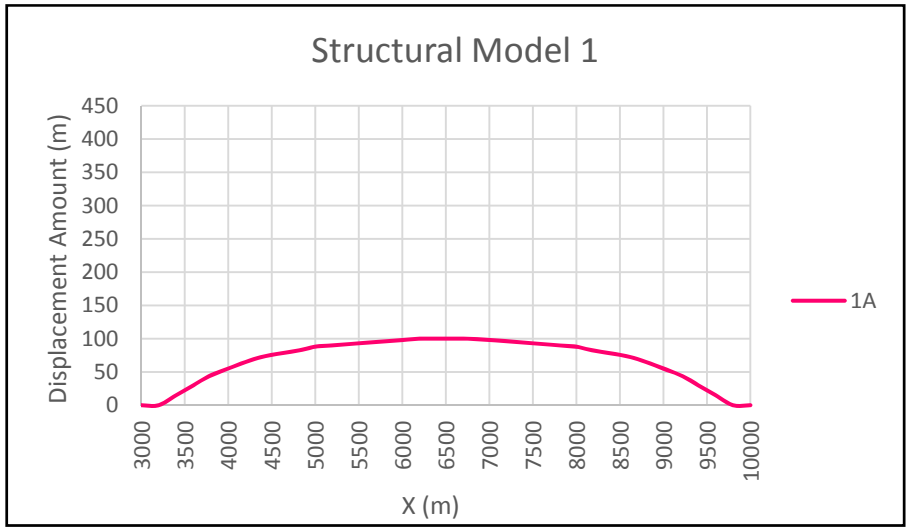

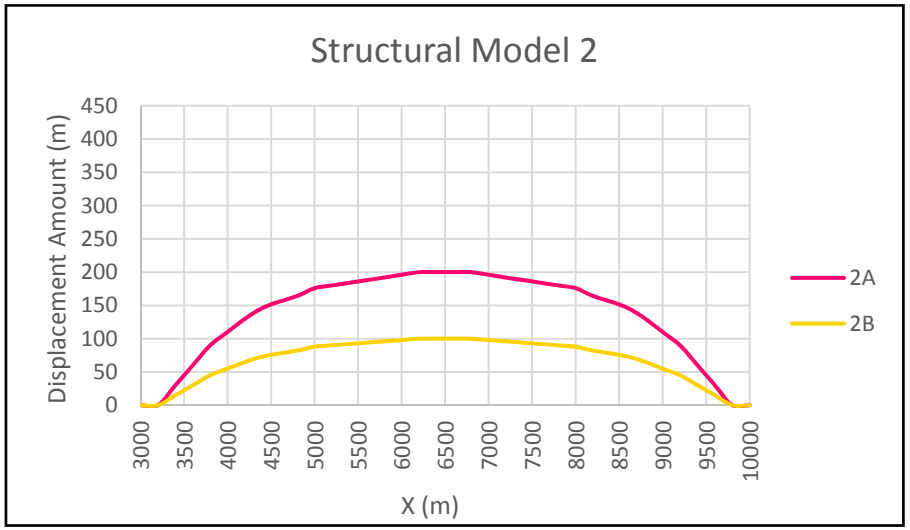

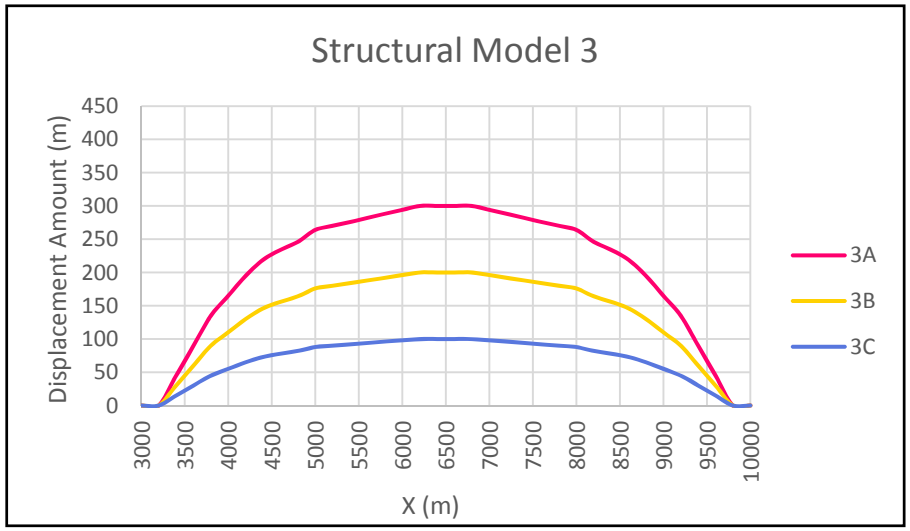

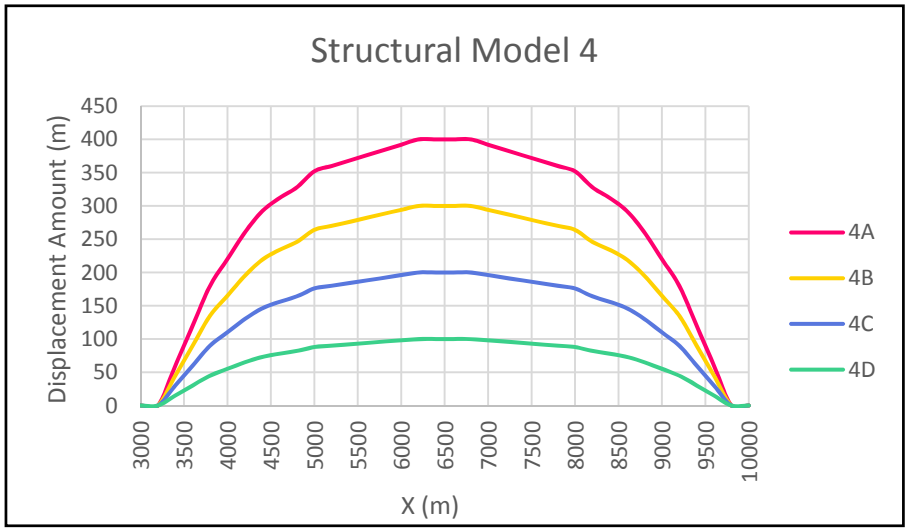

Experiment 3: Fault displacement attribute data linear charts

Experiment 3												
Displacement Point Location			Structural Model 1	Structural Model 2		Structural Model 3			Structural Model 4			
X	Y	Z	1A	2A	2B	3A	3B	3C	4A	4B	4C	4D
3000	5500	1500	0	0	0	0	0	0	0	0	0	0
3200	5500	1500	0	0	0	0	0	0	0	0	0	0
3400	5500	1500	15	30	15	45	30	15	60	45	30	15
3600	5500	1500	30	60	30	90	60	30	120	90	60	30
3800	5500	1500	45	90	45	135	90	45	180	135	90	45
4000	5500	1500	55	110	55	165	110	55	220	165	110	55
4200	5500	1500	65	130	65	195	130	65	260	195	130	65
4400	5500	1500	73	146	73	219	146	73	292	219	146	73
4600	5500	1500	78	156	78	234	156	78	312	234	156	78
4800	5500	1500	82	164	82	246	164	82	328	246	164	82
5000	5500	1500	88	176	88	264	176	88	352	264	176	88
5200	5500	1500	90	180	90	270	180	90	360	270	180	90
5400	5500	1500	92	184	92	276	184	92	368	276	184	92
5600	5500	1500	94	188	94	282	188	94	376	282	188	94
5800	5500	1500	96	192	96	288	192	96	384	288	192	96
6000	5500	1500	98	196	98	294	196	98	392	294	196	98
6200	5500	1500	100	200	100	300	200	100	400	300	200	100
6400	5500	1500	100	200	100	300	200	100	400	300	200	100
6600	5500	1500	100	200	100	300	200	100	400	300	200	100
6800	5500	1500	100	200	100	300	200	100	400	300	200	100
7000	5500	1500	98	196	98	294	196	98	392	294	196	98
7200	5500	1500	96	192	96	288	192	96	384	288	192	96
7400	5500	1500	94	188	94	282	188	94	376	282	188	94
7600	5500	1500	92	184	92	276	184	92	368	276	184	92
7800	5500	1500	90	180	90	270	180	90	360	270	180	90
8000	5500	1500	88	176	88	264	176	88	352	264	176	88
8200	5500	1500	82	164	82	246	164	82	328	246	164	82
8400	5500	1500	78	156	78	234	156	78	312	234	156	78
8600	5500	1500	73	146	73	219	146	73	292	219	146	73
8800	5500	1500	65	130	65	195	130	65	260	195	130	65
9000	5500	1500	55	110	55	165	110	55	220	165	110	55
9200	5500	1500	45	90	45	135	90	45	180	135	90	45
9400	5500	1500	30	60	30	90	60	30	120	90	60	30
9600	5500	1500	15	30	15	45	30	15	60	45	30	15
9800	5500	1500	0	0	0	0	0	0	0	0	0	0
10000	5500	1500	0	0	0	0	0	0	0	0	0	0

Experiment 3: Fault displacement attribute data

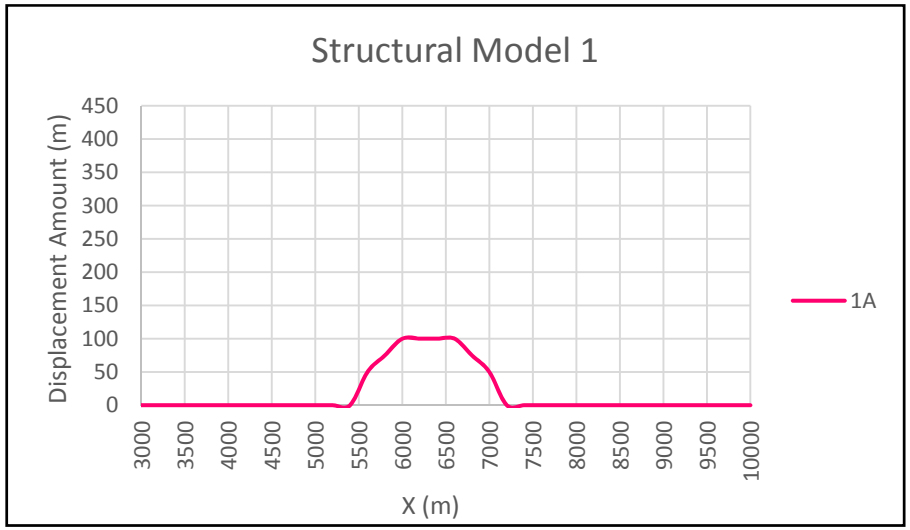

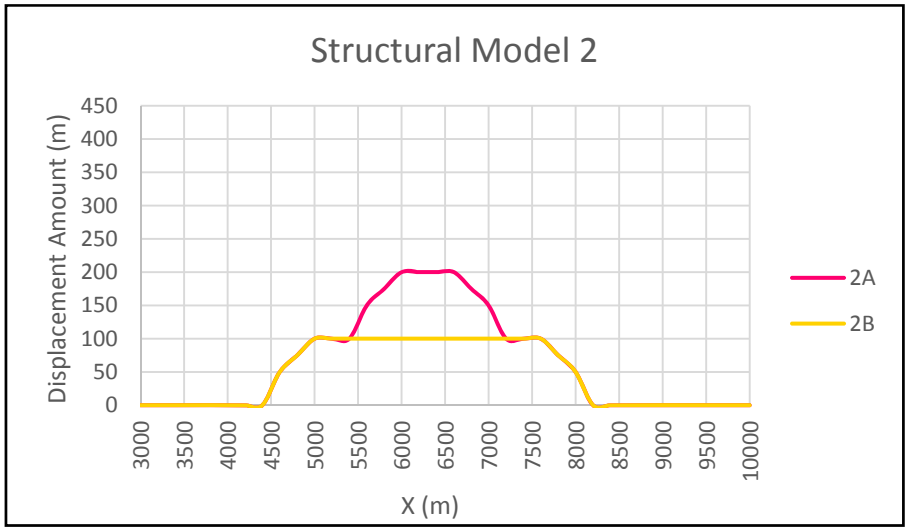

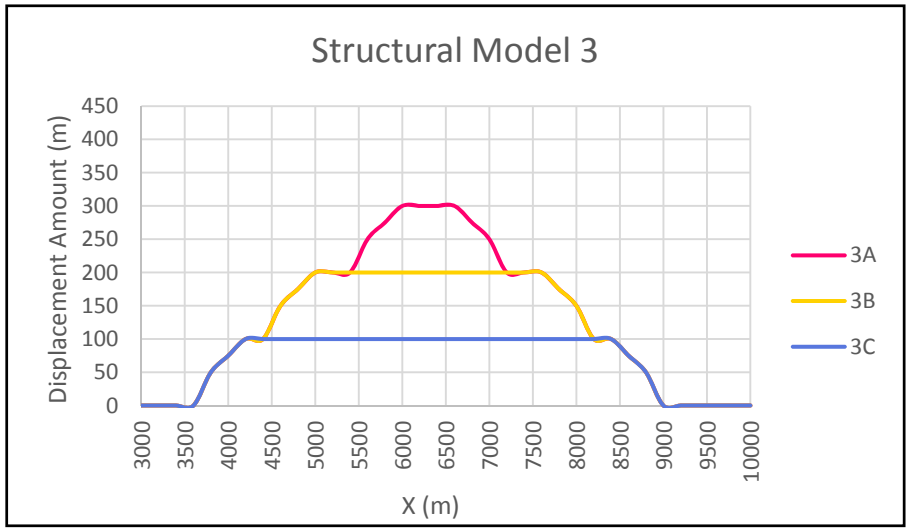

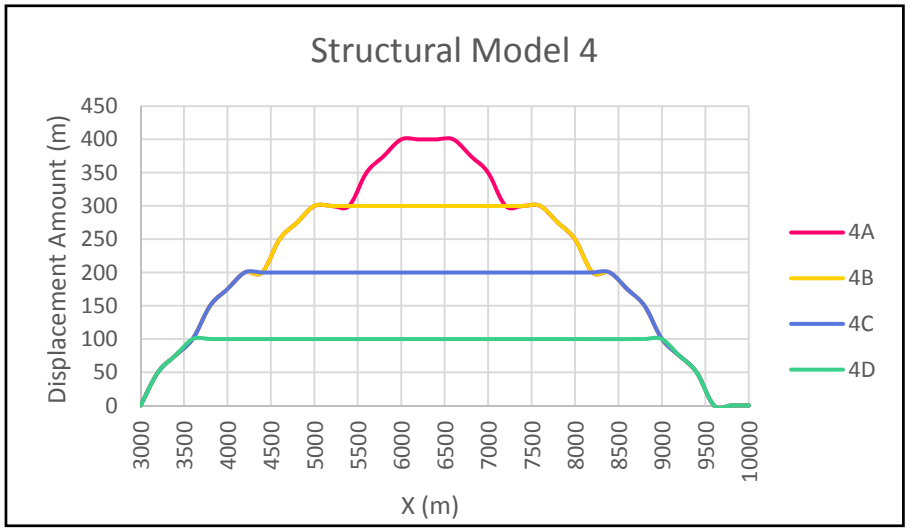

Experiment 4: Fault displacement attribute data linear charts

Experiment 4												
Displacement Point Location			Structural Model 1	Structural Model 2		Structural Model 3			Structural Model 4			
X	Y	Z	1A	2A	2B	3A	3B	3C	4A	4B	4C	4D
3000	5500	1500	0	0	0	0	0	0	0	0	0	0
3200	5500	1500	0	0	0	0	0	0	50	50	50	50
3400	5500	1500	0	0	0	0	0	0	75	75	75	75
3600	5500	1500	0	0	0	0	0	0	100	100	100	100
3800	5500	1500	0	0	0	50	50	50	150	150	150	100
4000	5500	1500	0	0	0	75	75	75	175	175	175	100
4200	5500	1500	0	0	0	100	100	100	200	200	200	100
4400	5500	1500	0	0	0	100	100	100	200	200	200	100
4600	5500	1500	0	50	50	150	150	100	250	250	200	100
4800	5500	1500	0	75	75	175	175	100	275	275	200	100
5000	5500	1500	0	100	100	200	200	100	300	300	200	100
5200	5500	1500	0	100	100	200	200	100	300	300	200	100
5400	5500	1500	0	100	100	200	200	100	300	300	200	100
5600	5500	1500	50	150	100	250	200	100	350	300	200	100
5800	5500	1500	75	175	100	275	200	100	375	300	200	100
6000	5500	1500	100	200	100	300	200	100	400	300	200	100
6200	5500	1500	100	200	100	300	200	100	400	300	200	100
6400	5500	1500	100	200	100	300	200	100	400	300	200	100
6600	5500	1500	100	200	100	300	200	100	400	300	200	100
6800	5500	1500	75	175	100	275	200	100	375	300	200	100
7000	5500	1500	50	150	100	250	200	100	350	300	200	100
7200	5500	1500	0	100	100	200	200	100	300	300	200	100
7400	5500	1500	0	100	100	200	200	100	300	300	200	100
7600	5500	1500	0	100	100	200	200	100	300	300	200	100
7800	5500	1500	0	75	75	175	175	100	275	275	200	100
8000	5500	1500	0	50	50	150	150	100	250	250	200	100
8200	5500	1500	0	0	0	100	100	100	200	200	200	100
8400	5500	1500	0	0	0	100	100	100	200	200	200	100
8600	5500	1500	0	0	0	75	75	75	175	175	175	100
8800	5500	1500	0	0	0	50	50	50	150	150	150	100
9000	5500	1500	0	0	0	0	0	0	100	100	100	100
9200	5500	1500	0	0	0	0	0	0	75	75	75	75
9400	5500	1500	0	0	0	0	0	0	50	50	50	50
9600	5500	1500	0	0	0	0	0	0	0	0	0	0
9800	5500	1500	0	0	0	0	0	0	0	0	0	0
10000	5500	1500	0	0	0	0	0	0	0	0	0	0

Experiment 4: Fault displacement attribute data

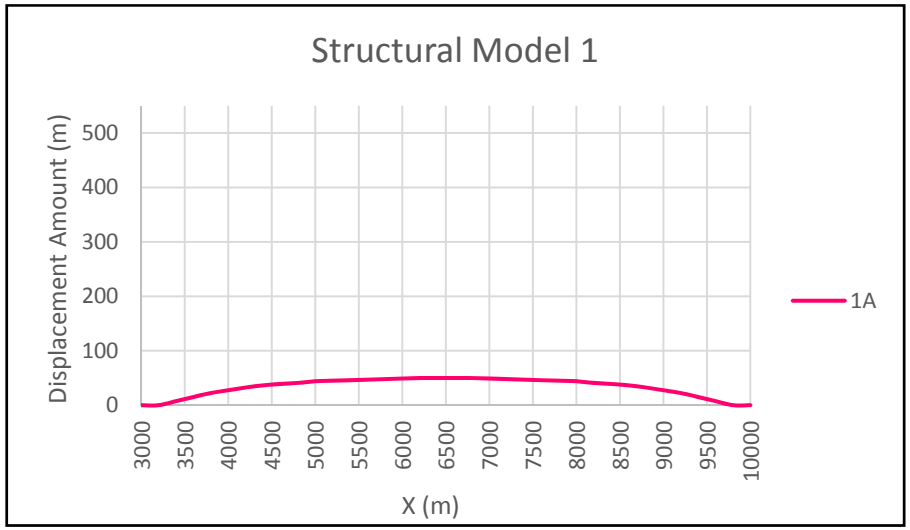

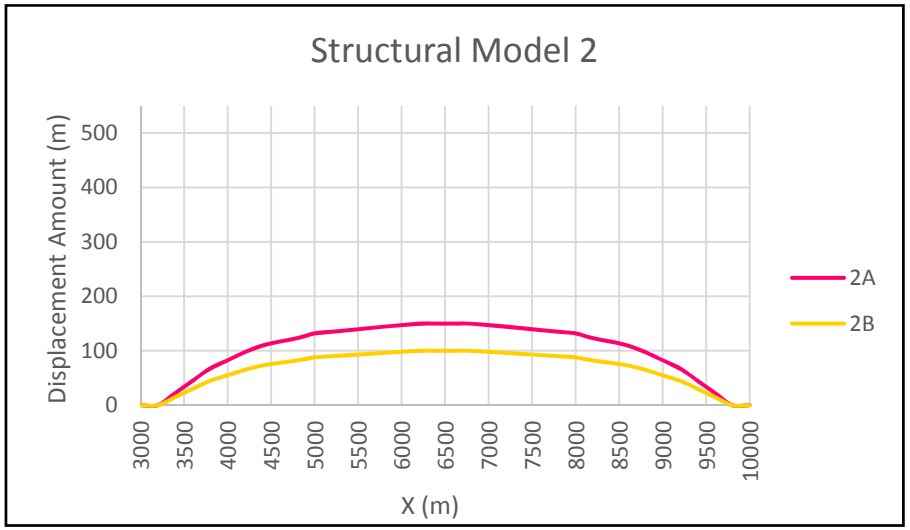

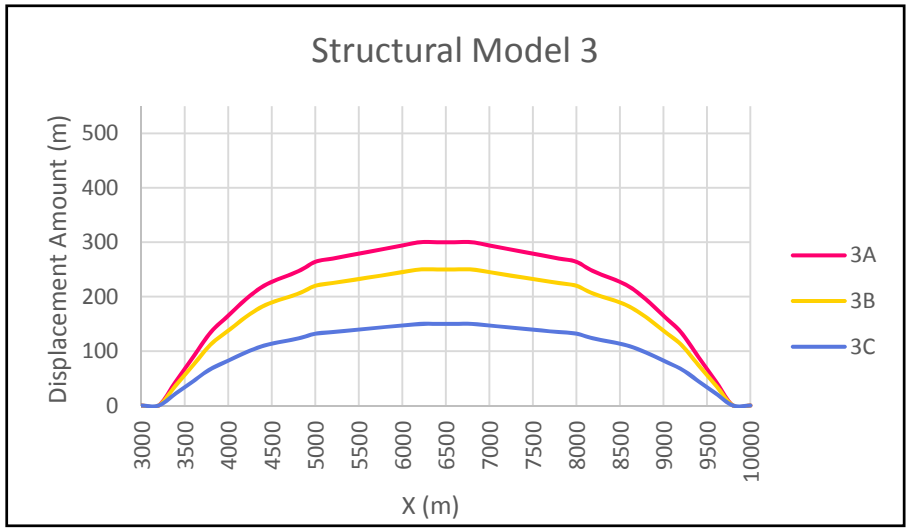

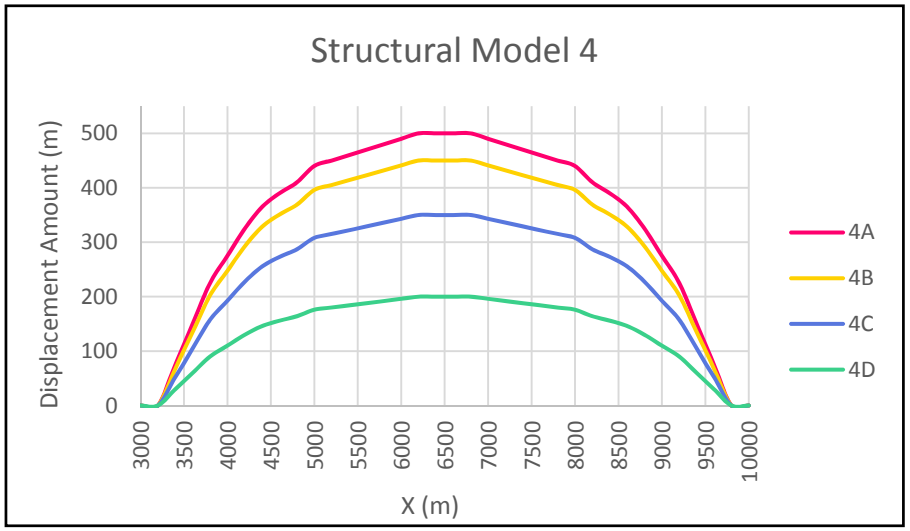

Experiment 5: Fault displacement attribute data linear charts

Experiment 5												
Displacement Point Location			Structural Model 1	Structural Model 2		Structural Model 3			Structural Model 4			
X	Y	Z	1A	2A	2B	3A	3B	3C	4A	4B	4C	4D
3000	5500	1500	0	0	0	0	0	0	0	0	0	0.00
3200	5500	1500	0	0	0	0	0	0	0	0	0	0.00
3400	5500	1500	7.5	22.5	15	45	37.5	22.5	75	67.5	52.5	30.00
3600	5500	1500	15	45	30	90	75	45	150	135	105	60.00
3800	5500	1500	22.5	67.5	45	135	112.5	67.5	225	202.5	157.5	90.00
4000	5500	1500	27.5	82.5	55	165	137.5	82.5	275	247.5	192.5	110.00
4200	5500	1500	32.5	97.5	65	195	162.5	97.5	325	292.5	227.5	130.00
4400	5500	1500	36.5	109.5	73	219	182.5	109.5	365	328.5	255.5	146.00
4600	5500	1500	39	117	78	234	195	117	390	351	273	156.00
4800	5500	1500	41	123	82	246	205	123	410	369	287	164.00
5000	5500	1500	44	132	88	264	220	132	440	396	308	176.00
5200	5500	1500	45	135	90	270	225	135	450	405	315	180.00
5400	5500	1500	46	138	92	276	230	138	460	414	322	184.00
5600	5500	1500	47	141	94	282	235	141	470	423	329	188.00
5800	5500	1500	48	144	96	288	240	144	480	432	336	192.00
6000	5500	1500	49	147	98	294	245	147	490	441	343	196.00
6200	5500	1500	50	150	100	300	250	150	500	450	350	200.00
6400	5500	1500	50	150	100	300	250	150	500	450	350	200.00
6600	5500	1500	50	150	100	300	250	150	500	450	350	200.00
6800	5500	1500	50	150	100	300	250	150	500	450	350	200.00
7000	5500	1500	49	147	98	294	245	147	490	441	343	196.00
7200	5500	1500	48	144	96	288	240	144	480	432	336	192.00
7400	5500	1500	47	141	94	282	235	141	470	423	329	188.00
7600	5500	1500	46	138	92	276	230	138	460	414	322	184.00
7800	5500	1500	45	135	90	270	225	135	450	405	315	180.00
8000	5500	1500	44	132	88	264	220	132	440	396	308	176.00
8200	5500	1500	41	123	82	246	205	123	410	369	287	164.00
8400	5500	1500	39	117	78	234	195	117	390	351	273	156.00
8600	5500	1500	36.5	109.5	73	219	182.5	109.5	365	328.5	255.5	146.00
8800	5500	1500	32.5	97.5	65	195	162.5	97.5	325	292.5	227.5	130.00
9000	5500	1500	27.5	82.5	55	165	137.5	82.5	275	247.5	192.5	110.00
9200	5500	1500	22.5	67.5	45	135	112.5	67.5	225	202.5	157.5	90.00
9400	5500	1500	15	45	30	90	75	45	150	135	105	60.00
9600	5500	1500	7.5	22.5	15	45	37.5	22.5	75	67.5	52.5	30
9800	5500	1500	0	0	0	0	0	0	0	0	0	0
10000	5500	1500	0	0	0	0	0	0	0	0	0	0

Experiment 5: Fault displacement attribute data

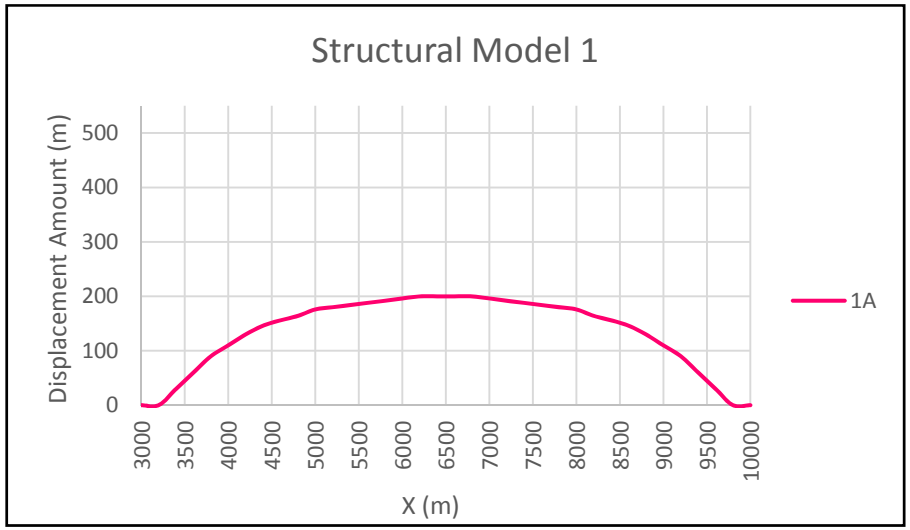

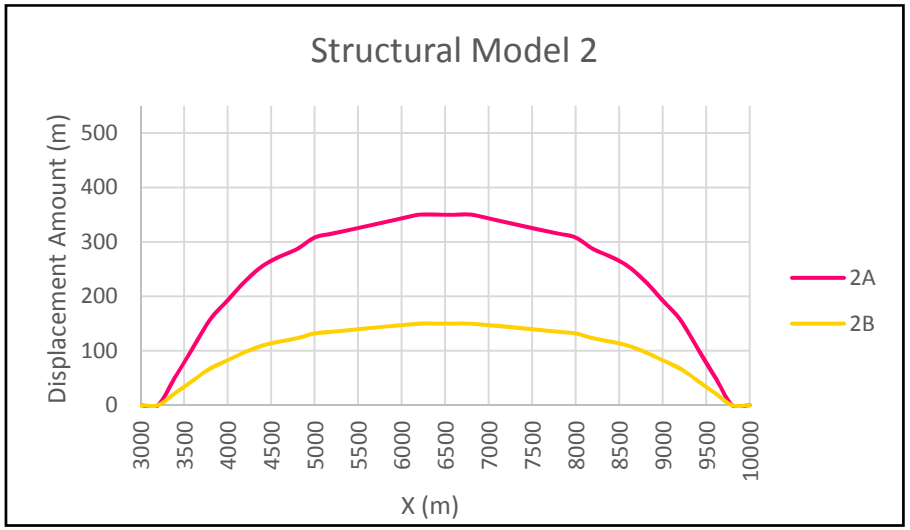

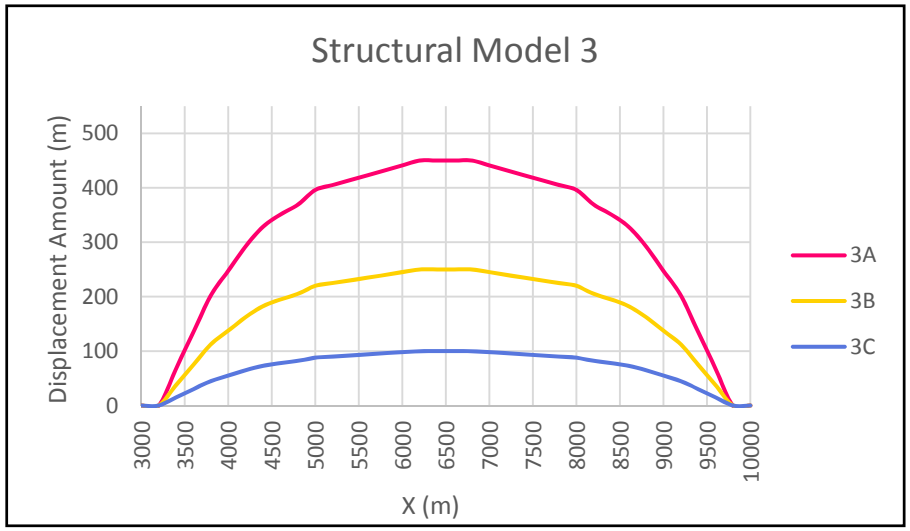

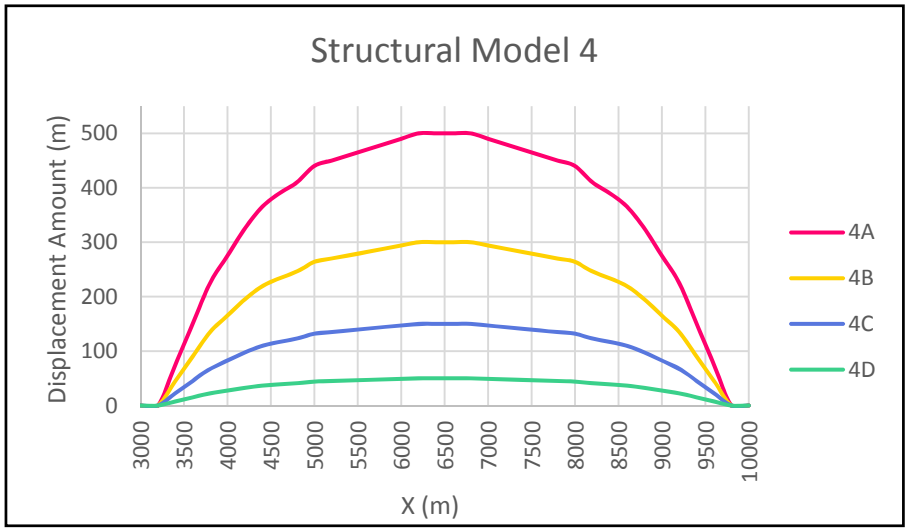

Experiment 6: Fault displacement attribute data linear charts

Experiment 6												
Displacement Point Location			Structural Model 1	Structural Model 2		Structural Model 3			Structural Model 4			
X	Y	Z	1A	2A	2B	3A	3B	3C	4A	4B	4C	4D
3000	5500	1500	0	0	0	0	0	0	0	0	0	0
3200	5500	1500	0	0	0	0	0	0	0	0	0	0
3400	5500	1500	30	52.5	22.5	67.5	37.5	15	75	45	22.5	7.5
3600	5500	1500	60	105	45	135	75	30	150	90	45	15
3800	5500	1500	90	157.5	67.5	202.5	112.5	45	225	135	67.5	22.5
4000	5500	1500	110	192.5	82.5	247.5	137.5	55	275	165	82.5	27.5
4200	5500	1500	130	227.5	97.5	292.5	162.5	65	325	195	97.5	32.5
4400	5500	1500	146	255.5	109.5	328.5	182.5	73	365	219	109.5	36.5
4600	5500	1500	156	273	117	351	195	78	390	234	117	39
4800	5500	1500	164	287	123	369	205	82	410	246	123	41
5000	5500	1500	176	308	132	396	220	88	440	264	132	44
5200	5500	1500	180	315	135	405	225	90	450	270	135	45
5400	5500	1500	184	322	138	414	230	92	460	276	138	46
5600	5500	1500	188	329	141	423	235	94	470	282	141	47
5800	5500	1500	192	336	144	432	240	96	480	288	144	48
6000	5500	1500	196	343	147	441	245	98	490	294	147	49
6200	5500	1500	200	350	150	450	250	100	500	300	150	50
6400	5500	1500	200	350	150	450	250	100	500	300	150	50
6600	5500	1500	200	350	150	450	250	100	500	300	150	50
6800	5500	1500	200	350	150	450	250	100	500	300	150	50
7000	5500	1500	196	343	147	441	245	98	490	294	147	49
7200	5500	1500	192	336	144	432	240	96	480	288	144	48
7400	5500	1500	188	329	141	423	235	94	470	282	141	47
7600	5500	1500	184	322	138	414	230	92	460	276	138	46
7800	5500	1500	180	315	135	405	225	90	450	270	135	45
8000	5500	1500	176	308	132	396	220	88	440	264	132	44
8200	5500	1500	164	287	123	369	205	82	410	246	123	41
8400	5500	1500	156	273	117	351	195	78	390	234	117	39
8600	5500	1500	146	255.5	109.5	328.5	182.5	73	365	219	109.5	36.5
8800	5500	1500	130	227.5	97.5	292.5	162.5	65	325	195	97.5	32.5
9000	5500	1500	110	192.5	82.5	247.5	137.5	55	275	165	82.5	27.5
9200	5500	1500	90	157.5	67.5	202.5	112.5	45	225	135	67.5	22.5
9400	5500	1500	60	105	45	135	75	30	150	90	45	15
9600	5500	1500	30	52.5	22.5	67.5	37.5	15	75	45	22.5	7.5
9800	5500	1500	0	0	0	0	0	0	0	0	0	0
10000	5500	1500	0	0	0	0	0	0	0	0	0	0

Experiment 6: Fault displacement attribute data

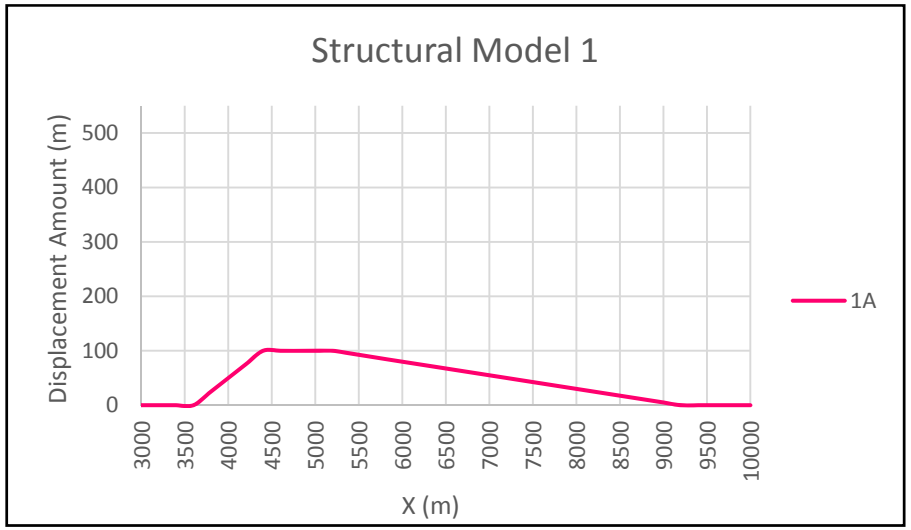

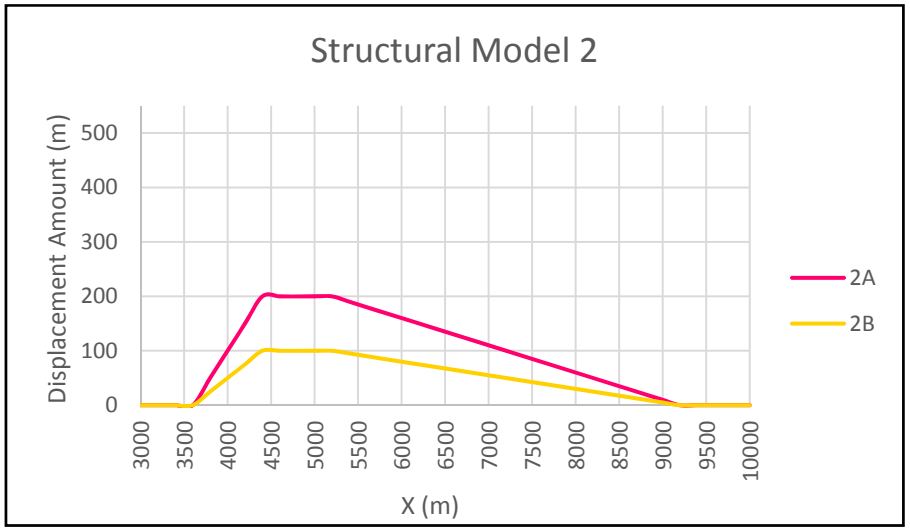

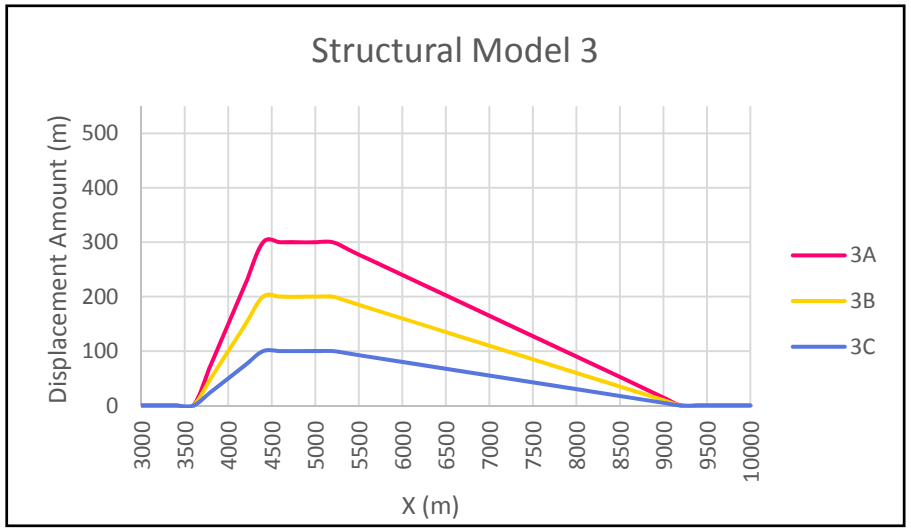

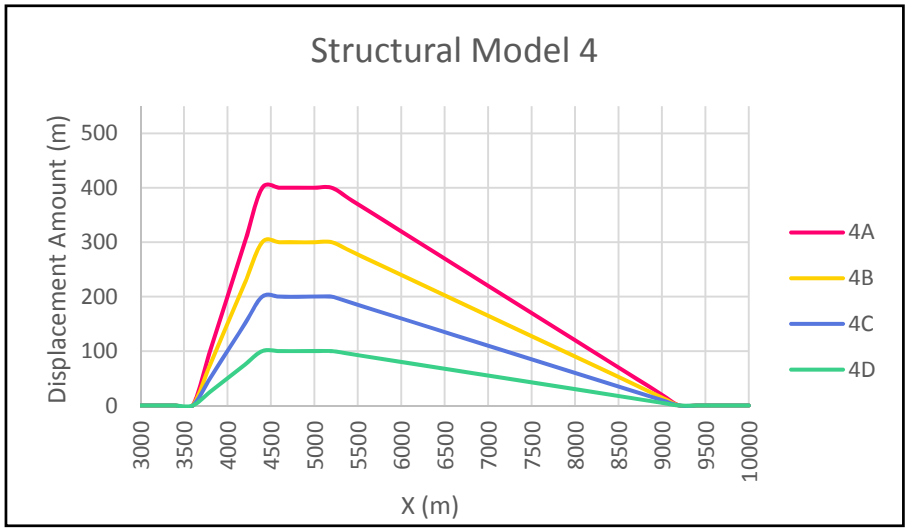

Experiment 7: Fault displacement attribute data linear charts

Experiment 7												
Displacement Point Location			Structural Model 1	Structural Model 2		Structural Model 3			Structural Model 4			
X	Y	Z	1A	2A	2B	3A	3B	3C	4A	4B	4C	4D
3000	5500	1500	0	0	0	0	0	0	0	0	0	0
3200	5500	1500	0	0	0	0	0	0	0	0	0	0
3400	5500	1500	0	0	0	0	0	0	0	0	0	0
3600	5500	1500	0	0	0	0	0	0	0	0	0	0
3800	5500	1500	25	50	25	75	50	25	100	75	50	25
4000	5500	1500	50	100	50	150	100	50	200	150	100	50
4200	5500	1500	75	150	75	225	150	75	300	225	150	75
4400	5500	1500	100	200	100	300	200	100	400	300	200	100
4600	5500	1500	100	200	100	300	200	100	400	300	200	100
4800	5500	1500	100	200	100	300	200	100	400	300	200	100
5000	5500	1500	100	200	100	300	200	100	400	300	200	100
5200	5500	1500	100	200	100	300	200	100	400	300	200	100
5400	5500	1500	95	190	95	285	190	95	380	285	190	95
5600	5500	1500	90	180	90	270	180	90	360	270	180	90
5800	5500	1500	85	170	85	255	170	85	340	255	170	85
6000	5500	1500	80	160	80	240	160	80	320	240	160	80
6200	5500	1500	75	150	75	225	150	75	300	225	150	75
6400	5500	1500	70	140	70	210	140	70	280	210	140	70
6600	5500	1500	65	130	65	195	130	65	260	195	130	65
6800	5500	1500	60	120	60	180	120	60	240	180	120	60
7000	5500	1500	55	110	55	165	110	55	220	165	110	55
7200	5500	1500	50	100	50	150	100	50	200	150	100	50
7400	5500	1500	45	90	45	135	90	45	180	135	90	45
7600	5500	1500	40	80	40	120	80	40	160	120	80	40
7800	5500	1500	35	70	35	105	70	35	140	105	70	35
8000	5500	1500	30	60	30	90	60	30	120	90	60	30
8200	5500	1500	25	50	25	75	50	25	100	75	50	25
8400	5500	1500	20	40	20	60	40	20	80	60	40	20
8600	5500	1500	15	30	15	45	30	15	60	45	30	15
8800	5500	1500	10	20	10	30	20	10	40	30	20	10
9000	5500	1500	5	10	5	15	10	5	20	15	10	5
9200	5500	1500	0	0	0	0	0	0	0	0	0	0
9400	5500	1500	0	0	0	0	0	0	0	0	0	0
9600	5500	1500	0	0	0	0	0	0	0	0	0	0
9800	5500	1500	0	0	0	0	0	0	0	0	0	0
10000	5500	1500	0	0	0	0	0	0	0	0	0	0

Experiment 7: Fault displacement attribute data

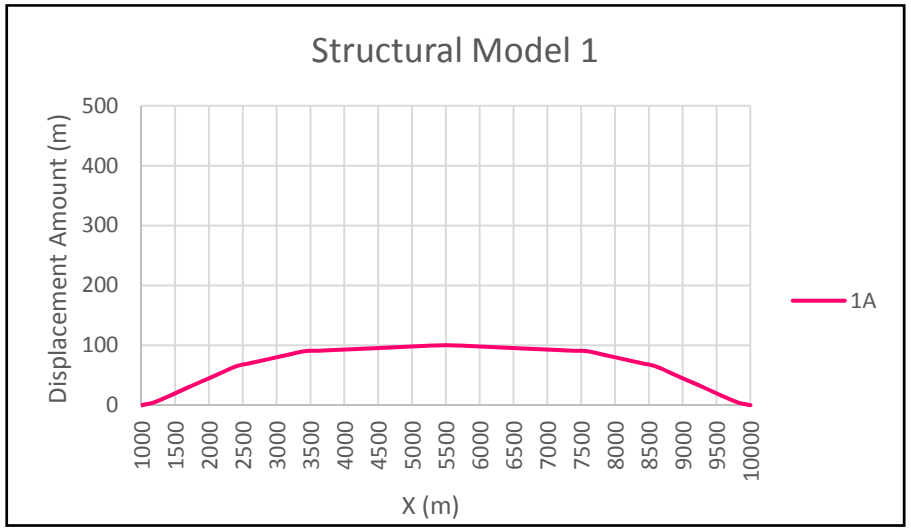

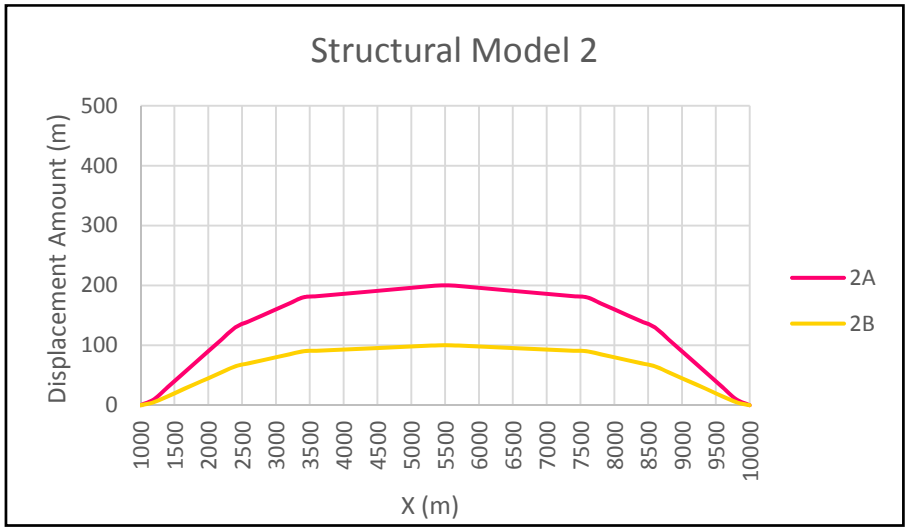

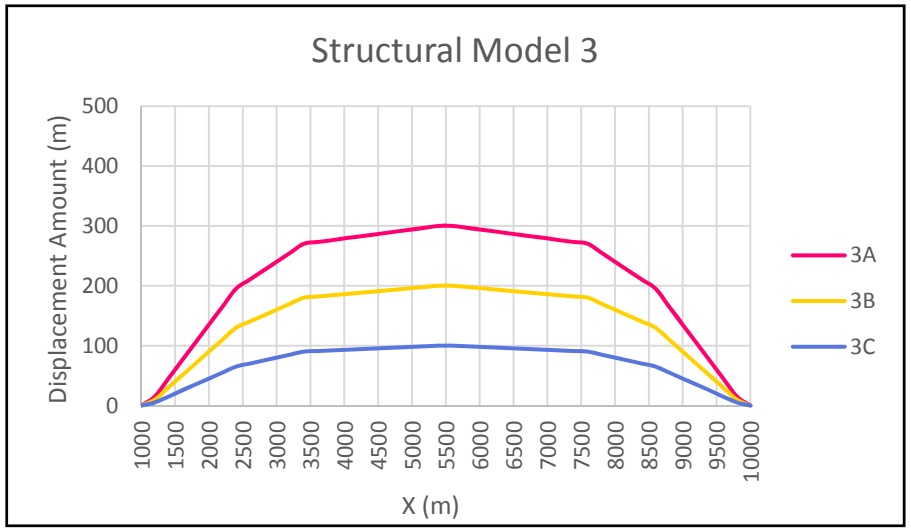

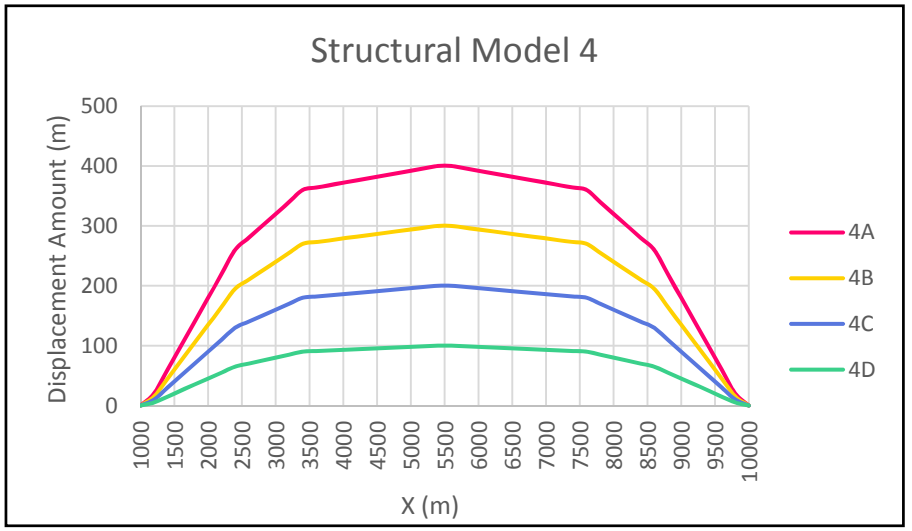

Experiment 8 Fault 1: Fault displacement attribute data linear charts

Experiment 8- Fault 1												
Displacement Point Location			Structural Model 1	Structural Model 2		Structural Model 3			Structural Model 4			
X	Y	Z	1A	2A	2B	3A	3B	3C	4A	4B	4C	4D
1000	8250	1500	0	0	0	0	0	0	0	0	0	0
1200	8250	1500	5	10	5	15	10	5	20	15	10	5
1400	8250	1500	15	30	15	45	30	15	60	45	30	15
1600	8250	1500	25	50	25	75	50	25	100	75	50	25
1800	8250	1500	35	70	35	105	70	35	140	105	70	35
2000	8250	1500	45	90	45	135	90	45	180	135	90	45
2200	8250	1500	55	110	55	165	110	55	220	165	110	55
2400	8250	1500	65	130	65	195	130	65	260	195	130	65
2600	8250	1500	70	140	70	210	140	70	280	210	140	70
2800	8250	1500	75	150	75	225	150	75	300	225	150	75
3000	8250	1500	80	160	80	240	160	80	320	240	160	80
3200	8250	1500	85	170	85	255	170	85	340	255	170	85
3400	8250	1500	90	180	90	270	180	90	360	270	180	90
3600	8250	1500	91	182	91	273	182	91	364	273	182	91
3800	8250	1500	92	184	92	276	184	92	368	276	184	92
4000	8250	1500	93	186	93	279	186	93	372	279	186	93
4200	8250	1500	94	188	94	282	188	94	376	282	188	94
4400	8250	1500	95	190	95	285	190	95	380	285	190	95
4600	8250	1500	96	192	96	288	192	96	384	288	192	96
4800	8250	1500	97	194	97	291	194	97	388	291	194	97
5000	8250	1500	98	196	98	294	196	98	392	294	196	98
5200	8250	1500	99	198	99	297	198	99	396	297	198	99
5400	8250	1500	100	200	100	300	200	100	400	300	200	100
5600	8250	1500	100	200	100	300	200	100	400	300	200	100
5800	8250	1500	99	198	99	297	198	99	396	297	198	99
6000	8250	1500	98	196	98	294	196	98	392	294	196	98
6200	8250	1500	97	194	97	291	194	97	388	291	194	97
6400	8250	1500	96	192	96	288	192	96	384	288	192	96
6600	8250	1500	95	190	95	285	190	95	380	285	190	95
6800	8250	1500	94	188	94	282	188	94	376	282	188	94
7000	8250	1500	93	186	93	279	186	93	372	279	186	93
7200	8250	1500	92	184	92	276	184	92	368	276	184	92
7400	8250	1500	91	182	91	273	182	91	364	273	182	91
7600	8250	1500	90	180	90	270	180	90	360	270	180	90
7800	8250	1500	85	170	85	255	170	85	340	255	170	85
8000	8250	1500	80	160	80	240	160	80	320	240	160	80
8200	8250	1500	75	150	75	225	150	75	300	225	150	75
8400	8250	1500	70	140	70	210	140	70	280	210	140	70
8600	8250	1500	65	130	65	195	130	65	260	195	130	65
8800	8250	1500	55	110	55	165	110	55	220	165	110	55
9000	8250	1500	45	90	45	135	90	45	180	135	90	45
9200	8250	1500	35	70	35	105	70	35	140	105	70	35
9400	8250	1500	25	50	25	75	50	25	100	75	50	25
9600	8250	1500	15	30	15	45	30	15	60	45	30	15
9800	8250	1500	5	10	5	15	10	5	20	15	10	5
10000	8250	1500	0	0	0	0	0	0	0	0	0	0

Experiment 8 Fault 1: Displacement attribute data

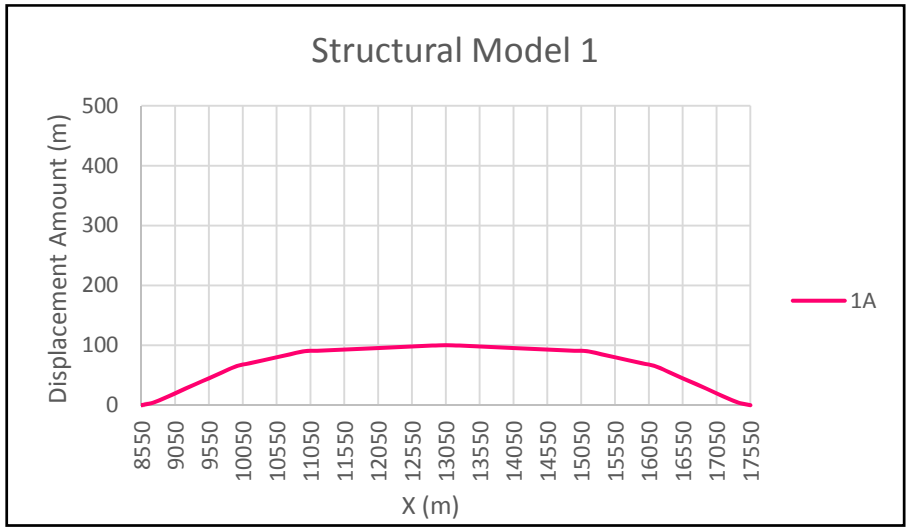

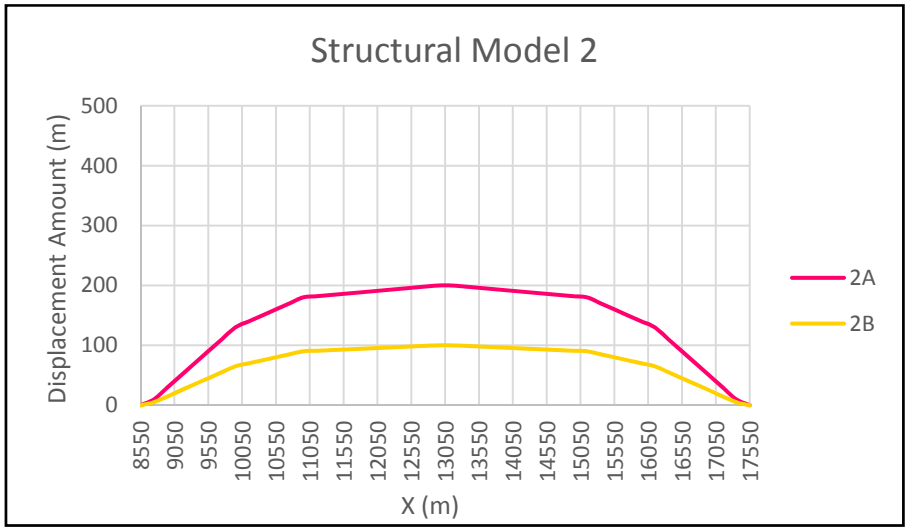

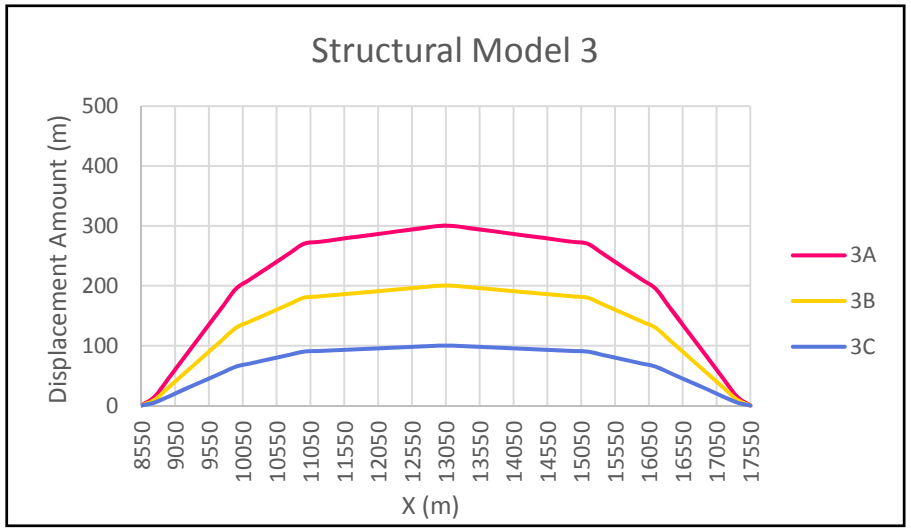

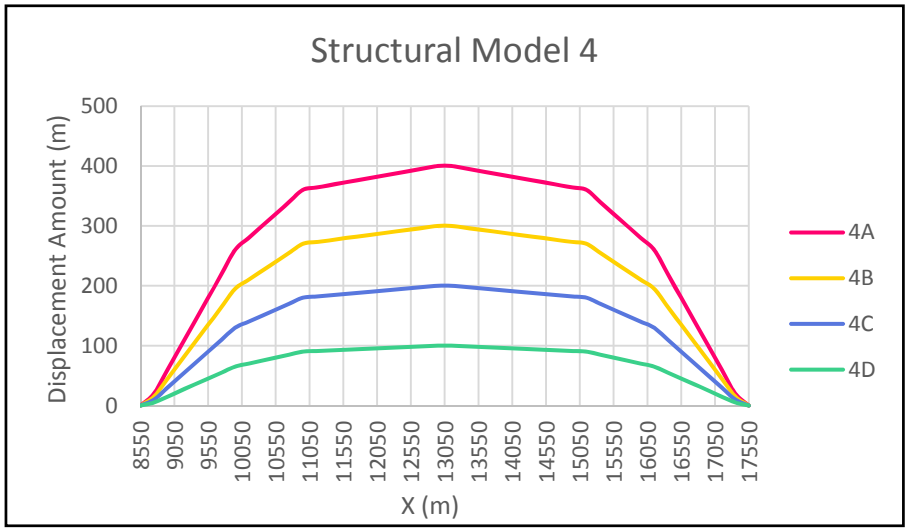

Experiment 8 Fault 2: Fault displacement attribute data linear charts

Experiment 8- Fault 2												
Displacement Point Location			Structural Model 1	Structural Model 2		Structural Model 3			Structural Model 4			
X	Y	Z	1A	2A	2B	3A	3B	3C	4A	4B	4C	4D
8550	9250	1500	0	0	0	0	0	0	0	0	0	0
8750	9250	1500	5	10	5	15	10	5	20	15	10	5
8950	9250	1500	15	30	15	45	30	15	60	45	30	15
9150	9250	1500	25	50	25	75	50	25	100	75	50	25
9350	9250	1500	35	70	35	105	70	35	140	105	70	35
9550	9250	1500	45	90	45	135	90	45	180	135	90	45
9750	9250	1500	55	110	55	165	110	55	220	165	110	55
9950	9250	1500	65	130	65	195	130	65	260	195	130	65
10150	9250	1500	70	140	70	210	140	70	280	210	140	70
10350	9250	1500	75	150	75	225	150	75	300	225	150	75
10550	9250	1500	80	160	80	240	160	80	320	240	160	80
10750	9250	1500	85	170	85	255	170	85	340	255	170	85
10950	9250	1500	90	180	90	270	180	90	360	270	180	90
11150	9250	1500	91	182	91	273	182	91	364	273	182	91
11350	9250	1500	92	184	92	276	184	92	368	276	184	92
11550	9250	1500	93	186	93	279	186	93	372	279	186	93
11750	9250	1500	94	188	94	282	188	94	376	282	188	94
11950	9250	1500	95	190	95	285	190	95	380	285	190	95
12150	9250	1500	96	192	96	288	192	96	384	288	192	96
12350	9250	1500	97	194	97	291	194	97	388	291	194	97
12550	9250	1500	98	196	98	294	196	98	392	294	196	98
12750	9250	1500	99	198	99	297	198	99	396	297	198	99
12950	9250	1500	100	200	100	300	200	100	400	300	200	100
13150	9250	1500	100	200	100	300	200	100	400	300	200	100
13350	9250	1500	99	198	99	297	198	99	396	297	198	99
13550	9250	1500	98	196	98	294	196	98	392	294	196	98
13750	9250	1500	97	194	97	291	194	97	388	291	194	97
13950	9250	1500	96	192	96	288	192	96	384	288	192	96
14150	9250	1500	95	190	95	285	190	95	380	285	190	95
14350	9250	1500	94	188	94	282	188	94	376	282	188	94
14550	9250	1500	93	186	93	279	186	93	372	279	186	93
14750	9250	1500	92	184	92	276	184	92	368	276	184	92
14950	9250	1500	91	182	91	273	182	91	364	273	182	91
15150	9250	1500	90	180	90	270	180	90	360	270	180	90
15350	9250	1500	85	170	85	255	170	85	340	255	170	85
15550	9250	1500	80	160	80	240	160	80	320	240	160	80
15750	9250	1500	75	150	75	225	150	75	300	225	150	75
15950	9250	1500	70	140	70	210	140	70	280	210	140	70
16150	9250	1500	65	130	65	195	130	65	260	195	130	65
16350	9250	1500	55	110	55	165	110	55	220	165	110	55
16550	9250	1500	45	90	45	135	90	45	180	135	90	45
16750	9250	1500	35	70	35	105	70	35	140	105	70	35
16950	9250	1500	25	50	25	75	50	25	100	75	50	25
17150	9250	1500	15	30	15	45	30	15	60	45	30	15
17350	9250	1500	5	10	5	15	10	5	20	15	10	5
17550	9250	1500	0	0	0	0	0	0	0	0	0	0

Experiment 8 Fault 2: Displacement attribute data

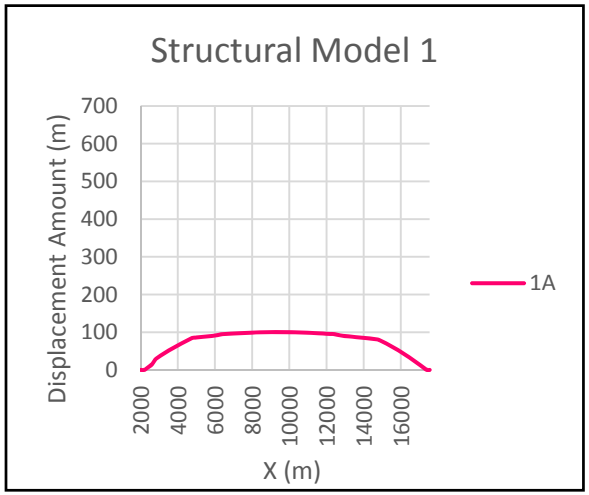

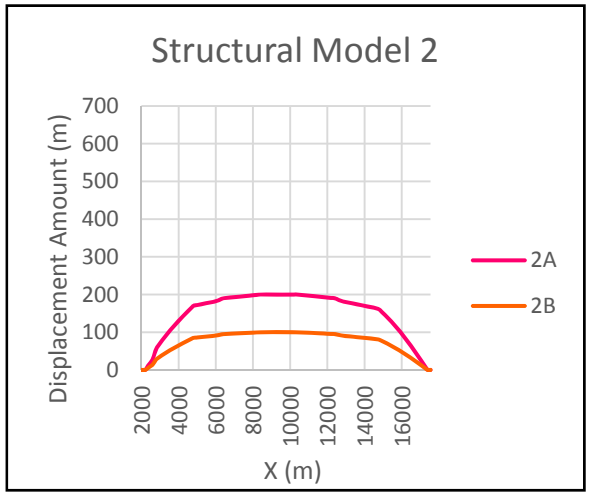

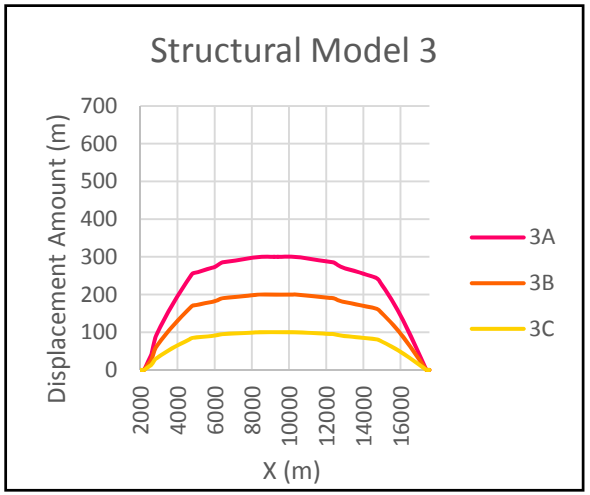

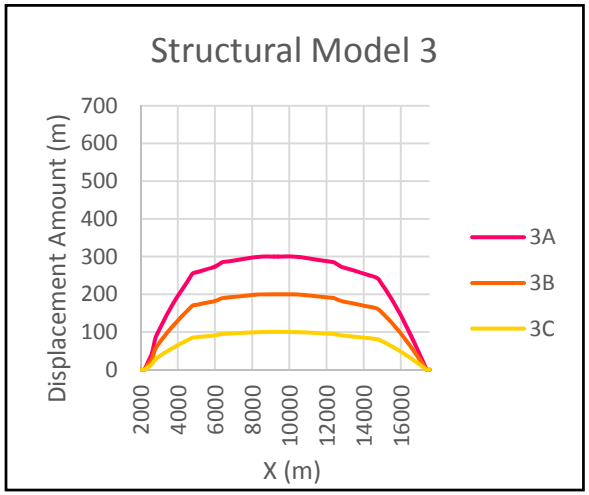

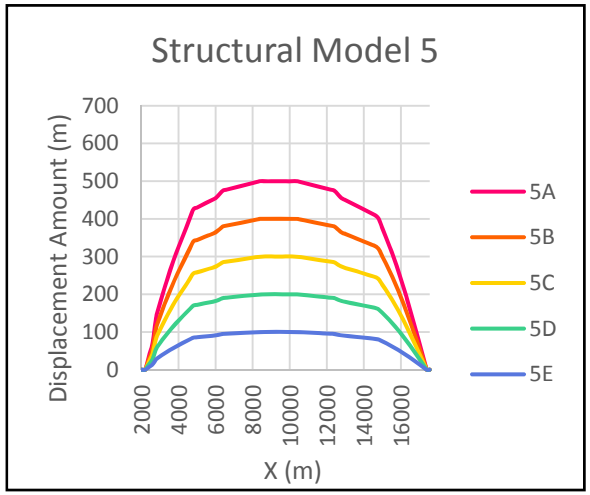

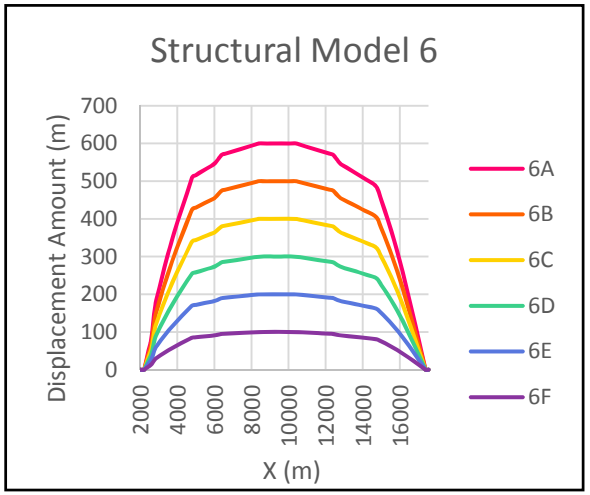

Experiment 9 Fault 1: Fault displacement attribute data linear charts

Experiment 9 Fault 1								
Displacement Point Location			Structural Model 1	Structural Model 2		Structural Model 3		
X	Y	Z	1A	2A	2B	3A	3B	3C
\	12250	1500	0	0	0	0	0	0
2200	12250	1500	0	0	0	0	0	0
2400	12250	1500	7	14	7	21	14	7
2600	12250	1500	14	28	14	42	28	14
2800	12250	1500	28	56	28	84	56	28
3000	12250	1500	35	70	35	105	70	35
3200	12250	1500	42	84	42	126	84	42
3400	12250	1500	48	96	48	144	96	48
3600	12250	1500	54	108	54	162	108	54
3800	12250	1500	60	120	60	180	120	60
4000	12250	1500	65	130	65	195	130	65
4200	12250	1500	70	140	70	210	140	70
4400	12250	1500	75	150	75	225	150	75
4600	12250	1500	80	160	80	240	160	80
4800	12250	1500	85	170	85	255	170	85
5000	12250	1500	86	172	86	258	172	86
5200	12250	1500	87	174	87	261	174	87
5400	12250	1500	88	176	88	264	176	88
5600	12250	1500	89	178	89	267	178	89
5800	12250	1500	90	180	90	270	180	90
6000	12250	1500	91	182	91	273	182	91
6200	12250	1500	93	186	93	279	186	93
6400	12250	1500	95	190	95	285	190	95
6600	12250	1500	95.5	191	95.5	286.5	191	95.5
6800	12250	1500	96	192	96	288	192	96
7000	12250	1500	96.5	193	96.5	289.5	193	96.5
7200	12250	1500	97	194	97	291	194	97
7400	12250	1500	97.5	195	97.5	292.5	195	97.5
7600	12250	1500	98	196	98	294	196	98
7800	12250	1500	98.5	197	98.5	295.5	197	98.5
8000	12250	1500	99	198	99	297	198	99
8200	12250	1500	99.5	199	99.5	298.5	199	99.5
8400	12250	1500	100	200	100	300	200	100
8600	12250	1500	100	200	100	300	200	100
8800	12250	1500	100	200	100	300	200	100
9000	12250	1500	100	200	100	300	200	100
9200	12250	1500	100	200	100	300	200	100
9400	12250	1500	100	200	100	300	200	100
9600	12250	1500	100	200	100	300	200	100
9800	12250	1500	100	200	100	300	200	100
10000	12250	1500	100	200	100	300	200	100
10200	12250	1500	100	200	100	300	200	100
10400	12250	1500	100	200	100	300	200	100
10600	12250	1500	99.5	199	99.5	298.5	199	99.5
10800	12250	1500	99	198	99	297	198	99
11000	12250	1500	98.5	197	98.5	295.5	197	98.5
11200	12250	1500	98	196	98	294	196	98
11400	12250	1500	97.5	195	97.5	292.5	195	97.5
11600	12250	1500	97	194	97	291	194	97
11800	12250	1500	96.5	193	96.5	289.5	193	96.5
12000	12250	1500	96	192	96	288	192	96
12200	12250	1500	95.5	191	95.5	286.5	191	95.5
12400	12250	1500	95	190	95	285	190	95
12600	12250	1500	93	186	93	279	186	93
12800	12250	1500	91	182	91	273	182	91
13000	12250	1500	90	180	90	270	180	90
13200	12250	1500	89	178	89	267	178	89
13400	12250	1500	88	176	88	264	176	88
13600	12250	1500	87	174	87	261	174	87
13800	12250	1500	86	172	86	258	172	86
14000	12250	1500	85	170	85	255	170	85
14200	12250	1500	84	168	84	252	168	84
14400	12250	1500	83	166	83	249	166	83
14600	12250	1500	82	164	82	246	164	82
14800	12250	1500	80	160	80	240	160	80
15000	12250	1500	75	150	75	225	150	75
15200	12250	1500	70	140	70	210	140	70
15400	12250	1500	65	130	65	195	130	65
15600	12250	1500	60	120	60	180	120	60
15800	12250	1500	54	108	54	162	108	54
16000	12250	1500	48	96	48	144	96	48
16200	12250	1500	42	84	42	126	84	42
16400	12250	1500	35	70	35	105	70	35
16600	12250	1500	28	56	28	84	56	28
16800	12250	1500	21	42	21	63	42	21
17000	12250	1500	14	28	14	42	28	14
17200	12250	1500	7	14	7	21	14	7
17400	12250	1500	0	0	0	0	0	0
17550	12250	1500	0	0	0	0	0	0

Experiment 9 Fault 1: Structural models 1-3 displacement attribute data

Experiment 9 Fault 1														
Structural Model 4				Structural Model 5					Structural Model 6					
4A	4B	4C	4D	5A	5B	5C	5D	5E	6A	6B	6C	6D	6E	6F
0	0	0	0	0	0	0	0	0	0	0	0	0	0	0
0	0	0	0	0	0	0	0	0	0	0	0	0	0	0
28	21	14	7	35	28	21	14	7	42	35	28	21	14	7
56	42	28	14	70	56	42	28	14	84	70	56	42	28	14
112	84	56	28	140	112	84	56	28	168	140	112	84	56	28
140	105	70	35	175	140	105	70	35	210	175	140	105	70	35
168	126	84	42	210	168	126	84	42	252	210	168	126	84	42
192	144	96	48	240	192	144	96	48	288	240	192	144	96	48
216	162	108	54	270	216	162	108	54	324	270	216	162	108	54
240	180	120	60	300	240	180	120	60	360	300	240	180	120	60
260	195	130	65	325	260	195	130	65	390	325	260	195	130	65
280	210	140	70	350	280	210	140	70	420	350	280	210	140	70
300	225	150	75	375	300	225	150	75	450	375	300	225	150	75
320	240	160	80	400	320	240	160	80	480	400	320	240	160	80
340	255	170	85	425	340	255	170	85	510	425	340	255	170	85
344	258	172	86	430	344	258	172	86	516	430	344	258	172	86
348	261	174	87	435	348	261	174	87	522	435	348	261	174	87
352	264	176	88	440	352	264	176	88	528	440	352	264	176	88
356	267	178	89	445	356	267	178	89	534	445	356	267	178	89
360	270	180	90	450	360	270	180	90	540	450	360	270	180	90
364	273	182	91	455	364	273	182	91	546	455	364	273	182	91
372	279	186	93	465	372	279	186	93	558	465	372	279	186	93
380	285	190	95	475	380	285	190	95	570	475	380	285	190	95
382	286.5	191	95.5	477.5	382	286.5	191	95.5	573	477.5	382	286.5	191	95.5
384	288	192	96	480	384	288	192	96	576	480	384	288	192	96
386	289.5	193	96.5	482.5	386	289.5	193	96.5	579	482.5	386	289.5	193	96.5
388	291	194	97	485	388	291	194	97	582	485	388	291	194	97
390	292.5	195	97.5	487.5	390	292.5	195	97.5	585	487.5	390	292.5	195	97.5
392	294	196	98	490	392	294	196	98	588	490	392	294	196	98
394	295.5	197	98.5	492.5	394	295.5	197	98.5	591	492.5	394	295.5	197	98.5
396	297	198	99	495	396	297	198	99	594	495	396	297	198	99
398	298.5	199	99.5	497.5	398	298.5	199	99.5	597	497.5	398	298.5	199	99.5
400	300	200	100	500	400	300	200	100	600	500	400	300	200	100
400	300	200	100	500	400	300	200	100	600	500	400	300	200	100
400	300	200	100	500	400	300	200	100	600	500	400	300	200	100
400	300	200	100	500	400	300	200	100	600	500	400	300	200	100
400	300	200	100	500	400	300	200	100	600	500	400	300	200	100
400	300	200	100	500	400	300	200	100	600	500	400	300	200	100
400	300	200	100	500	400	300	200	100	600	500	400	300	200	100
400	300	200	100	500	400	300	200	100	600	500	400	300	200	100
400	300	200	100	500	400	300	200	100	600	500	400	300	200	100
400	300	200	100	500	400	300	200	100	600	500	400	300	200	100
400	300	200	100	500	400	300	200	100	600	500	400	300	200	100
398	298.5	199	99.5	497.5	398	298.5	199	99.5	597	497.5	398	298.5	199	99.5
396	297	198	99	495	396	297	198	99	594	495	396	297	198	99
394	295.5	197	98.5	492.5	394	295.5	197	98.5	591	492.5	394	295.5	197	98.5
392	294	196	98	490	392	294	196	98	588	490	392	294	196	98
390	292.5	195	97.5	487.5	390	292.5	195	97.5	585	487.5	390	292.5	195	97.5
388	291	194	97	485	388	291	194	97	582	485	388	291	194	97
386	289.5	193	96.5	482.5	386	289.5	193	96.5	579	482.5	386	289.5	193	96.5
384	288	192	96	480	384	288	192	96	576	480	384	288	192	96
382	286.5	191	95.5	477.5	382	286.5	191	95.5	573	477.5	382	286.5	191	95.5
380	285	190	95	475	380	285	190	95	570	475	380	285	190	95
372	279	186	93	465	372	279	186	93	558	465	372	279	186	93
364	273	182	91	455	364	273	182	91	546	455	364	273	182	91
360	270	180	90	450	360	270	180	90	540	450	360	270	180	90
356	267	178	89	445	356	267	178	89	534	445	356	267	178	89
352	264	176	88	440	352	264	176	88	528	440	352	264	176	88
348	261	174	87	435	348	261	174	87	522	435	348	261	174	87
344	258	172	86	430	344	258	172	86	516	430	344	258	172	86
340	255	170	85	425	340	255	170	85	510	425	340	255	170	85
336	252	168	84	420	336	252	168	84	504	420	336	252	168	84
332	249	166	83	415	332	249	166	83	498	415	332	249	166	83
328	246	164	82	410	328	246	164	82	492	410	328	246	164	82
320	240	160	80	400	320	240	160	80	480	400	320	240	160	80
300	225	150	75	375	300	225	150	75	450	375	300	225	150	75
280	210	140	70	350	280	210	140	70	420	350	280	210	140	70
260	195	130	65	325	260	195	130	65	390	325	260	195	130	65
240	180	120	60	300	240	180	120	60	360	300	240	180	120	60
216	162	108	54	270	216	162	108	54	324	270	216	162	108	54
192	144	96	48	240	192	144	96	48	288	240	192	144	96	48
168	126	84	42	210	168	126	84	42	252	210	168	126	84	42
140	105	70	35	175	140	105	70	35	210	175	140	105	70	35
112	84	56	28	140	112	84	56	28	168	140	112	84	56	28
84	63	42	21	105	84	63	42	21	126	105	84	63	42	21
56	42	28	14	70	56	42	28	14	84	70	56	42	28	14
28	21	14	7	35	28	21	14	7	42	35	28	21	14	7
0	0	0	0	0	0	0	0	0	0	0	0	0	0	0
0	0	0	0	0	0	0	0	0	0	0	0	0	0	0

Experiment 9 Fault 1: Structural models 4-6 displacement attribute data

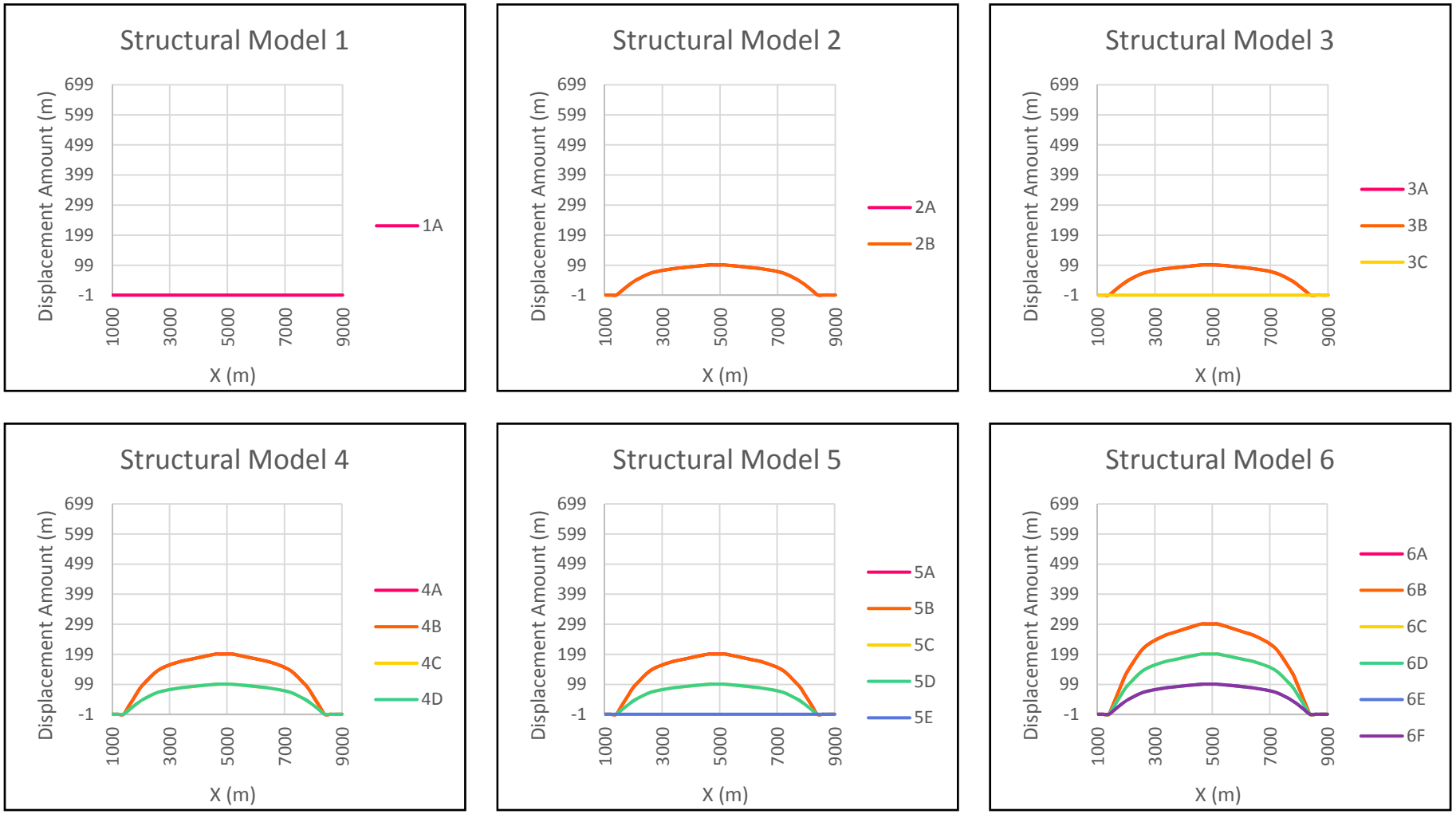

Experiment 9 Fault 2: Fault displacement attribute data linear charts

Experiment 9 Fault 2																							
Displacement Point Location			Structural Model 1	Structural Model 2		Structural Model 3			Structural Model 4				Structural Model 5					Structural Model 6					
X	Y	Z	1A	2A	2B	3A	3B	3C	4A	4B	4C	4D	5A	5B	5C	5D	5E	6A	6B	6C	6D	6E	6F
1000	8000	1500	0	0	0	0	0	0	0	0	0	0	0	0	0	0	0	0	0	0	0	0	0
1200	8000	1500	0	0	0	0	0	0	0	0	0	0	0	0	0	0	0	0	0	0	0	0	0
1400	8000	1500	0	0	0	0	0	0	0	0	0	0	0	0	0	0	0	0	0	0	0	0	0
1600	8000	1500	0	15	15	15	15	0	30	30	15	15	30	30	15	15	0	45	45	30	30	15	15
1800	8000	1500	0	30	30	30	30	0	60	60	30	30	60	60	30	30	0	90	90	60	60	30	30
2000	8000	1500	0	45	45	45	45	0	90	90	45	45	90	90	45	45	0	135	135	90	90	45	45
2200	8000	1500	0	55	55	55	55	0	110	110	55	55	110	110	55	55	0	165	165	110	110	55	55
2400	8000	1500	0	65	65	65	65	0	130	130	65	65	130	130	65	65	0	195	195	130	130	65	65
2600	8000	1500	0	73	73	73	73	0	146	146	73	73	146	146	73	73	0	219	219	146	146	73	73
2800	8000	1500	0	78	78	78	78	0	156	156	78	78	156	156	78	78	0	234	234	156	156	78	78
3000	8000	1500	0	82	82	82	82	0	164	164	82	82	164	164	82	82	0	246	246	164	164	82	82
3200	8000	1500	0	85	85	85	85	0	170	170	85	85	170	170	85	85	0	255	255	170	170	85	85
3400	8000	1500	0	88	88	88	88	0	176	176	88	88	176	176	88	88	0	264	264	176	176	88	88
3600	8000	1500	0	90	90	90	90	0	180	180	90	90	180	180	90	90	0	270	270	180	180	90	90
3800	8000	1500	0	92	92	92	92	0	184	184	92	92	184	184	92	92	0	276	276	184	184	92	92
4000	8000	1500	0	94	94	94	94	0	188	188	94	94	188	188	94	94	0	282	282	188	188	94	94
4200	8000	1500	0	96	96	96	96	0	192	192	96	96	192	192	96	96	0	288	288	192	192	96	96
4400	8000	1500	0	98	98	98	98	0	196	196	98	98	196	196	98	98	0	294	294	196	196	98	98
4600	8000	1500	0	100	100	100	100	0	200	200	100	100	200	200	100	100	0	300	300	200	200	100	100
4800	8000	1500	0	100	100	100	100	0	200	200	100	100	200	200	100	100	0	300	300	200	200	100	100
5000	8000	1500	0	100	100	100	100	0	200	200	100	100	200	200	100	100	0	300	300	200	200	100	100
5200	8000	1500	0	100	100	100	100	0	200	200	100	100	200	200	100	100	0	300	300	200	200	100	100
5400	8000	1500	0	98	98	98	98	0	196	196	98	98	196	196	98	98	0	294	294	196	196	98	98
5600	8000	1500	0	96	96	96	96	0	192	192	96	96	192	192	96	96	0	288	288	192	192	96	96
5800	8000	1500	0	94	94	94	94	0	188	188	94	94	188	188	94	94	0	282	282	188	188	94	94
6000	8000	1500	0	92	92	92	92	0	184	184	92	92	184	184	92	92	0	276	276	184	184	92	92
6200	8000	1500	0	90	90	90	90	0	180	180	90	90	180	180	90	90	0	270	270	180	180	90	90
6400	8000	1500	0	88	88	88	88	0	176	176	88	88	176	176	88	88	0	264	264	176	176	88	88
6600	8000	1500	0	85	85	85	85	0	170	170	85	85	170	170	85	85	0	255	255	170	170	85	85
6800	8000	1500	0	82	82	82	82	0	164	164	82	82	164	164	82	82	0	246	246	164	164	82	82
7000	8000	1500	0	78	78	78	78	0	156	156	78	78	156	156	78	78	0	234	234	156	156	78	78
7200	8000	1500	0	73	73	73	73	0	146	146	73	73	146	146	73	73	0	219	219	146	146	73	73
7400	8000	1500	0	65	65	65	65	0	130	130	65	65	130	130	65	65	0	195	195	130	130	65	65
7600	8000	1500	0	55	55	55	55	0	110	110	55	55	110	110	55	55	0	165	165	110	110	55	55
7800	8000	1500	0	45	45	45	45	0	90	90	45	45	90	90	45	45	0	135	135	90	90	45	45
8000	8000	1500	0	30	30	30	30	0	60	60	30	30	60	60	30	30	0	90	90	60	60	30	30
8200	8000	1500	0	15	15	15	15	0	30	30	15	15	30	30	15	15	0	45	45	30	30	15	15
8400	8000	1500	0	0	0	0	0	0	0	0	0	0	0	0	0	0	0	0	0	0	0	0	0
8600	8000	1500	0	0	0	0	0	0	0	0	0	0	0	0	0	0	0	0	0	0	0	0	0
8800	8000	1500	0	0	0	0	0	0	0	0	0	0	0	0	0	0	0	0	0	0	0	0	0
9000	8000	1500	0	0	0	0	0	0	0	0	0	0	0	0	0	0	0	0	0	0	0	0	0

Experiment 9 Fault 2: Displacement attribute data

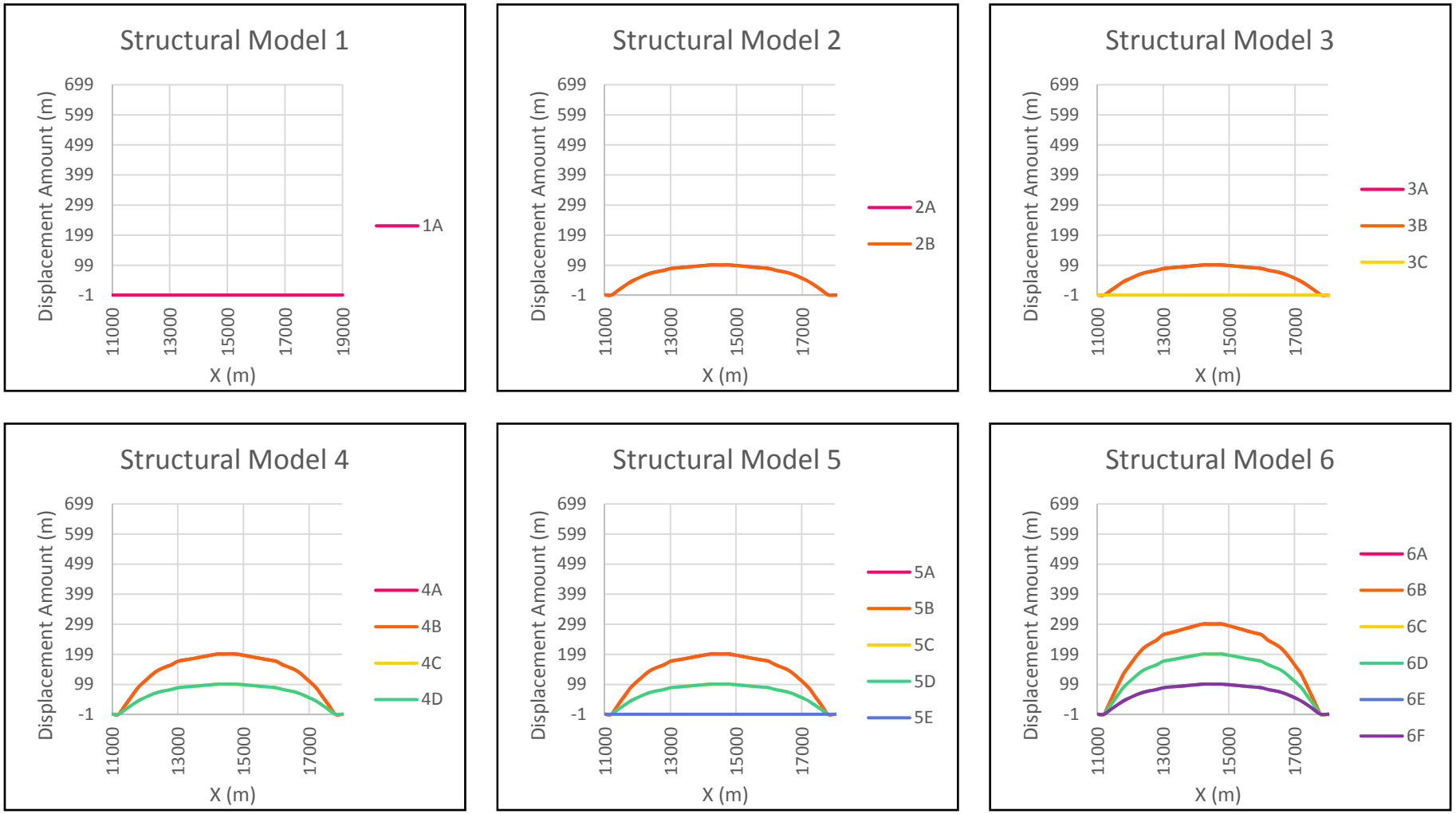

Experiment 9 Fault 3: Fault displacement attribute data linear charts

Experiment 9 Fault 3																							
Displacement Point Location			Structural Model 1	Structural Model 2		Structural Model 3			Structural Model 4				Structural Model 5					Structural Model 6					
X	Y	Z	1A	2A	2B	3A	3B	3C	4A	4B	4C	4D	5A	5B	5C	5D	5E	6A	6B	6C	6D	6E	6F
11000	8000	1500	0	0	0	0	0	0	0	0	0	0	0	0	0	0	0	0	0	0	0	0	0
11200	8000	1500	0	0	0	0	0	0	0	0	0	0	0	0	0	0	0	0	0	0	0	0	0
11400	8000	1500	0	15	15	15	15	0	30	30	15	15	30	30	15	15	0	45	45	30	30	15	15
11600	8000	1500	0	30	30	30	30	0	60	60	30	30	60	60	30	30	0	90	90	60	60	30	30
11800	8000	1500	0	45	45	45	45	0	90	90	45	45	90	90	45	45	0	135	135	90	90	45	45
12000	8000	1500	0	55	55	55	55	0	110	110	55	55	110	110	55	55	0	165	165	110	110	55	55
12200	8000	1500	0	65	65	65	65	0	130	130	65	65	130	130	65	65	0	195	195	130	130	65	65
12400	8000	1500	0	73	73	73	73	0	146	146	73	73	146	146	73	73	0	219	219	146	146	73	73
12600	8000	1500	0	78	78	78	78	0	156	156	78	78	156	156	78	78	0	234	234	156	156	78	78
12800	8000	1500	0	82	82	82	82	0	164	164	82	82	164	164	82	82	0	246	246	164	164	82	82
13000	8000	1500	0	88	88	88	88	0	176	176	88	88	176	176	88	88	0	264	264	176	176	88	88
13200	8000	1500	0	90	90	90	90	0	180	180	90	90	180	180	90	90	0	270	270	180	180	90	90
13400	8000	1500	0	92	92	92	92	0	184	184	92	92	184	184	92	92	0	276	276	184	184	92	92
13600	8000	1500	0	94	94	94	94	0	188	188	94	94	188	188	94	94	0	282	282	188	188	94	94
13800	8000	1500	0	96	96	96	96	0	192	192	96	96	192	192	96	96	0	288	288	192	192	96	96
14000	8000	1500	0	98	98	98	98	0	196	196	98	98	196	196	98	98	0	294	294	196	196	98	98
14200	8000	1500	0	100	100	100	100	0	200	200	100	100	200	200	100	100	0	300	300	200	200	100	100
14400	8000	1500	0	100	100	100	100	0	200	200	100	100	200	200	100	100	0	300	300	200	200	100	100
14600	8000	1500	0	100	100	100	100	0	200	200	100	100	200	200	100	100	0	300	300	200	200	100	100
14800	8000	1500	0	100	100	100	100	0	200	200	100	100	200	200	100	100	0	300	300	200	200	100	100
15000	8000	1500	0	98	98	98	98	0	196	196	98	98	196	196	98	98	0	294	294	196	196	98	98
15200	8000	1500	0	96	96	96	96	0	192	192	96	96	192	192	96	96	0	288	288	192	192	96	96
15400	8000	1500	0	94	94	94	94	0	188	188	94	94	188	188	94	94	0	282	282	188	188	94	94
15600	8000	1500	0	92	92	92	92	0	184	184	92	92	184	184	92	92	0	276	276	184	184	92	92
15800	8000	1500	0	90	90	90	90	0	180	180	90	90	180	180	90	90	0	270	270	180	180	90	90
16000	8000	1500	0	88	88	88	88	0	176	176	88	88	176	176	88	88	0	264	264	176	176	88	88
16200	8000	1500	0	82	82	82	82	0	164	164	82	82	164	164	82	82	0	246	246	164	164	82	82
16400	8000	1500	0	78	78	78	78	0	156	156	78	78	156	156	78	78	0	234	234	156	156	78	78
16600	8000	1500	0	73	73	73	73	0	146	146	73	73	146	146	73	73	0	219	219	146	146	73	73
16800	8000	1500	0	65	65	65	65	0	130	130	65	65	130	130	65	65	0	195	195	130	130	65	65
17000	8000	1500	0	55	55	55	55	0	110	110	55	55	110	110	55	55	0	165	165	110	110	55	55
17200	8000	1500	0	45	45	45	45	0	90	90	45	45	90	90	45	45	0	135	135	90	90	45	45
17400	8000	1500	0	30	30	30	30	0	60	60	30	30	60	60	30	30	0	90	90	60	60	30	30
17600	8000	1500	0	15	15	15	15	0	30	30	15	15	30	30	15	15	0	45	45	30	30	15	15
17800	8000	1500	0	0	0	0	0	0	0	0	0	0	0	0	0	0	0	0	0	0	0	0	0
18000	8000	1500	0	0	0	0	0	0	0	0	0	0	0	0	0	0	0	0	0	0	0	0	0
18200	8000	1500	0	0	0	0	0	0	0	0	0	0	0	0	0	0	0	0	0	0	0	0	0
18400	8000	1500	0	0	0	0	0	0	0	0	0	0	0	0	0	0	0	0	0	0	0	0	0
18600	8000	1500	0	0	0	0	0	0	0	0	0	0	0	0	0	0	0	0	0	0	0	0	0
18800	8000	1500	0	0	0	0	0	0	0	0	0	0	0	0	0	0	0	0	0	0	0	0	0
19000	8000	1500	0	0	0	0	0	0	0	0	0	0	0	0	0	0	0	0	0	0	0	0	0

Experiment 9 Fault 3: Displacement attribute data

Appendix 4: All modeling information and workflows for Experiments 1-10

Structural Model 1
Experiments 1-9

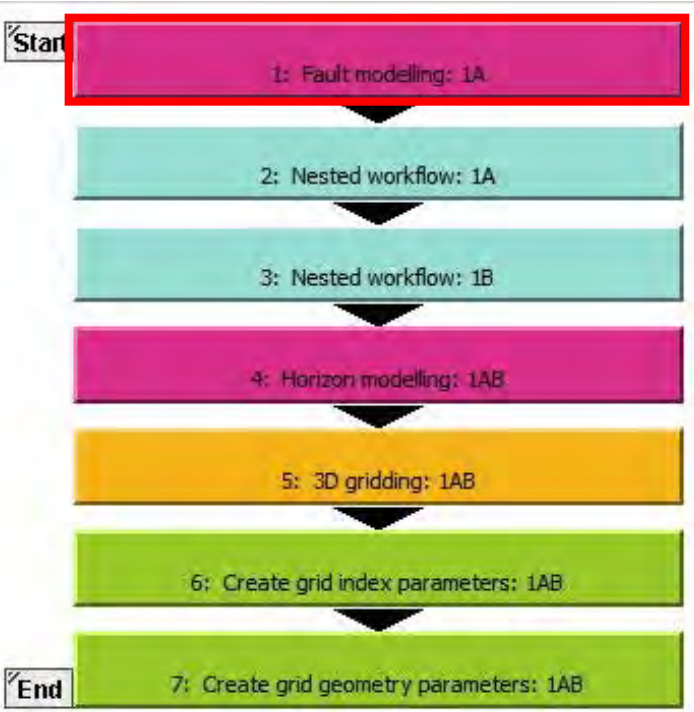

Under Gridding Grid Increment was changed form 25 to 100 to increase fault displacement ellipse detail

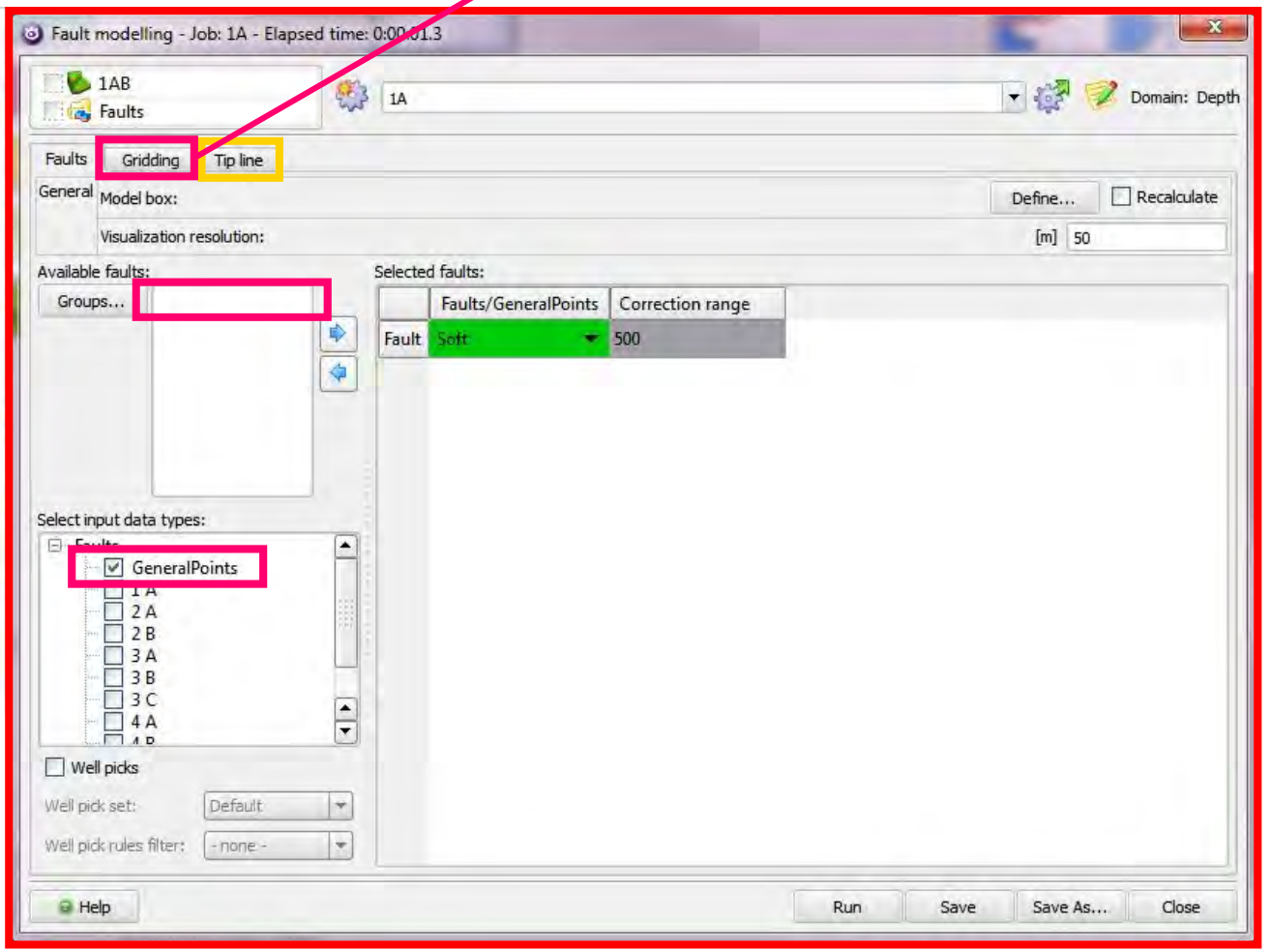

Legend

Select

Input Value

No Changes

Structural Model 1
Experiments 1-9

This is where the displacement distribution is set to 0.5 for 50/50 hanging wall/footwall displacement distribution

Nested Workflow A

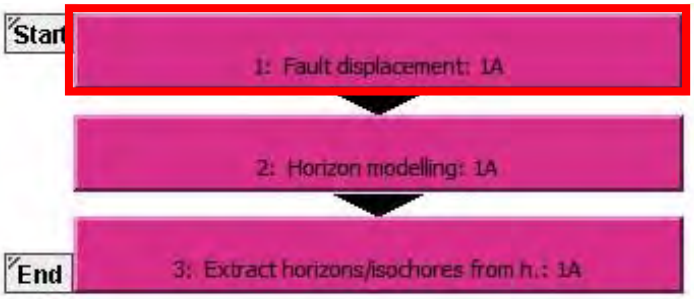

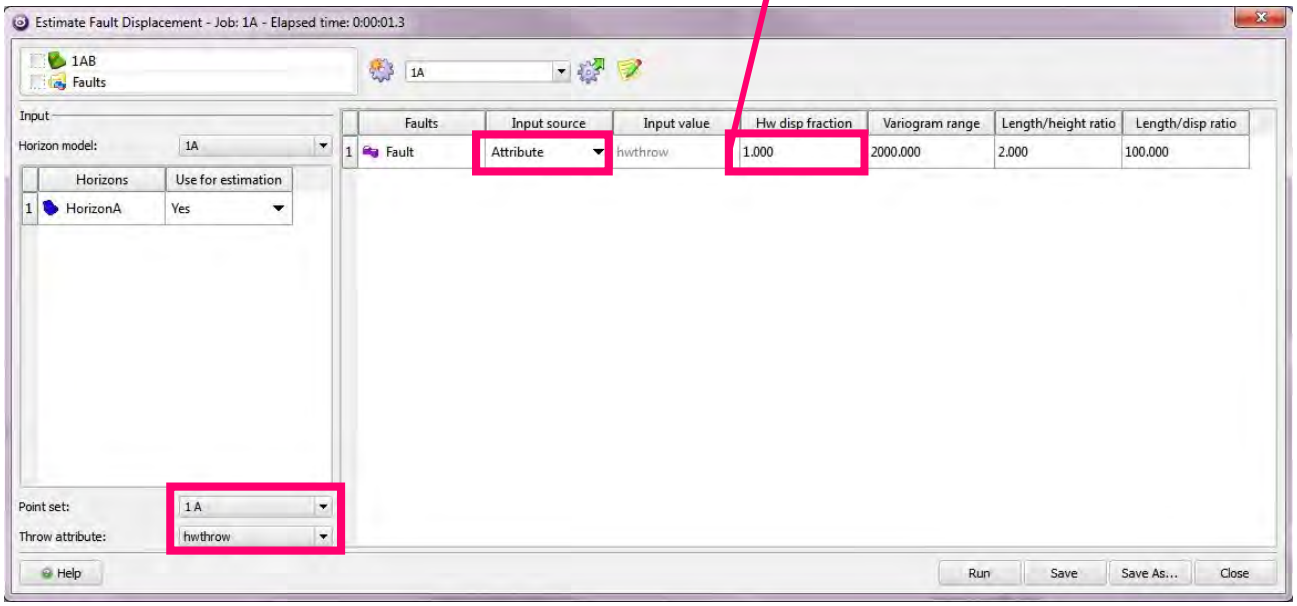

Legend

Select

Input Value

No Changes

Structural Model 1
Experiments 1-9

Change correction range to desired reverse drag distance in meters.

Select fault and turn on displacement.

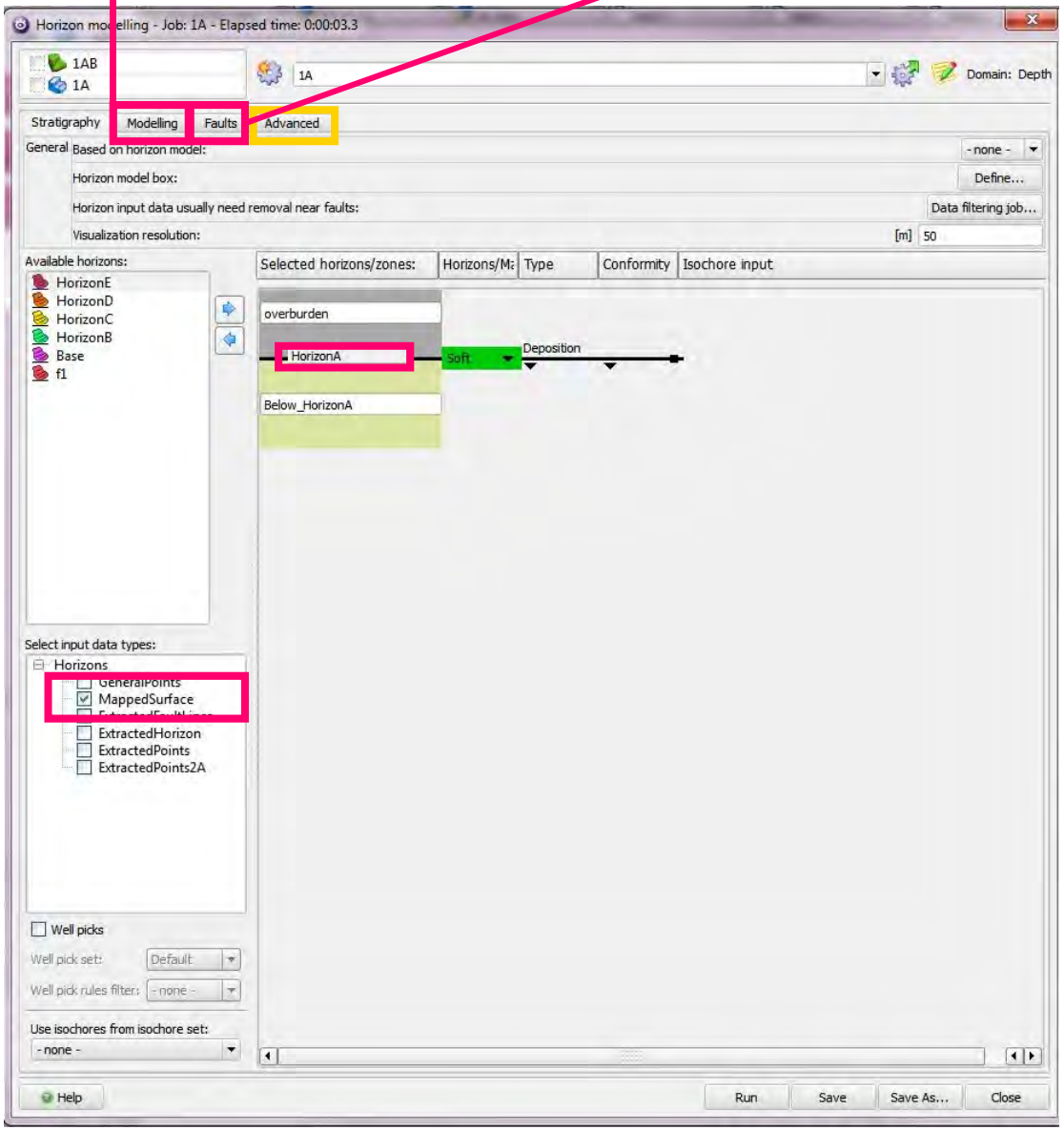

Nested Workflow A

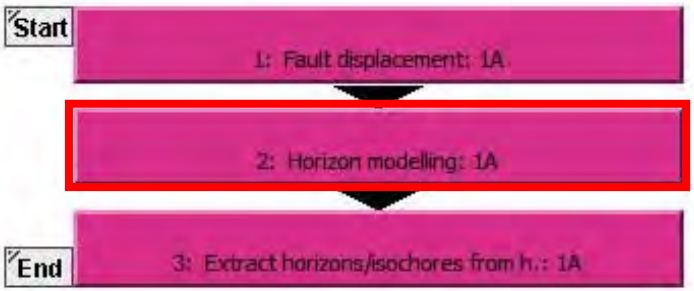

Legend

Select

Input Value

No Changes

Structural Model 1
Experiments 1-9

Nested Workflow A

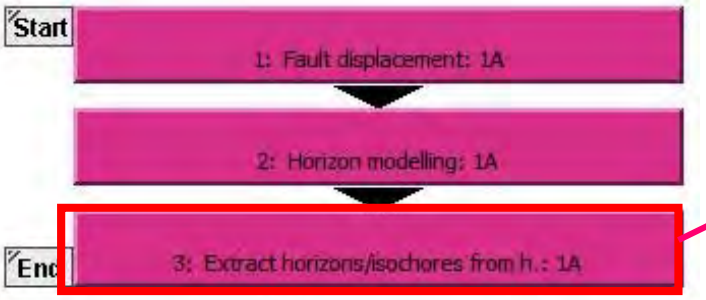

Select generate horizons- the results will be found in the original horizon folder in data tree.

Legend

Select

Input Value

No Changes

Structural Model 1
Experiments 1-9

Change correction range to desired reverse drag distance in meters.

Select fault and turn on displacement.

Nested Workflow B

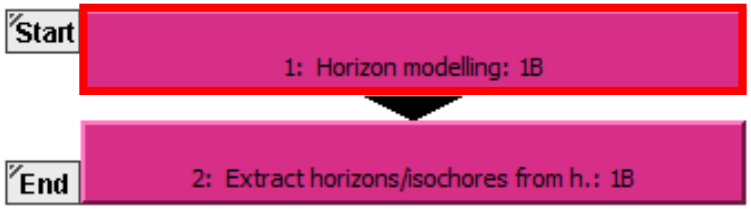

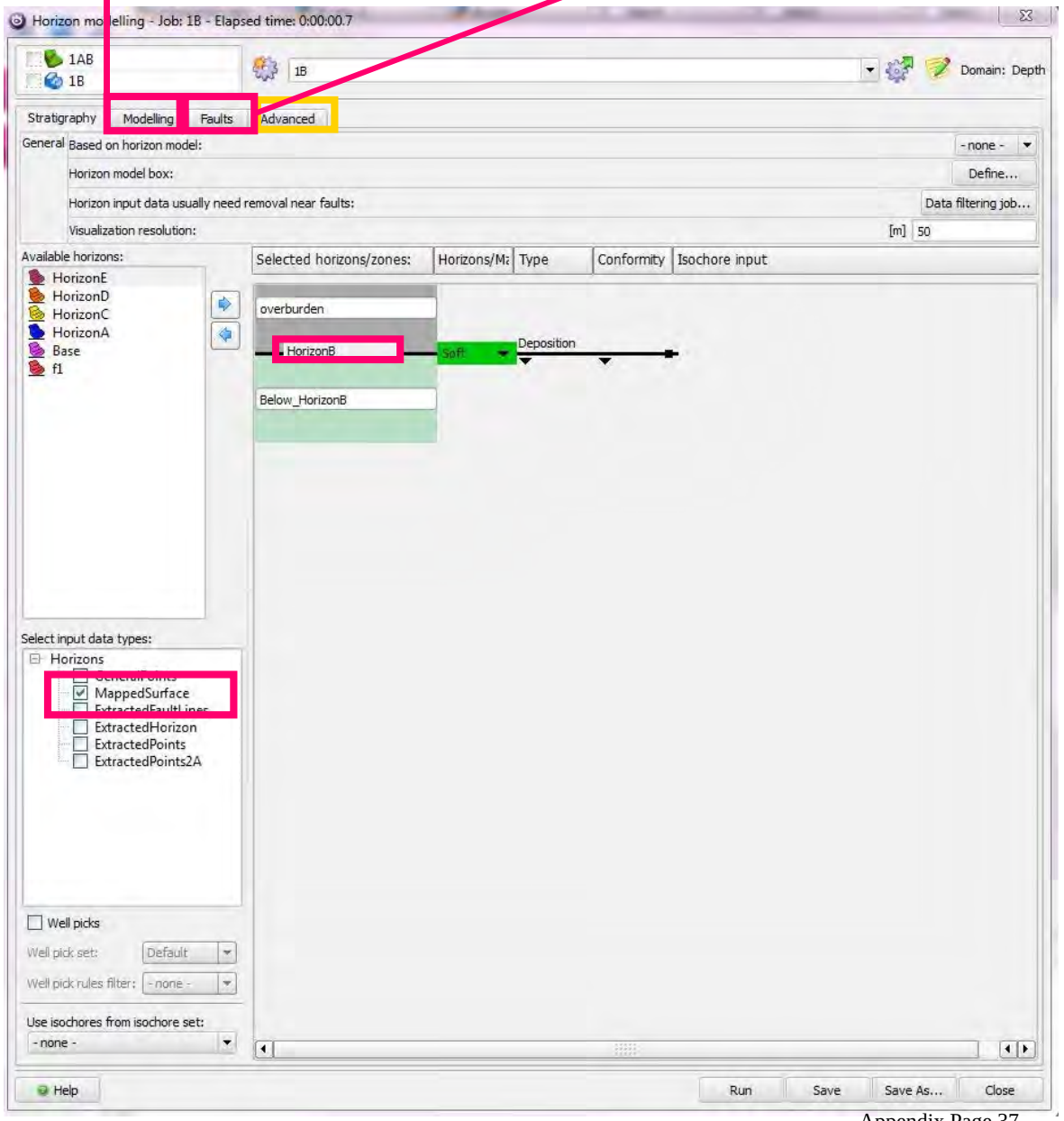

Legend

Select

Input Value

No Changes

Structural Model 1
Experiments 1-9

Nested Workflow B

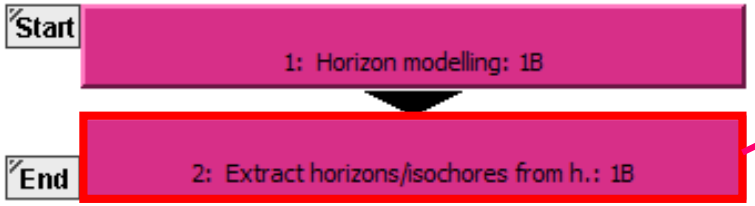

Select Generate Horizons- the results will be found in the original horizon folder in data tree.

Legend

Select

Input Value

No Changes

Structural Model 1
Experiments 1-9

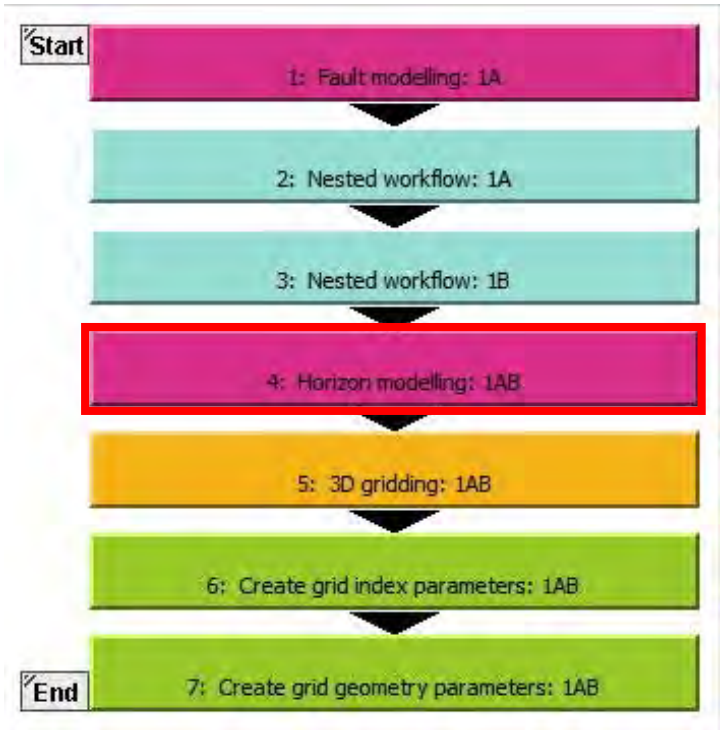

Under Gridding Grid Increment was changed form 25 to 100 to increase fault displacement ellipse detail.

Select Fault (s) and do not apply displacement.

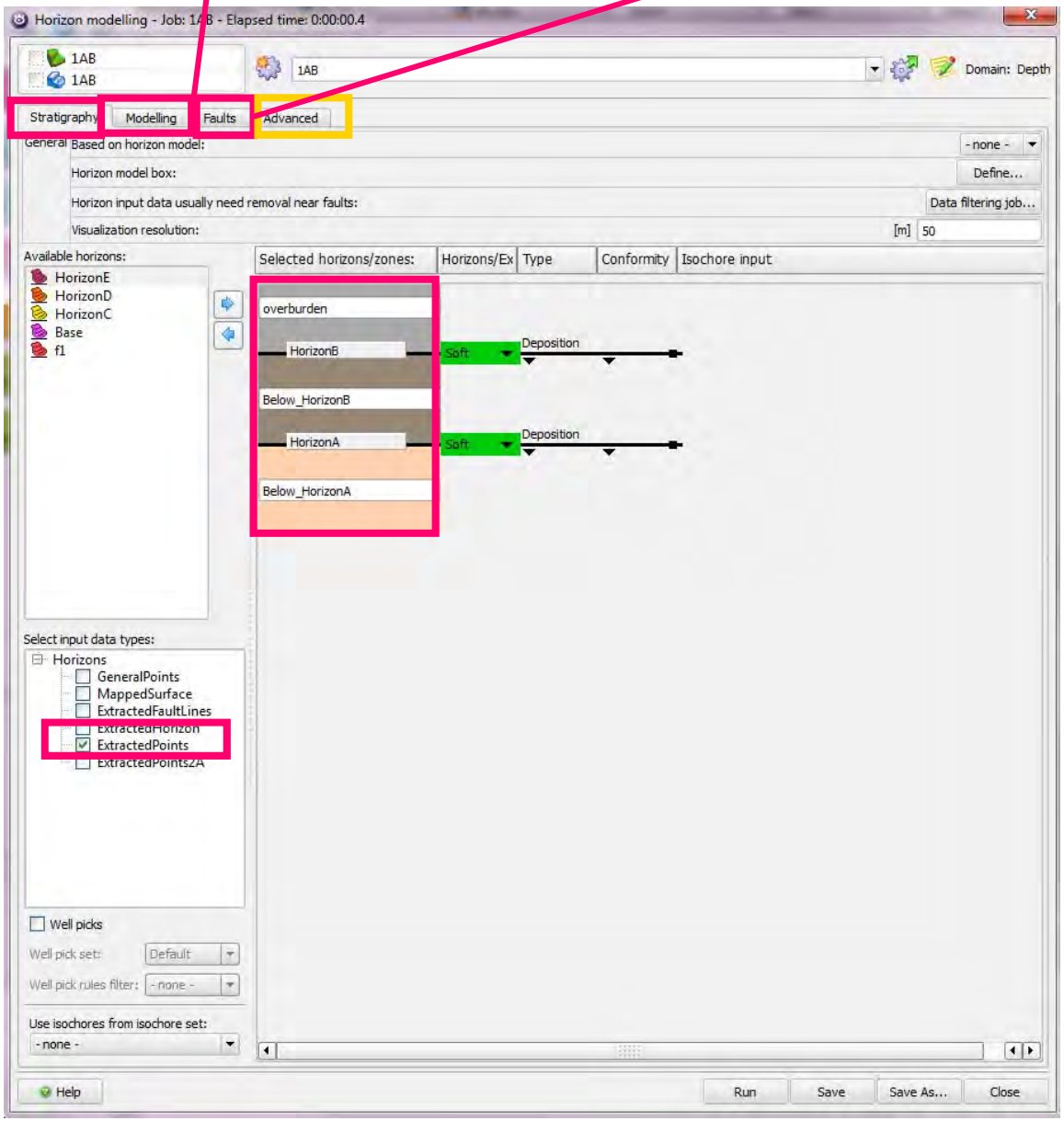

Legend

Select

Input Value

No Changes

Structural Model 1
Experiments 1-9

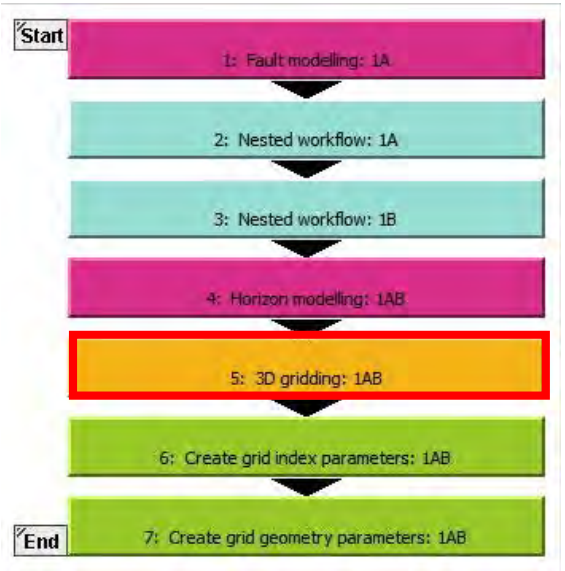

Legend

Select

Input Value

No Changes

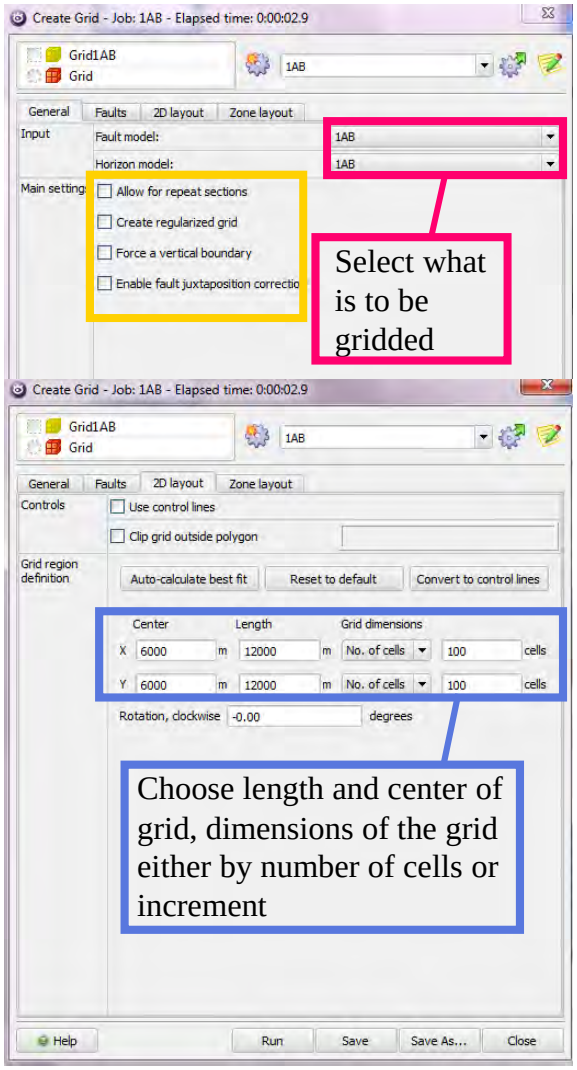

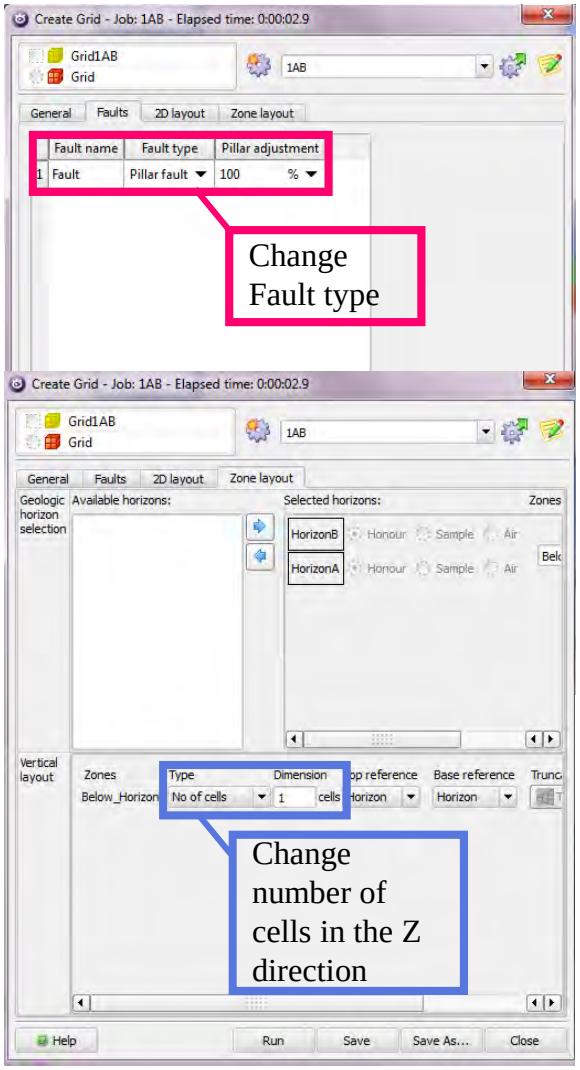

Structural Model 1
Experiments 1-9

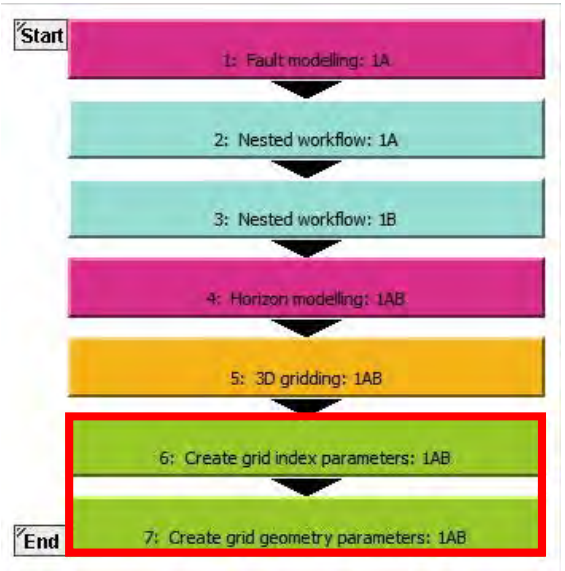

Legend

Select

Input Value

No Changes

All grid index parameters can be selected but only the Zone filter was used in these experiments

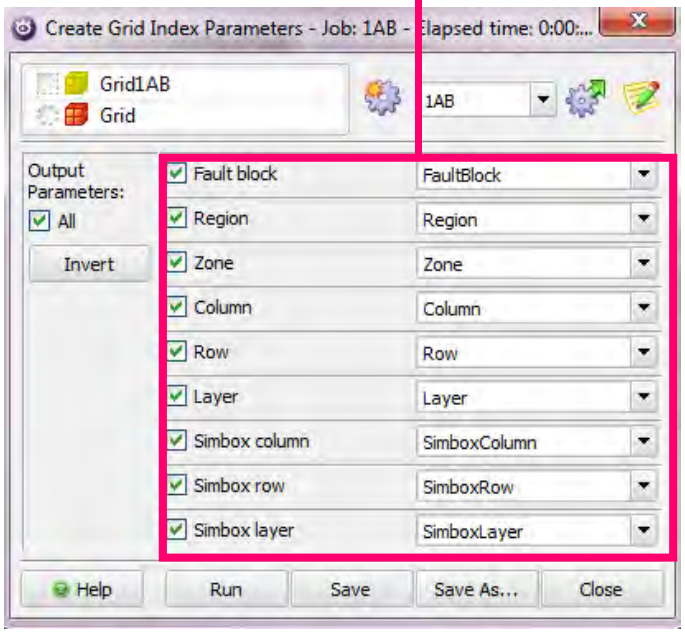

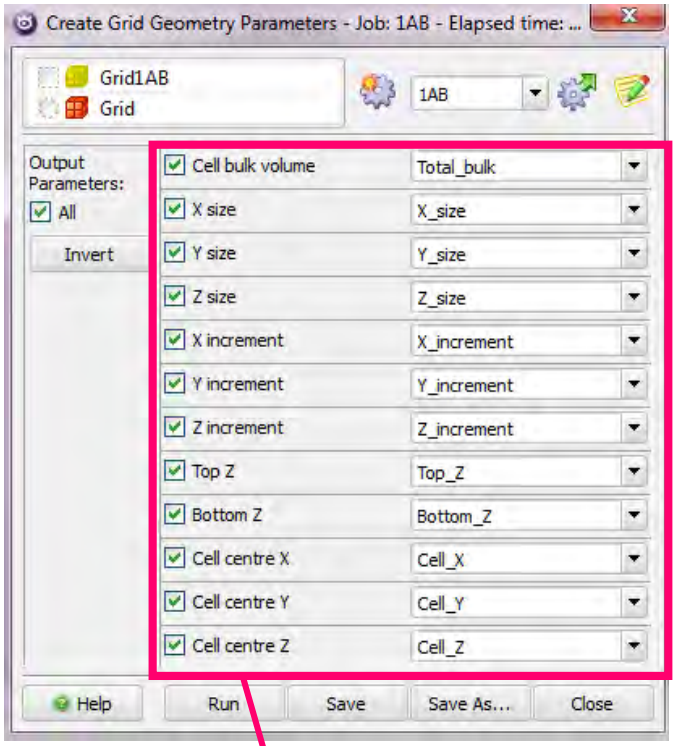

All grid geometry parameters can be selected but only the Cell_Z filter was used in these experiments.

Workflow for
Structural Model 2
Experiments 1-8

Workflow for
Structural Model 3
Experiments 1-8

Workflow for
Structural Model 4
Experiments 1-8

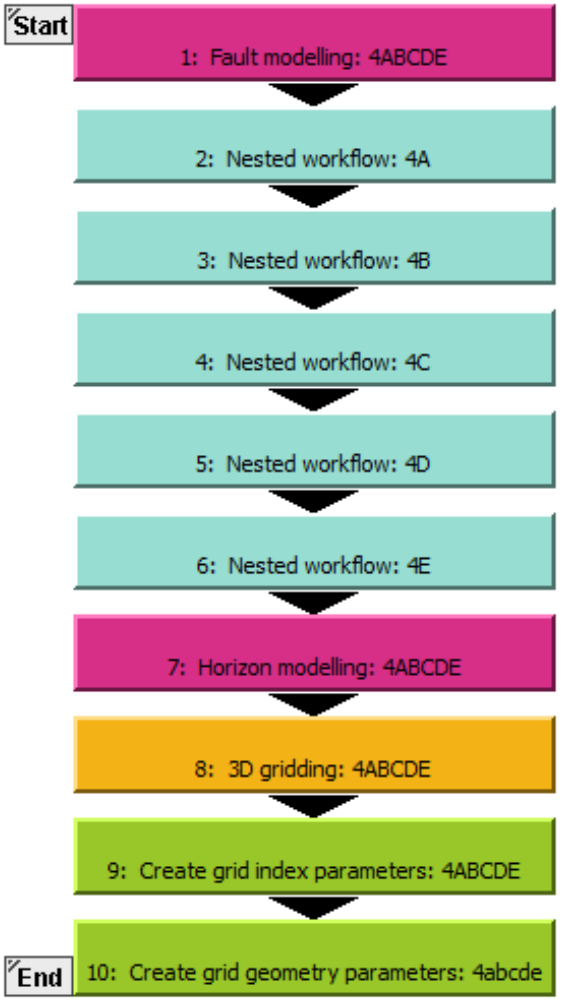

Workflow for
Structural Model 5
Experiment 9

Workflow for
Structural Model 6
Experiments 9

Workflow for
Structural Model 1
Experiment 10

Workflow for
Structural Model 2
Experiments10

Appendix 5: Color bars used in 3D grid experiment visualization

Color Bars with RGB input values: Experiments 1-8

Color	R	G	B
Yellow	255	209	0
Red	255	0	110

Structural Model 1

Color	R	G	B
Yellow	255	209	0
Red	255	0	110

Structural Model 2

Color	R	G	B
Blue	88	119	222
Yellow	255	209	0
Red	255	0	110

Structural Model 3

Color	R	G	B
Green	58	208	138
Blue	88	119	222
Yellow	255	209	0
Red	255	0	110

Structural Model 4

Red: Zone A in Models, Yellow: Zone B, Blue: Zone C, Green: Zone D

Color Bars with RGB input values: Experiment 9

Color	R	G	B
Orange	255	98	0
Red	255	0	110

Structural Model 1

Color	R	G	B
Orange	255	98	0
Red	255	0	110

Structural Model 2

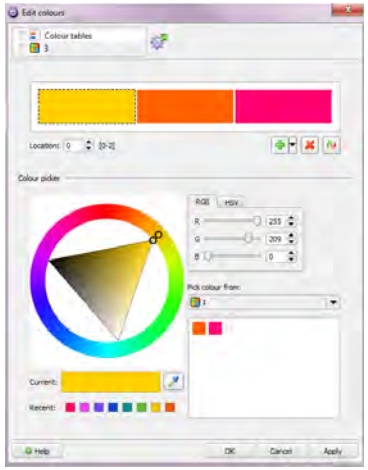

Color	R	G	B
Yellow	255	209	0
Orange	255	98	0
Red	255	0	110

Structural Model 3

Color	R	G	B
Green	58	208	138
Yellow	255	209	0
Orange	255	98	0
Red	255	0	110

Structural Model 4

Red: Zone A, Orange: Zone B, Yellow: Zone C, Green: Zone D

Color Bars with RGB input values: Experiment 9

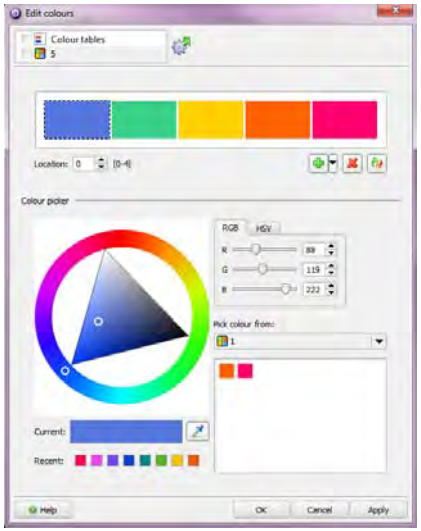

Color	R	G	B
Blue	88	119	222
Green	58	208	138
Yellow	255	209	0
Orange	255	98	0
Red	255	0	110

Structural Model 5

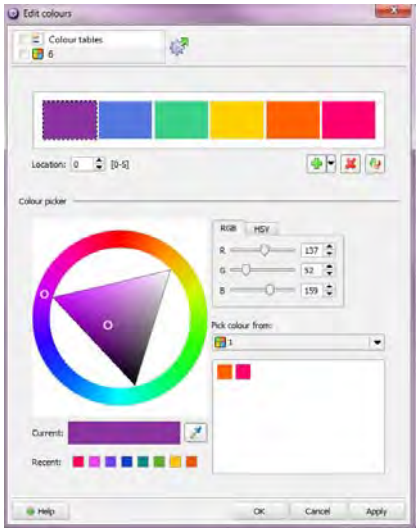

Color	R	G	B
Purple	137	52	159
Blue	88	119	222
Green	58	208	138
Yellow	255	209	0
Orange	255	98	0
Red	255	0	110

Structural Model 6

Red: Zone A, Orange: Zone B, Yellow: Zone C, Green: Zone D, Blue: Zone E, Purple: Zone F

Color Bars with RGB input values: Experiment 10

Color	R	G	B
Dark Pink	193	19	106
Purple	137	52	159
Blue	88	119	222
Green	58	208	138
Yellow	255	209	0
Lt. Orange	255	157	0
Orange	255	98	0
Red	255	0	21
Pink	255	0	89
Grey	173	173	173

Structural Model 1

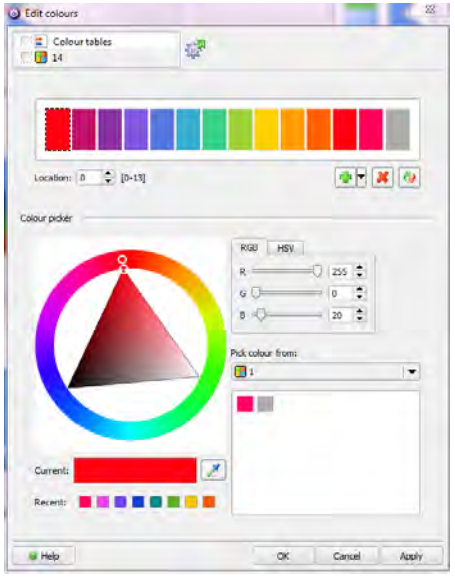

Color	R	G	B
Red	225	0	20
Dark Pink	193	19	106
Purple	137	52	159
Violet	128	88	222
Blue	88	119	222
Teal	255	173	208
Green	58	208	138
Lime	158	208	58
Yellow	255	209	0
Lt. Orange	255	157	0
Orange	255	98	0
Red	255	0	21
Pink	255	0	89
Grey	173	173	173

Structural Model 2

Red: Zone A, Orange: Zone B, Yellow: Zone C, Green: Zone D, Blue: Zone E, Purple: Zone F

Appendix 6: CD with Sample RMS File: Experiment 1

Sample RMS file Experiment 1